AFRL-RX-WP-TR-2011-4148

NANOCATALYSIS FOR PRIMARY AND SECONDARY HIGH ENERGY LITHIUM OXYGEN CELLS

D. "Pera"Peramunage, Gary Pabst, and Christina M. Gasbarro

EIC Laboratories, Inc.

April 2011
Final Report

AIR FORCE RESEARCH LABORATORY
MATERIALS AND MANUFACTURING DIRECTORATE
WRIGHT-PATTERSON AIR FORCE BASE, OH 45433-7750
AIR FORCE MATERIEL COMMAND
UNITED STATES AIR FORCE

NOTICE AND SIGNATURE PAGE

Using Government drawings, specifications, or other data included in this document for any purpose other than Government procurement does not in any way obligate the U.S. Government. The fact that the Government formulated or supplied the drawings, specifications, or other data does not license the holder or any other person or corporation; or convey any rights or permission to manufacture, use, or sell any patented invention that may relate to them.

This report was cleared for public release by the Wright-Patterson Air Force Base (WPAFB) Public Affairs Office and is available to the general public, including foreign nationals. Copies may be obtained from the Defense Technical Information Center (DTIC)
(http://www.dtic.mil).

AFRL-RX-WP-TR-2011-4148 HAS BEEN REVIEWED AND IS APPROVED FOR PUBLICATION IN ACCORDANCE WITH THE ASSIGNED DISTRIBUTION STATEMENT.

*//signature//

PATRICK S. CARLIN, Project Engineer,
Nanostructured and Biological Materials Branch,
Nonmetallic Materials Division

//signature//

RICHARD A. VAIA, Acting Chief
Nanostructured and Biological Materials Branch,
Nonmetallic Materials Division

//signature//

SHASHI SHARMA, Deputy Division Chief
Nonmetallic Materials Division,
Materials and Manufacturing Directorate

This report is published in the interest of scientific and technical information exchange, and its publication does not constitute the Government's approval or disapproval of its ideas or findings.

*Disseminated copies will show "//signature//" stamped or typed above the signature blocks

REPORT DOCUMENTATION PAGE

Form Approved
OMB No. 0704-0188

1. REPORT DATE *(DD-MM-YY)*	2. REPORT TYPE	3. DATES COVERED *(From - To)*
April 2011	Final	24 September 2008 – 24 September 2010

4. TITLE AND SUBTITLE
NANOCATALYSIS FOR PRIMARY AND SECONDARY HIGH ENERGY LITHIUM OXYGEN CELLS

5a. CONTRACT NUMBER
FA8650-08-C-5042

5b. GRANT NUMBER

5c. PROGRAM ELEMENT NUMBER
62102F

6. AUTHOR(S)
D. "Pera"Peramunage, Gary Pabst and Christina M. Gasbarro

5d. PROJECT NUMBER
4347

5e. TASK NUMBER
ML

5f. WORK UNIT NUMBER
BP112100-A

7. PERFORMING ORGANIZATION NAME(S) AND ADDRESS(ES)

EIC Laboratories, Inc.
111 Downey Street
Norwood, MA 02062

8. PERFORMING ORGANIZATION REPORT NUMBER

9. SPONSORING/MONITORING AGENCY NAME(S) AND ADDRESS(ES)

Air Force Research Laboratory
Materials and Manufacturing Directorate
Wright-Patterson Air Force Base, OH 45433-7750
Air Force Materiel Command
United States Air Force

10. SPONSORING/MONITORING AGENCY ACRONYM(S)
AFRL/RXBN

11. SPONSORING/MONITORING AGENCY REPORT NUMBER(S)
AFRL-RX-WP-TR-2011-4148

12. DISTRIBUTION/AVAILABILITY STATEMENT
Approved for public release; distribution unlimited.

13. SUPPLEMENTARY NOTES
Report contains color. Case Number RX11-0438; Clearance Date: 29 Apr 2011.

14. ABSTRACT ***(Maximum 200 words)***

The objective of the technical program was to develop practical Lithium–Air battery technology towards achieving high specific energy and power densities. It involved a unique cathode material based on elastic hollow carbon spheres (200 and ~500 nm) with a Co_3O_4 nano-cluster catalyst encapsulated in it, designated as Co@C. We evaluated the Co@C/O_2 cathodes based on the silica templates of 500nm and 200 nm in an electrolyte consisting of a carbonate-based mixed solvent and a blend of lithium salts. Cold pressed carbon composites with the PTFE binder were found to provide the highest capacities involved in O_2 reduction. The dual shell architecture of these materials was well preserved in these electrodes despite the high pressure used in electrode fabrication. The Co@C cathodes exhibited capacities of 2500 to 3000 mAh/g range in Li/O_2 cells at a low current density, 0.1mA/cm^2, whereas cathodes based on a commercial carbon blend provided capacities in the 800 mAh/g range. Higher discharge currents resulted in a sharp decrease in the capacity, but without losing the capacity advantage of the Co@C material. Despite the very high capacities observed for Co@C materials, there was no evidence to support that lithium oxide was preferentially deposited inside the nanoshells. Uniform coverage of lithium oxide over the entire exposed carbon surfaces was observed instead. Despite the very high discharge capacities observed with the Co@C/O_2 cathode, it was poorly rechargeable. Only one charging cycle with nearly equal specific capacities was possible.

15. SUBJECT TERMS
dual shells, nanocatalyst, Co@C, Li/O2 cells, Cathode, capacity, carbonate-electrolyte, cobalt catalyst, encapsulated-catalyst

16. SECURITY CLASSIFICATION OF:			17. LIMITATION OF ABSTRACT:	18. NUMBER OF PAGES	19a. NAME OF RESPONSIBLE PERSON (Monitor)
a. REPORT	b. ABSTRACT	c. THIS PAGE			Patrick S. Carlin
Unclassified	Unclassified	Unclassified	SAR	67	19b. TELEPHONE NUMBER *(Include Area Code)* (937) 255-9162

TABLE OF CONTENTS

LIST OF FIGURES

LIST OF TABLES

SUMMARY

The objective of the technical program was to develop practical Lithium–Air battery technology towards achieving high specific energy and power densities. It involved the development of a unique cathode material based on elastic hollow carbon spheres (200 and ~500 nm) with a Co_3O_4 nano-cluster catalyst encapsulated in it (designated throughout this text as “Co@C”).

We have attempted all Tasks included in this effort fully and obtained promising results. Synthesis of the cobalt encapsulated carbon nanoshells was full of challenges that were successfully overcome. Silica-NS templates of 500 and ~200 nm sized were prepared using a spreadsheet-based work plan. The process was scaled up to produce about 50g at a time in a one liter reactor. Deposition of the cobalt catalyst and the carbon shell were perfected leading to the synthesis of Co@C materials with two Cobalt/Carbon ratios. We evaluated a broad matrix of variables pertaining to Li/O_2 cells using a liquid electrolyte. Electrolyte solvent blends, lithium salt blends, and cathode binders were of interest. For reference, a cathode was first evaluated using a blend of two commercial carbons. Based on the evaluations of a large number of Li/O_2 cells, the electrolyte, PC 30.8 mol% / DEGME 30.8 mol% /DMFA 30.8 / Li-Imide 7.3 mol% / LiBOB 0.2 mol% emerged as the best electrolyte. Cold pressed carbon composites with the PTFE binder were found to provide the highest capacities involved in O_2 reduction. Ionic groups anchored to the surface of the commercial carbon blend were not effective in improving the performance of Li/O_2 cells based on them.

Guided by the results of the preliminary evaluations involving commercial carbons, we evaluated $Co@C/O_2$ cathodes based on the silica templates of 500nm and 200 nm. The dual shell architecture of these materials was well preserved in the electrodes despite the high pressure used in electrode fabrication. The Co@C electrodes exhibited capacities of 2500 to 3000 mAh/g range in Li/O_2 cells at a low current density, $0.1mA/cm^2$, whereas cathodes based on the commercial blends provided capacities in the 800 mAh/g range. Higher discharge currents resulted in a sharp decrease in the capacity, but without losing the capacity advantage of the Co@C material. Despite the very high capacities observed for Co@C materials, there was no evidence to support that lithium oxide was preferentially deposited inside the nanoshells. Uniform coverage of lithium oxide over the entire exposed carbon surfaces was observed instead. Despite the very high discharge capacities observed with the $Co@C/O_2$ cathode, it was poorly rechargeable. Only one charging cycle with nearly equal specific capacities was possible.

1 INTRODUCTION

The military has a general requirement for batteries to power a wide range of equipment. There is a further need for a range of new applications to extend the energy density and power density of batteries beyond what is currently available. These applications include micro-UAVs, increasingly sophisticated integrated uniform instrument suites, electronic weapons and lightweight energy storage for expeditionary units. Currently, the lithium ion battery has the highest energy density of commercially available rechargeable systems, with values (in hardware) ranging up to about 150 Wh/kg. The current top end of energy density is the Li (metal)/S battery, which is currently being marketed by SION Power with an energy density for individual cells of ~350 Wh/kg, with the possibility of >500 Wh/kg being claimed.

Standing in contrast to these more or less established technologies is the Li/O_2 or Li/air battery, a "holy grail" of battery technology. The overall reaction in the Li-air cell can be represented by:

$$2Li + ½\ O_2 = Li_2O \qquad E^0 = 2.91\ V \qquad [1]$$

The theoretical specific energies calculated without and with O_2 are a remarkable 11140 and 5200 Wh/kg, respectively, compared to ~2600 Wh/kg for Li/S. The battery would have a simple construction in principle, consisting of a Li metal anode, a separator containing an electrolyte, and an "air breathing" cathode based on high surface area carbon on which the O_2 reduction to Li_2O takes place. Unfortunately, investigations to date of the Li/air battery, including work at EIC Laboratories, have resulted in limited discharge capacities and low discharge rates due to rapid passivation of the cathode matrix. Therefore, the principal objective of our cathode development effort was to adopt strategies to establish this co-continuous three phase structure that is not subjected to the capacity-limiting effect of lithium oxides precipitating inside the cathode.

We were convinced that proper control over nucleation and growth of the insulating Li-oxides remains the key factor for a successful Li-air battery. In operation during discharge, the reduction of O_2 takes place at a three phase interface, comprising the electrical conductor cathode matrix material, the ion conducting electrolyte and O_2. As a basic requirement, we would like the passivating product to be minimized on the electroactive conductive surfaces of the nanospheres and to accumulate instead in the free internal volume.

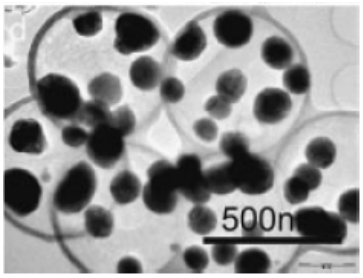

We sought to achieve this by constructing the cathode matrix using uniform semiporous carbon spheres. The spheres contained a payload of oxygen electrocatalysts (e.g. Co_3O_4). Prior work by Ming et al [1] has demonstrated hollow shell carbon nanospheres with Sn nanoparticles. When reduced in a Li^+ electrolyte, the product, Li_xSn, formed inside the nanoshells, indicating some molecular level of carbon porosity. Therefore, lithium oxide that forms in a Li/O_2 cell as the discharge product could preferentially occupy the space inside carbon shells without significantly

1) Wei-Ming Zhang et al., *Adv. Mat.*, **20**. 1160 (2008**).**

disrupting the electron conductive matrix outside the shells. Oxygen reduction is likely to occur on the outer surfaces of the spheres as well. In this case, we wished to promote formation of product away from the carbon surface. This was to be accomplished by derivatizing the carbon surface with species capable of conducting ions. These species were supposed to create a zone for uninterrupted Li^+ ion and gas transport, and to divert the insoluble lithium oxide product away from these ion conductive zones. Accordingly, the three-phase interface is preserved and the oxygen reduction could continue until the entire free volume of the electrode is filled with lithium oxide. Other anionic species such as quaternary ammonium groups, capable of transporting anionic oxide species away from the carbon surface, were also under consideration.

1.1 Objectives/goals

The objective of the technical program was to develop practical Lithium–Air battery technology towards achieving extremely high specific energy and power densities. A key expectation was to demonstrate 600 Wh/kg at moderate to high rates and to develop an extensive technology base to enable design and fabrication of mission specific Li-Air batteries. Specific Objectives are:

- Preparation of elastic hollow carbon spheres (200 and ~500 nA) with a Co_3O_4 nano-cluster catalyst encapsulated in it (designated throughout this text as “Co@C”).
- Develop Li^+ and anion conductive solid electrolyte phases covalently attached to the carbon surface
- Optimize the co-continuous, interpenetrating carbon/polymer electrolyte-gas channel cathode structure
- Identify and optimize alternative electrolytes that are capable of stabilizing the oxide ion.
- Determine operating characteristics for the developed Li-Air cells including specifically cell voltage and capacity as a function of discharge rate
- Investigate rechargeability of the spent cathodes based on hollow carbon spheres
- Analyze experimental data to identify the limiting components and processes
- Develop a data base enabling subsequent design and fabrication of Li-Air batteries for specific applications
- Fabricate prototype demonstration cells for testing by AFRL

1.2 Work plan

The Project Work Plan was organized into the following six tasks. All tasks were carried out solely at EIC Laboratories.

Task 1. Synthesis of the Hollow Carbon Sphere-Material
Task 2. Anchoring of the Cation and the Anion Conductive Ionic Brushes
Task 3. Li/O_2 Cell Fabrication
Task 4. Performance Demonstration of Li/O_2 Cells
Task 5. Analysis and Performance Projection
Task 6. Reporting.

A Gantt chart showing duration and schedule of tasks are provided in Tables 1. respectively. Milestones and deliverables are included. A detail description of the work

related to each task will follow.

2 EXPERIMENTAL APPROACH AND PROCEDURES

2.1 Synthesis of the Hollow Carbon Sphere-Material

This multistep task involved synthesis of monodispersed silica spheres, coating them with nano-clusters of the cobalt oxide catalyst, overcoating the structure with carbon and then removing the silica core leaving behind the target dual shell structure. Some of these steps involved sub-tasks that will be described below in conjunction with those steps. A schematic of the synthesis is given in Figure 1. We prepared the nanospheres in two sizes (500 nm and 200 nm). Synthesis of the monodispersed silica spheres of 100 nm, although originally targeted, did not materialize due to difficulties encountered with the synthesis and recovery.

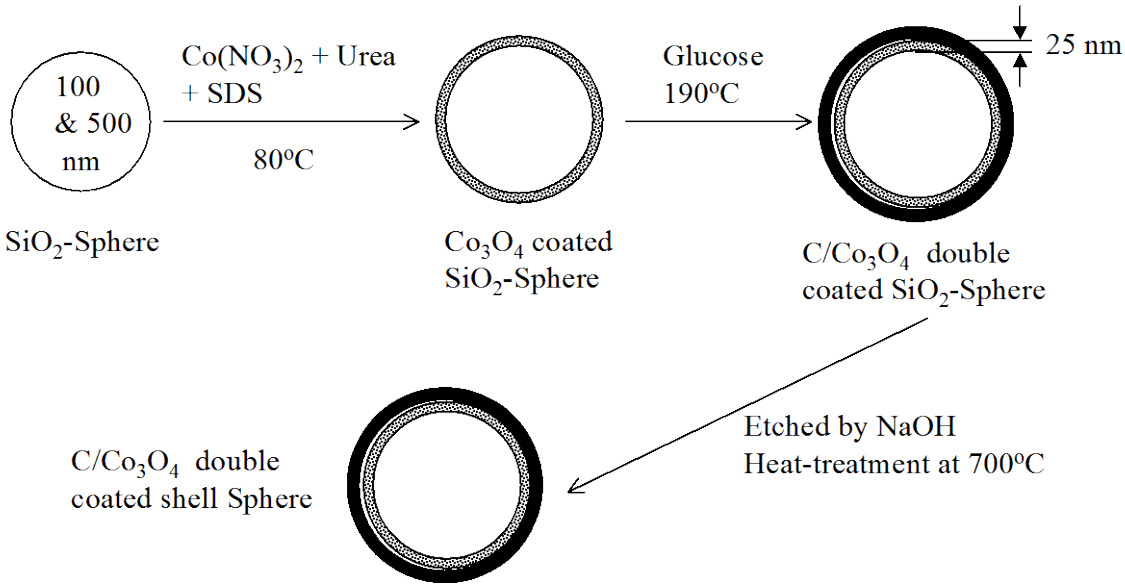

Figure 1. Synthetic scheme of nano-clusters of Co_3O_4 encapsulated in 200 & 500 nm elastic hollow carbon spheres.

2.1.1 Synthesis of the spherical monodispersed SiO_2, silica-NS template

SiO_2 spheres were freshly synthesized according to the method of Bogush et al. [2] using tetraethyl orthosilicate (TEOS) which will be hydrolyzed in a water/ethanol medium with NH_3 as the catalyst. The procedure involved preparation of "seed particles" of smaller dimension followed by growing them to a particular size by sequential addition of the two reactants, TEOS and H_2O, at a 1:2 ratio. A reaction time of 8 to 12 hours was observed between additions. An Excel spreadsheet modeling the entire seeding and growth sequences was key to our experimental design. Two such spreadsheets for 180 nm and 500 nm silica-NS, respectively, are shown in Figs. 2 and 3.

2) G.H. Bogush, M.A. Tracy, and C.F. Zukoski IV, *J. non-cryst. Solids*, **104**, 95 (1988).

Table 1. Program schedule for Program Tasks

	Months after beginning of program																			
	1	2	3	4	5	6	7	8	9	10	11	12	13	14	15	16	17	18	19	20	21
Task 1	Preparation of the Hollow Carbon Sphere-Material																				
Task 2				Anchoring of ion Conductive Brushes on carbon																	
Task 3							Li/O_2 Cell Fabrication														
Task 4												Performance Demonstration of Li/O_2 Cells									
Task 5																Analysis of Performance					
Reports	1	2	3	4	5	6	7	8	9	10	11	12	13	14	15	16	17	18	Final Report		

Milestones & Deliverables

Milestone 1: All nanocatalyst containing carbon will have synthesized - month 5

Milestone 2: Successful methodology to introduce surface functionalities on carbon will have been worked out – month 8

Milestone 3: cathode structures suitable for fabricating Li-air cells will have been completed – month 11

Milestone 4: High specific energy Li-Air cell will have demonstrated – month 17

Deliverable 1: Li-Air cells based on cathodes containing nanocatalysts ready for evaluation at AFRL – month 18

1		**Correlation of SiO_2 Particle Size to Initial Reagent Concentration**							
2									
3	***Materials***								
4			Mol. Wt.	Density	Molarity	Assay			
5			g/mol	g/ml	mol/l	w%			
6	Ammonia conc. Aq.		17.031	0.88	15.04	29.03	(NH_3)		
7	Ammonia (EtOH.)		17.031	0.766	4.28	9.512	(NH_3)		
8	TEOS		208.33	0.934	-	-			
9	Water		18.016	0.996	-	-			
10	Ethanol		46.07	0.790	-	-			
11									
12	***Estimated size of seed particles***								
13	Concentration of NH_3, (mol/l), $[NH_3]$ =						1.082		
14	Total water content, (mol/l), H_2O =						1.747		
15	Concentration of TEOS, (mol/l), [TEOS] =						0.091		
16									
17	Constant "A" = $[TEOS]^{1/2}$ (82+ 151$[NH_3]$ + 1200 $[NH_3]^2$ - 366 $[NH_3]^3$)								
18						A =	357.96		
19	Constant "B" = 1.05 + 0.523$[NH_3]$ - 0.128$[NH_3]^2$								
20						B =	1.47		
21	Particle size d, nm =A$[H_2O]^2$ exp(-B$[H_2O]^{1/2}$)								
22						d =	157		
23									
24	***Pot composition***								
25				*Weight*	*Volume*	*Molarity*			
26				*g*	*ml*	*mol/l*			
27	EtOH-NH_3:			153.30	200.0	-			
28	Ammonia, (NH_3):			14.58	-	1.082			
29	Water added			24.90	25.00	1.747			
30	TEOS:			14.94	16.00	0.091			
31	Ethanol from (EtOH-NH_3):			138.72	-				
32	Ethanol added			434.5	550.0				
33									
34			Total	627.64	791.03				
35									
36	***SiO_2 nano-sphere yield:***								
37									
38	TEOS one mole reacting with H_2O two moles produces SiO_2 one mole								
39	SiO_2 molecular weight, (g/mol) =				60.08				
40	Expected SiO_2 yield, (g) =				4.31				
41	W% of SiO_2 in the reaction mix, (%) =				0.69				
42									
43	***Seeded Growth Process:***								
44									
45	Equation : $d = d_o (V/V_o)^{1/3}$.....[1]								
46	Where, d and d_o are the new and seed particle sizes respectively								
47	V and Vo are the intial volume and the total volume of TEOS added (sequentially) to the pot								
48	Initial volume of TEOS, (ml) =				16.0				
49	Initial SiO_2 seed particle size, (nm) =				157.36				
50	Additional volume of conc. Ammonia added in each step, ml =						2.21	ml	
51	(Ammonia added will be about 1/20 of the initial concentration making up for any loss)								
52	Additional Water added with ammonia =				1.4	g			
53	*Addition Step #*		*TEOS*	*TEOS-total*	*Water*	*Water-total*	*SiO_2 size*	*SiO_2 yield*	*SiO_2 in pot*
54			*ml*	*ml*	*ml*	*ml*	*nm*	*g*	w%
55									
56	1		20.0	36.0	1.86	28.2	206	9.7	1.5
57	2		20.0	56.0	1.86	31.5	260	15.1	2.3
58	3		20.0	76.0	1.86	34.7	282	20.5	3.2
59	4		20.0	96.0	1.86	38.0	301	25.9	4.0
60	5		20.0	116.0	1.86	41.2	318	31.2	4.8
61	6		20.0	136.0	1.86	44.5	333	36.6	5.6
62									
63	(TEOS and water added corresponds to 1:2 molar ratio in each step)								

Fig 2. Spreadsheet-based experimental plan utilizing the seeded growth technique to prepare silica-NS of a particular size 180 nm.

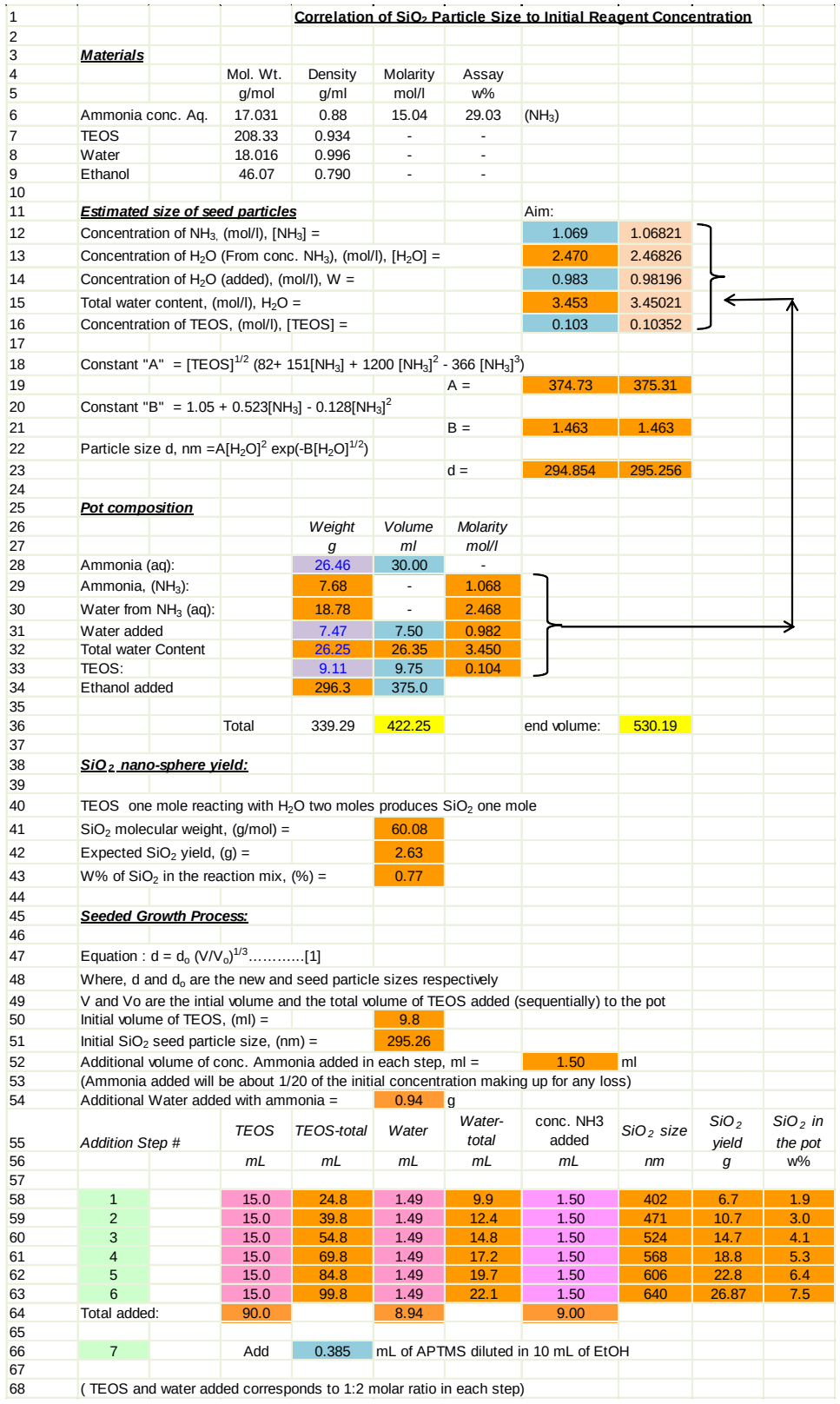

1				**Correlation of SiO_2 Particle Size to Initial Reagent Concentration**						
2										
3	***Materials***									
4			Mol. Wt.	Density	Molarity	Assay				
5			g/mol	g/ml	mol/l	w%				
6	Ammonia conc. Aq.		17.031	0.88	15.04	29.03	(NH_3)			
7	TEOS		208.33	0.934	-	-				
8	Water		18.016	0.996	-	-				
9	Ethanol		46.07	0.790	-	-				
10										
11	***Estimated size of seed particles***						Aim:			
12	Concentration of NH_3, (mol/l), [NH_3] =						1.069	1.06821		
13	Concentration of H_2O (From conc. NH_3), (mol/l), [H_2O] =						2.470	2.46826		
14	Concentration of H_2O (added), (mol/l), W =						0.983	0.98196		
15	Total water content, (mol/l), H_2O =						3.453	3.45021		
16	Concentration of TEOS, (mol/l), [TEOS] =						0.103	0.10352		
17										
18	Constant "A" = $[TEOS]^{1/2}$ (82+ 151[NH_3] + 1200 $[NH_3]^2$ - 366 $[NH_3]^3$)									
19						A =	374.73	375.31		
20	Constant "B" = 1.05 + 0.523[NH_3] - 0.128$[NH_3]^2$									
21						B =	1.463	1.463		
22	Particle size d, nm =A$[H_2O]^2$ exp(-B$[H_2O]^{1/2}$)									
23						d =	294.854	295.256		
24										
25	***Pot composition***									
26				*Weight*	*Volume*	*Molarity*				
27				*g*	*ml*	*mol/l*				
28	Ammonia (aq):			26.46	30.00	-				
29	Ammonia, (NH_3):			7.68	-	1.068				
30	Water from NH_3 (aq):			18.78	-	2.468				
31	Water added			7.47	7.50	0.982				
32	Total water Content			26.25	26.35	3.450				
33	TEOS:			9.11	9.75	0.104				
34	Ethanol added			296.3	375.0					
35										
36			Total	339.29	422.25		end volume:	530.19		
37										
38	***SiO_2 nano-sphere yield:***									
39										
40	TEOS one mole reacting with H_2O two moles produces SiO_2 one mole									
41	SiO_2 molecular weight, (g/mol) =				60.08					
42	Expected SiO_2 yield, (g) =				2.63					
43	W% of SiO_2 in the reaction mix, (%) =				0.77					
44										
45	***Seeded Growth Process:***									
46										
47	Equation : $d = d_o (V/V_o)^{1/3}$.....[1]									
48	Where, d and d_o are the new and seed particle sizes respectively									
49	V and Vo are the intial volume and the total volume of TEOS added (sequentially) to the pot									
50	Initial volume of TEOS, (ml) =				9.8					
51	Initial SiO_2 seed particle size, (nm) =				295.26					
52	Additional volume of conc. Ammonia added in each step, ml =						1.50	ml		
53	(Ammonia added will be about 1/20 of the initial concentration making up for any loss)									
54	Additional Water added with ammonia =				0.94	g				
55	*Addition Step #*		*TEOS*	*TEOS-total*	*Water*	*Water-total*	conc. NH3 added	*SiO_2 size*	*SiO_2 yield*	*SiO_2 in the pot*
56			*mL*	*mL*	*mL*	*mL*	*mL*	*nm*	*g*	w%
57										
58	1		15.0	24.8	1.49	9.9	1.50	402	6.7	1.9
59	2		15.0	39.8	1.49	12.4	1.50	471	10.7	3.0
60	3		15.0	54.8	1.49	14.8	1.50	524	14.7	4.1
61	4		15.0	69.8	1.49	17.2	1.50	568	18.8	5.3
62	5		15.0	84.8	1.49	19.7	1.50	606	22.8	6.4
63	6		15.0	99.8	1.49	22.1	1.50	640	26.87	7.5
64	Total added:		90.0		8.94		9.00			
65										
66	7		Add	0.385	mL of APTMS diluted in 10 mL of EtOH					
67										
68	(TEOS and water added corresponds to 1:2 molar ratio in each step)									

Fig 3. Spreadsheet-based experimental plan utilizing the seeded growth technique to prepare silica-NS of a particular size 500 nm.

As indicated in Fig.3, seed particles of about 300 nm (theoretically) are grown to 640 nm (theoretically) in six steps. In practice this preparation affords a monodispersed product with a particle size closer to 500 nm. As a result, several iterations were required to determine the exact number of growth steps to arrive at the desired particle size at the end. In the preparation of 500 nm particles, the seed particles were prepared at 25^{o}C from a solution with the following composition: 9.7 ml tetraethyl orthosilicate, TEOS (Alfa): 30.0 ml 29 wt% conc. ammonia (Aldrich):7.5 ml H_2O:375 ml abs. ethanol (Alfa). All reagents except TEOS were added to ethanol and stirred for 0.5 hour before TEOS was mixed in. Then the solution was stirred for another 6 hours in order to establish the seed population. During the growth stage, TEOS and water were added at the 1:2 mole ratio in the amounts shown in Fig.3 into the seed suspension prepared above. Additions were repeated at 8-16h intervals. The product was recovered by centrifugation. The particles were evaluated for their shape and size under SEM. The same methodology was used in the preparation of silica-NS of 180 nm. In this case, the theoretical target at the end of the three-step growth process was 333 nm (Fig. 2). The discrepancy between the theoretical target sizes shown in Fig 2 and 3 and the actual sizes reflects the uncertainties in the rate equations pertaining to the growth of silica-NS via hydrolysis of TEOS.

2.1.2 Coating of silica-NS with the cobalt catalyst

Several published procedures described below were attempted to coat silica-NS with the cobalt catalyst layer. These procedures involved precipitation of cobalt as hydroxide from a solution of the nitrate salt under controlled conditions.

Method 1.- A procedure reported by Li et al. [3] using the cobalt acetylacetonate complex [$Co(acac)_2$] in hexadecaylamine (HDA) as the solvent was used. Cobalt(III) acetylacetonate, 0.356 g (1 mmol), was taken in a 100 ml round bottomed flask equipped with a stirrer. The material was dissolved in hexadecyl amine (30.0 g, 0.3 mol) (Aldrich). The reaction was heated at 240^{o}C for 3 hours. The reaction mixture, which was initially pink, turned to purple and slowly became dark green. Silica-NS (1g) was added into the reactor, which was heated at 260^{o}C for 1 hour. The dark green reaction product was brought to room temperature, dissolved in methylene chloride and centrifuged several times to wash off all the hexadecyl amine. The product was air dried at 80^{o}C for two days.

Method 2.- Silica-NS of 500 nm (2.5 g) were suspended in a solution of $Co(NO_3)_2 \cdot 6H_2O$ (2.73 g , 9.3 mmol) and cetyl triethyl ammonium bromide (CTAB) (0.68, 1.9 mmol) in 50 ml of deionized water. After stirring for 20 minutes, triethylamine (TEA) (1.12 g, 18.6 mmol) was rapidly added into the above solution under vigorous stirring. The mixture was allowed to stir at that temperature for overnight, and the suspension was isolated by centrifuging. The solid product was washed twice with deionized water and finally was suspended in pure ethanol. The product was evaluated by SEM.

Method 3.- Silica-NS of 500 nm (1.0 g) were suspended in a solution of $Co(NO_3)_2 \cdot 6H_2O$ (1.5 g, 0.02M) and urea (9.0 g, 0.6M) in 250 ml of 37.5 vol% aqueous ethanol. The suspension was heated at 190-210 ^{o}C in a stainless steel autoclave for 18 hours.

3) Y. Li, M. Afzaal, and P. O'Brian, *J. Mater. Chem.,* **16**, 2175 (2006).

The resulting suspension was isolated by centrifugation and washed three times with water and once with ethanol. The product was evaluated by SEM.

Method 4.- A procedure reported by Narayan et al. [4] was adopted. A solution of cobalt nitrate, (0.69g, 2.4 mmol), sodium dodecyl sulphate, (SDS) (1.36 g, 4.7 mmol), and urea, (4.249 g, 0.071 mol), (molar ratios of 1 : 2 : 30 respectively) were taken in a 1L round bottomed flask. Total volume was adjusted to ~500 ml by adding DI water before stirring the mixture for 60 minutes at 40^{o}C. Into this clear solution was added Silica-NS 500nm (10.0 g) which was suspended in ~25-50 ml DI water and the pH adjusted to 6.5 with 5.8M acetic acid. The temperature was immediately raised to 105^{o}C and the reactor was allowed to stir overnight during which the color turned from pink to crimson. After cooling, the $Co(OH)_2$ coated product was centrifuged and washed with deionized water (20ml x 10 times). The product was allowed to remain as a suspension in water and was used immediately to coat with the carbon prepolymer (section 2.1.4. below). The product was evaluated by SEM.

2.1.3 Modification of the silica-NS with $–NH_2$ surface functionality

Modification of the silica-NS surface with amine groups was necessary in order to assure the deposition of a uniform coating of cobalt hydroxide. These groups could be conveniently introduced by a simple modification to the growth process typically used to synthesize silica-NS. It involved injecting the reactor with 3-propylaminotrimethoxysilane (APTMS) after the last regular growth step was completed. A quantity of APTMS sufficient to produce about 5 monolayers of hydrolyzed/condensed aminosilane was used for this purpose as shown in Figs. 2 and 3. The amine-modified product was isolated and cleaned by repeated centrifuging and re-dispersion in denatured ethanol. The product was evaluated by SEM and FT-IR.

2.1.4 Hydrothermal synthesis of carbon from D-glucose

Carbon prepolymer coatings were conveniently deposited following a procedure reported by Wan et. al. [5] which involved the decomposition of a dilute glucose solution under hydrothermal conditions. A Solution of glucose 2.0 g (~10 mmol) in 100 ml water was heated in an autoclave at 190^{o}C for 18 hours. The resulting dark-brown suspension was centrifuged to recover the carbon prepolymer as a dark brown powder, which was washed with deionized water and ethanol before drying at 125^{o}C . The same procedure was adopted to obtain a thin coating of the carbon prepolymer on the cobalt hydroxide coated silica-NS as well. Cobalt hydroxide coated silica-NS (the product of the cobalt hydroxide deposition step using 10.0 g Silica-NS 500nm) was dispersed in 800 ml of water containing 9.6 g of dissolved glucose. The mixture was heated in an autoclave at 190^{o}C for 18 hours. The product was isolated by filtration and washed three times with water and once with ethanol before drying at 125^{o}C in air. The dried prepolymer coating was carbonized by heating at 700^{o}C in a slow stream of argon which had flowed through Cu turnings at 450^{o}C to remove traces of oxygen. The product was evaluated by SEM.

4) R.V. Narayan, V. Kanniah, and A. Dhathathreyan, *J. Chem. Sci.,* **118**, 179 (2006).
5) W-M Zhang, J-S Hu, Y-G Guo, S-F Zheng, L-S Zhong, W-G Song, and L-J Wan, *Adv. Mater.* **20**, 1160 (2008).

2.1.5 Removal of silica core from carbon coated silica-NS/$Co(OH)_2$

Method 1.- The dual shell product consisting of the silica-NS core and cobalt hydroxide and carbon shells was treated with 2% HF for 2 hours in order to etch away the silica core.

Method 2.- The silica-NS core/cobalt hydroxide /carbon dual shell product was treated with 60 ml of 2M NaOH for two days at 45°C. The product was dispersed in 0.2% aqueous ammonia in 45 ml centrifuge tubes in order for the remaining NaOH and silicates to leach out of the product. Leaching continued for 24 hours with occasional shaking. Afterwards, the suspension was mildly centrifuged to recover the product. The leaching and recovery process was repeated three times followed by a final wash in deionized water. The product was then isolated and dried in an oven at 125°C. The dried product was heat treated at 700°C in a furnace under a flow of oxygen-free argon for four hours.

2.2 Anchoring of the Cation and the Anion Conductive Ionic Brushes

Task 2 of the work plan involved derivatization of the carbon surface of the cobalt-catalyst/carbon dual shell structure with groups that are of either ionic or have the ability to solvate ions. Some groups of interest are shown in Fig. 4.

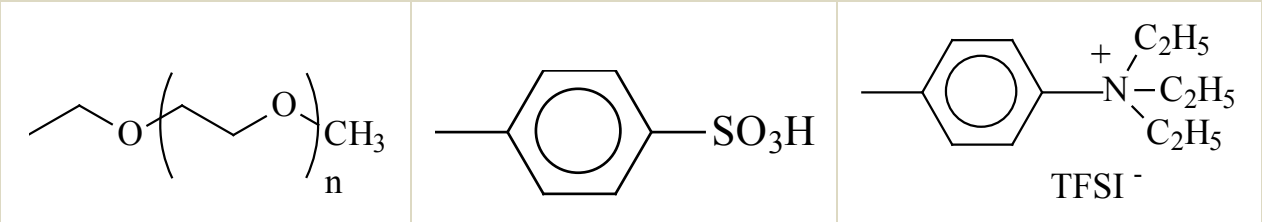

Figure 4. Groups suitable as Ionic brushes anchored to the carbon surface

In order to develop a workable procedure introduction of carboxyl, -COOH and sulfonyl, $-SO_3H$ to mixture of commercial carbons, XC-72 and P-2000 or glucose-derived carbon was undertaken.

2.2.1 General procedure for the surface derivatization of carbons with COOH

Using a modification of a literature procedure, carbon (1 g) was stirred with a solution of p-carboxyphenyldiazonium tetrafluoroborate (500 mg in 20 ml water) [6]. Hypophosphorous acid (50%, 20 ml) was then added. Bubbling was observed, indicating that the reaction was proceeding. The reaction mixture was stirred 30 minutes and then isolated by vacuum filtration using a fritted glass filter. The carbon was washed repeatedly with water (10 x 50 ml) to remove excess acid, followed by acetonitrile (5 x 30 ml). Finally, the carbon washed further by overnight Soxhlet extraction with CH_2Cl_2.

Synthesis of p-carboxyphenyldiazonium tetrafluoroborate.- p-Aminobenzoic acid (13.71g, 0.10 mol) was dissolved in 180 ml 2N HCl by heating to 60°C and stirring. The solution was then cooled to 0°C. Next, sodium nitrite (7.59g, 0.11 mol) was dissolved in 40 ml water and also cooled to 0°C. The nitrite solution was then added dropwise to the

6) P. Abiman, A. Crossley, G.G. Wildgoose, J.H. Jones, and R.G. Compton, *Langmuir* **23**, 7847 (2007).

p-aminobenzoic acid solution over 20 min. The cloudy solution turned to clear yellow during the addition, as the diazonium salt formed. Sodium tetrafluoroborate (14.8 g, 0.13 mol) was then added in small portions, and the reaction mixture was concentrated to ~50% volume by evaporation under vacuum. The resulting white crystals were isolated by vacuum filtration and washed with ice cold ether. Yield: 10.26 g (44 %). Several variations of this procedure were performed in which the amount of hypophosphorous acid was varied (from stoichiometric to excess), sodium hypophosphite was used in place of the acid, and the reaction was performed in the absence of acid.

2.2.2 General procedure for the surface derivatization of carbons with SO_3H

This procedure was similar to that described above for COOH functionalization, except that sulfoxyphenyldiazonium chloride was used in place of carboxyphenyldiazonium tetrafluoroborate, as mentioned above.

Synthesis of sulfoxyphenyldiazonium Chloride.- Attempts to prepare sulfoxyphenyl-diazonium tetrafluoroborate from sulfanilic acid and tetrafluoroboric acid (following literature procedures) was unsuccessful due to the very low solubility of the starting material in the HBF_4. However, a reaction in which the sulfanilic acid was first stirred with sodium carbonate followed by addition of sodium nitrite and then tetrafluoroboric acid did afford a salt which could be isolated, although this was very difficult due to the products high solubility in water. We successfully modified this procedure so that the chloride salt could be isolated. Here, sodium carbonate (3.00g, 28.31 mmol) was first dissolved in 25 ml water. Sulfanilic acid (1.00 g, 5.77 mmol) was then added and the solution was heated with stirring at 80^{o}C for 20 min. The solution was then cooled to room temperature and sodium nitrite (0.400g, 5.80 mmol) was added while stirring. The solution was then cooled to 0^{o}C and concentrated HCl was added dropwise (4 ml). At this point, the pH of the mixture was ~5, and a yellow precipitate was isolated. However, IR analysis showed that this first crop was not a diazonium salt. While still at 0^{o}C, a further 2 ml HCl was added to the filtrate (total = 6mL, 72 mmol). A second precipitate, which was white was then isolated. IR showed the diazonium stretch at 2284 cm^{-1} and 1078 cm^{-1} due to sulfoxide, expected for the product. The yield was 0.324g, 27%. The product was stored under vacuum at 4^{o}C over P_2O_5.

2.2.3 Assessment of -COOH and $–SO_3H$ surface groups on carbon

Carboxylic and sulfonic acid groups anchored to the carbon surface were quantitatively assessed by using a back-titration method. The carbon sample (0.1-1 g) was mixed with 0.01N NaOH (30 ml, standardized by titration against 0.1M HCl) in a sealed tube and shaken for 15 minutes. The sample was vortexed briefly at 5 minute intervals to ensure efficient mixing. The mixture was then rapidly filtered through a fritted glass funnel and 25 ml of the filtrate was titrated vs. standard 0.01 N HCl. The pH was monitored while stirring using a pH meter and ph 7.0 was taken as the end point [7].

7) Phenolphthalein was used initially in some titrations involving unreacted carbon. However, in most cases the filtrate was quite dark, rendering phenolphthalein unusable. However, good correlation was obtained between results obtained with phenolphthalein and those using the pH meter.

2.3 Li/O_2 Cell Fabrication

Li/O_2 prototype cells consisted of three key components, the anode, electrolyte, and the cathode. The anode typically consisted of a thin lithium foil. The electrolyte and the cathode development were the key objectives of this task.

2.3.1 Electrolytes for Li/O_2 prototype cells

The electrolyte consisted of a mixture of lithium salts dissolved in a mixed solvent. Varies solvents and lithium salts typically used in lithium batteries were evaluated in prototype Li/O_2 cells. Electrolyte compositions of interest are shown in Table 2. Mixed solvents were prepared from, Propylene carbonate (PC) (Grant), Ethylenecarbonate (EC) (Grant), Dimethoxy ethane (DME) (Aldrich), Diethylene glycol dimethyl ether (DEGME) (Aldrich), N,N Dimethyl acetamide (DMA) (Aldrich), and Dimethyl trifluoro acetamide (DMFA) (Oakwood).

Table 2. Electrolyte evaluated in Li/O_2 cells based on a commercial carbon mixture

Electrolyte	Composition
C1D1	PC 64.8 mol% / EC 27.8 mol% / Li-Imide 7.3 mol% / LiBOB 0.2 mol%
C1D2	PC 64.8 mol% / EC 27.8 mol% / LiPF6 7.3 mol% / LiBOB 0.2 mol%
C1D6	PC 64.8 mol% / EC 27.8 mol% / Li-Imide 7.1 mol% / LiBF4 0.4 mol%
C1D7	PC 64.8 mol% / EC 27.8 mol% / LiPF6 7.5 mol%
C2D1	PC 46.2 mol% / DME 46.2 mol% / Li-Imide 7.3 mol% / LiBOB 0.2 mol%
C3D1	PC 46.2 mol% / DEGME 46.2 mol% / Li-Imide 7.3 mol% / LiBOB 0.2 mol%
C4D1	PC 46.2 mol% / DMA 46.2 mol% / Li-Imide 7.3 mol% / LiBOB 0.2 mol%
C5D1	PC 46.2 mol% / DMFA 46.2 mol% / Li-Imide 7.3 mol% / LiBOB 0.2 mol%
C6D1	PC 46.2 mol% / MPC 46.2 mol% / Li-Imide 7.3 mol% / LiBOB 0.2 mol%
C7D1	MPC 30.8 mol% / DEGME 30.8 mol% /DMFA 30.8 / Li-Imide 7.3 mol% / LiBOB 0.2 mol%
C8D1	PC 30.8 mol% / DEGME 30.8 mol% /DMFA 30.8 / Li-Imide 7.3 mol% / LiBOB 0.2 mol%
C8D2	PC 30.8 mol% / DEGME 30.8 mol% /DMFA 30.8 / $LiPF_6$ 7.3 mol% / LiBOB 0.2 mol%
C8D3	PC 30.8 mol% / DEGME 30.8 mol% /DMFA 30.8 / $LiBF_4$ 7.3 mol% / LiBOB 0.2 mol%
C8D4	PC 30.8 mol% / DEGME 30.8 mol% /DMFA 30.8 / Li-Imide 7.5 mol%
C8D5	PC 30.8 mol% / DEGME 30.8 mol% /DMFA 30.8 / LiBOB 7.5 mol%
C8D7	PC 30.8 mol% / DEGME 30.8 mol% /DMFA 30.8 / $LiPF_6$ 7.5 mol%

All solvents were of vendor certified anhydrous quality and were stored over activated Linde 4Å molecular sieves before use. Methyl propyl carbonate (MPC) was synthesized

in-house and distilled before use. The mixed solvents were passed through an activated basic alumina column before used for electrolyte preparation.

Synthesis of the electrolyte solvent, methyl n-propyl carbonate (MPC).- The electrolyte co-solvent methyl n-propylcarbonate was prepared employing a one-pot reaction as described previously [8] and shown in Figure 5.

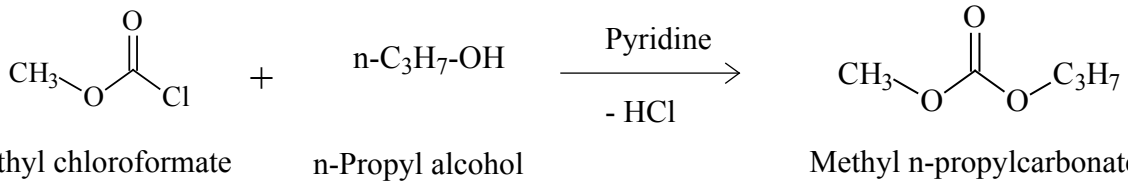

Figure. 5 Preparative scheme for the electrolyte co-solvent methyl n-propylcarbonate, MPC.

To a precursor mixture consisting of 1.1 mol (109.3g) methylchloroformate and 1.0 mol (60.3 g) n-propanol in 300 ml of anhydrous dichloroethane maintained at 0.0^{o}C in a 1 liter reactor, 1.1 mol (87.2 g) pyridine was introduced dropwise. After stirring overnight at the ambient temperature, the entire reaction mixture containing a white precipitate was transferred to a separatory funnel and washed three times with 150 ml aliquots of water. The organic phase that was retained in the funnel was shaken with sufficient 10% HCl until the aqueous layer pH was close to 2. The acidic aqueous layer was removed and the organic phase was washed three times with 50 ml aliquots of water. The organic phase was shaken thoroughly with 125 ml of saturated brine, separated and dried over anhydrous $MgSO_4$ for three hours. After removing the solvent using a rotary evaporator, the residual liquid was distilled at the ambient pressure. The middle portion distilled at ~135^{o}C was collected in a dry-ice cooled receiver in an argon atmosphere. The yield was ~52% of theoretical. The product was characterized by GC-MS, FT-IR and NMR.

Purification of the commercially available lithium bis(trifluoromethylsulfonyl)imide, $Li(CF_3SO_2)_2N$.- The salt was purified by a procedure reported in the patent literature [9]. The impure salt 100g (3M) was added with stirring to 300 ml anhydrous 1,4-dioxane (Aldrich) and stirred at room temperature for 5 minutes before heating to 80^{o}C under reflux until all the salt was dissolved. The solution was allowed to cool to room temperature and held for 12 hours before mixing with 100 ml of hexane. The white crystals that had separated were filtered and washed with 100 ml of a dioxane/hexane (4:1 volume) mixture. The product was dried under vacuum at room temperature followed by 140^{o}C for another 72 hours.

2.3.2 Cathode fabrication

Fabrication of cathodes typically involved 1) mixing of the carbon of interest with a conductivity additive (Carbon Black (Alfa Aesar)) or expanded graphite (Superior Graphite, grade #205-110) and a suitable polymeric binder (Teflon), making a paste or a

8) Y Ein-Eli, S. F. McDevitt, and R. Laura, *J. Electrochem. Soc.,* 1**45**, L1 (1998)
9) United States Patent, No. 6, 248, 883 to A. Grokovenko, and G. L. Soloveichik (2001).

slurry with a suitable solvent (50 vol% 2-propanol in DI water), application of the paste/slurry to a metallic support (Ni mesh (SN: 5-5/0 Exmet)), compaction of the composite layer under pressure, and, for composites with the Teflon binder, thermal curing, if necessary. Screening of the electrolytes, binders, and procedures were typically carried out using a 1:1 wt% mixture of commercial carbons, Black Pearls 2000 and Vulcan XC-72 (both from Cabot) and, to a limited extent, hydrothermally prepared carbon from glucose. The target carbon material, cobalt-catalyst encapsulated carbon shells, was used in more refined experiments. Polymeric binders of interest included emulsified Teflon (Fuel Cell Earth, 60 wt% in water), and mixtures of styrene butadiene latex (SBR, Euclid Chemical Company) and sodium carboxymethyl cellulose (CMC, Aldrich).

In a typical procedure the carbons were mixed together with the conductivity additive and the mixture was made into a paste with 50 vol% 2-propanol and the binder. The paste was then spread on a cleaned Ni mesh (SN: 5-5/0 Exmet) on both sides using a sandwich style template (125 µm) by the "Doctor Blade" method. Electrodes were then pressed at 18000 lbs for 20 seconds. In some instances, the electrodes with the Teflon binder was heat cured at 300°C for 15 minutes to melt the binder. The coated electrode strips were then dried under vacuum at 125°C and processed into 2.5 cm x 5 cm electrodes with 2.5 cm x 4 cm area of active material inside the argon-filled glove box (Vacuum Atmospheres). Slight modifications to this process were necessary to fabricate electrodes based on carbon nanoshells that were robust enough to be considered for Li/O_2 cells, as will be described later with the Results.

Preparation of the Co-phthalocyanine-catalyzed Commercial Carbon.- Carbon modified with cobalt phthalocyanine was prepared according to our reported procedure [10]. For example, 0.5 g of Co-phthalocyanine was dissolved in 30 ml of concentrated sulfuric acid. 4.75 g each of Vulcan XC-72 and Black Pearls 2000 carbon was slowly mixed into the solution while stirring manually until a smooth paste was obtained. Upon water addition to this paste the compound was precipitated on carbon. The product was filtered and washed thoroughly with water until the filtrate was neutral to pH paper. The washed product was dried in air at 100^{o}C and, finally heated at 800^{o}C for 5 hours under a flow of argon. This resulted in a carbon with a very coarse texture.

Coating commercial carbons with polyaniline-polystyrene sulfonic acid complex. - A previously published synthetic approach for polyaniline-polystyrene sulfonic acid complex [11] was carried out in the presence of a 50:50 mixture of Black Pearls 2000 and Vulcan XC in the reactor. The two carbons, five grams each, were dispersed in 125 deionized water containing 2 ml of methanol. Commercially available sodium polystyrene sulfonic acid (Aldrich, 30 weight%, 20000 mol. wt.) 2.6 ml (3.8 mmol) was added to the reactor. The reactor was chilled in an ice bath below 4^{o}C under stirring. Separately, a solution of 0.35 g aniline (Aldrich, 3.8 mmol) and 0.9 ml conc. HCl (Aldrich, 11 mmol) in 6 ml of DI-water was prepared and added to the reactor while stirring vigorously. A solution of 3.38 g ammonium persulfate, $(NH_4)_2S_2O_8$ (1.9 mmol) in 19 ml of DI-water was then added dropwise into the reactor. The reactor was allowed to

10) K. M. Abraham and Z. Jiang, *J. Electrochem. Soc*. **143**, 1 (1996)
11) S.Y. Park, M.S. Cho, "Synthesis and electrical characteristics of polyaniline nanopartcles and their polymeric composite", *Curr. Appl Phys.,* **4**, 581 (2004).

stir overnight in the ice bath before filtering and washing the coated product with DI-water until free of acid.

Preparation of the cobalt-doped polyaniline-polystyrene sulfonic acid complex,-

Polyaniline coated carbon (6.3 g) prepared above was dispersed in ~100 ml methanol under ultrasonication. Into it 0.270 g $CoCl_2$ in 50 ml of anhydrous methanol was added (2 weight% Co). The solvent was evaporated at 100^oC to obtain the Co-complexed material. Carbonization of a PANI coated mixture of carbons with and without complexed $CoCl_2$ was carried out at 700^oC under a flow of oxygen free carbon for 6 hours.

2.4 Performance Demonstration of Li/O_2 Cells

Li/O_2 prototype Configuration.- The test cells consisted of a Li foil (Foote Mineral, 0.025cm) anode, a polypropylene microporous membrane (Celgard 2400 or 3401), non-woven glass fiber mat separator soaked with the electrolyte, the carbon cathode and a woven polypropylene mesh as a gas distribution screen. This component package was contained between two polypropylene plates and held under compression by spring clamps. The cell assembly was placed in a polyethylene bag with inlet and outlet valves, filled with oxygen and sealed. All materials handling and processing prior to the final testing in air was performed in a dry argon filled glove box (Vacuum Atmospheres).

Test procedure.- The cells were discharged galvanostatically 1.2 V while maintaining a blanket of pure oxygen inside the cell. Total discharge time was generally between 40 and 70 hours. Some cells underwent a routine of repeated discharge at the same current density. In this case the cell was allowed to remain in open-circuit potential for 4 hours in order for the potential to stabilize followed by further discharge to 1.2 V. The procedure was repeated for 20 or more iterations with rest periods in between. Cell discharge was conducted at room temperature in dry oxygen.

3 RESULTS AND DISCUSSION

3.1 Synthesis of the Hollow Carbon Sphere-Material

We successfully executed the synthetic scheme sown in Fig.1 for the synthesis of the dual shell structure consisting of a Co_3O_4 inner shell and glucose derived carbon outer shell. The structures were built upon silica-NS templates with diameters approximately 200 and 500 nm.

3.1.1 Synthesis of the spherical monodispersed SiO_2, silica-NS template

The spreadsheet-based experimental approach is shown in Figs.2 and 3. It is based on the polynomial expressions developed by Bogush. et. al. [2] to fit the experimental observations in their seminal study on the synthesis of silica nanospheres. Accordingly,

$$d = A\,[H_2O]^2 \exp(-B[H_2O]^{1/2}), \quad (1)$$

with $A = [TEOS]^{1/2}(82 + 151[NH_3] + 1200[NH_3]^2 - 366[NH_3]^3$ and

$B = 1.05 + 0.523[NH_3] - 0.128[NH_3]^2$,

where, d is the average diameter in nanometers with reagents in molar concentrations. During seeded growth the size of the particles can be related to the total volume of TEOS added to the solution by a simple relation

$$d = d_o [V/V_o)^{1/3}), \quad (2)$$

where d is the average diameter of the target particles, d_o is the average diameter of the seed particles, V_o is the moles (or volume or weight) if TEOS used to produce the seed particles and V is the total moles of TEOS added to the solution (including V_o).

These empirical relations were used to generate the spreadsheet-based experimental plan shown in Figs. 2 and 3 to guide the synthesis of the monodispersed silica-NS of approximate diameters 180 and 500nm. The equations shown above are not exact and as a result many iterations were required to adjust the diameters predicted by the model to the actual size resulting from the synthesis. For example, a model predicting 333 nm silica-NS resulted in particles of approximately 180 nm. The predictions are better for large sizes, for example 640 nm predicted size resulting in approximately 500 nm silica-NS (Fig. 3).

The synthesis itself proved to be somewhat challenging initially in that proper cleaning of the glass reactor, purity of TEOS and, more importantly, preventing ammonia gas leaking out of the reactor during the week-long synthesis, appeared crucial for a successful outcome. These difficulties could be circumvented by cleaning the reactor thoroughly with aqua regia followed by etching with 2% HF prior to use, distilling the commercially available high purity TEOS, and using a septa-sealed reactor for the synthesis. Product of a synthesis obtained prior to observing these precautions is shown in Fig. 5.

Figure 6. SEM image of the product obtained with TEOS (Alfa Aesar 99.9% purity) following the seeded growth approach (Fig. 2).

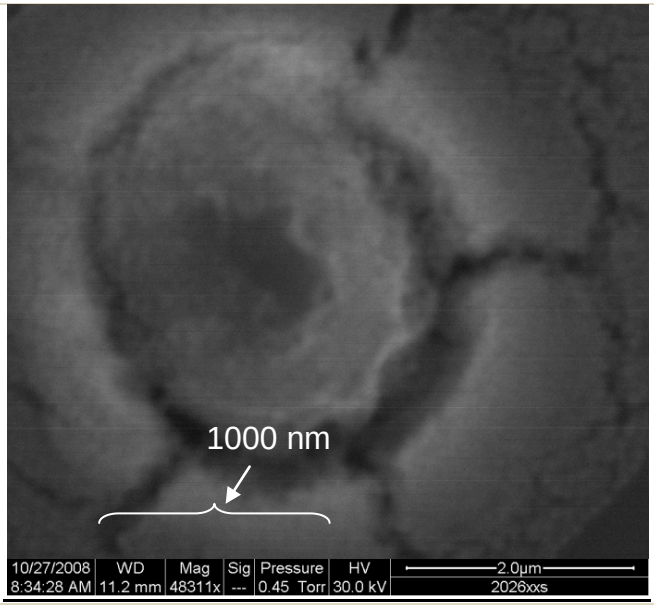

Once these precautions were observed the synthesis of Silica-NS became routine and consistent. We have succeeded in reaching a particle density of about 7.5% for 500 nm silica-NS without any appreciable polydispersity. SEM pictures for a typical batch are

shown in Fig. 6.

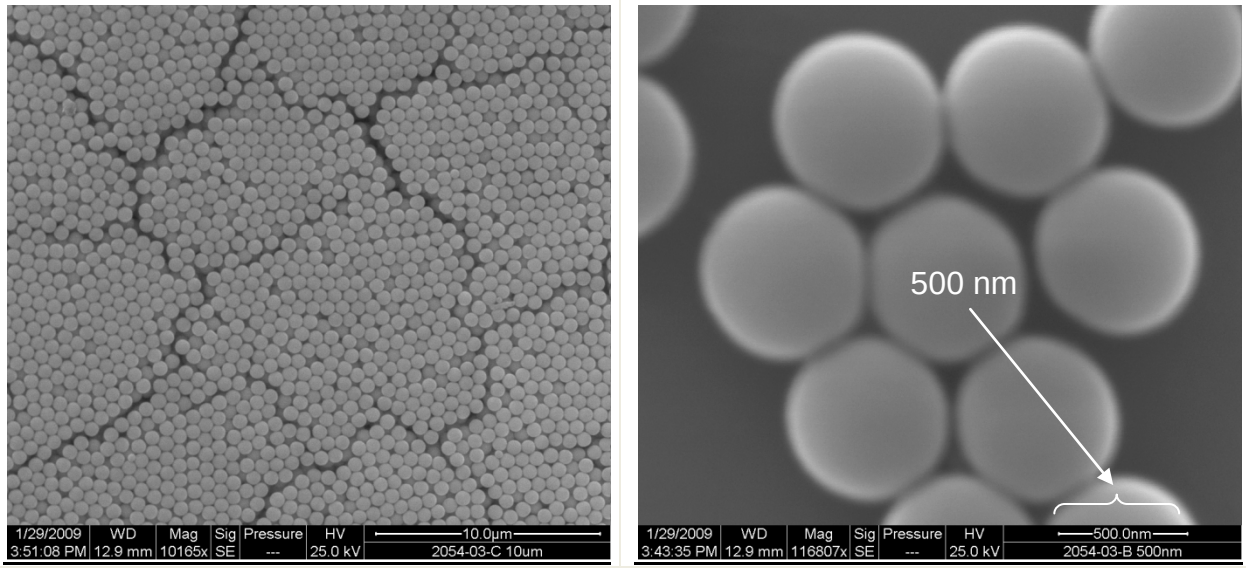

Figure 7. SEM image of the monodispersed silica nanospheres of ~500 nm synthesized using the seeded growth process which resulted in a particle concentration of 7.5 weight% in the reaction mix.

SEM pictures of silica-NS of approximately 180 nm size obtained using the spreadsheet in Fig 2 as the guide are shown in Fig. 8.

Figure 8. SEM image of the silica nanospheres obtained in a “single-step” preparative procedure.

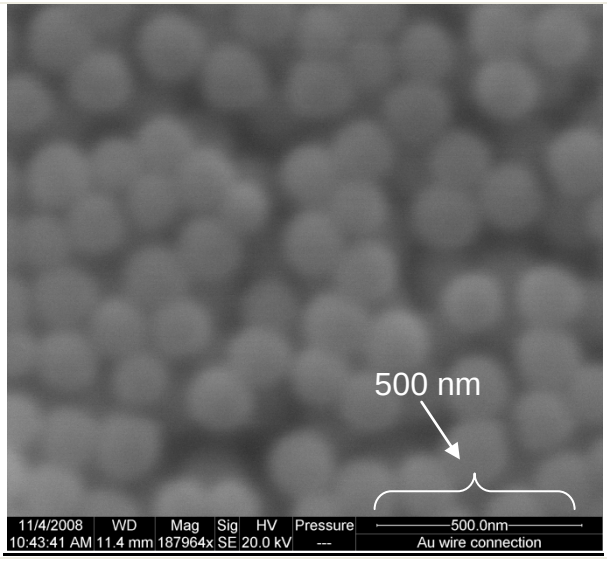

3.1.2 Coating of silica-NS with the cobalt catalyst

Precipitation of $Co(OH)_2$ in hexadecaylamine (HDA) medium.- Several procedures were attempted to coat silica-NS with the cobalt catalyst as described in the Experimental section. The first method, hydrolysis of the cobalt pentandionato complex

[$Co(acac)_2$], in hexadecaylamine (HDA) solvent was validated without silica-NS in the reaction medium. Formation of $Co(OH)_2$ was verified by the IR spectroscopic analysis of the product formed. The reaction was repeated with silica –NS of approximately 550 nm diameter present in the reaction medium. The objective was to determine whether a uniform coating of $Co(OH)_2$ would be possible over the surface of the suspended silica-NS. The product of the reaction was isolated and evaluated by TEM as shown in FIG. 9.

Figure 9. Transmission electron microscopic (TEM) image of the product obtained by the hydrolysis of the cobalt pentandionato complex [$Co(acac)_2$], in hexadecaylamine (HDA) solvent with ~550 nm silica-NS in the reaction medium.

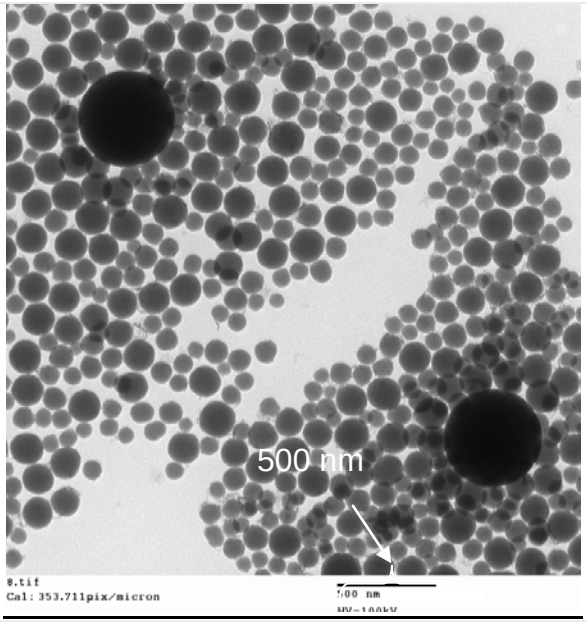

Fig. 9 clearly shows that the cobalt hydroxide precipitating in the medium has coalesced into spherical nano-particles of 20-~100 nm without depositing on the silica nanospheres. The silica-NS present in the image appears to be smooth and of the same dimensions as the original silica-NS. High resolution images further gave no evidence for any significant coverage of cobalt hydroxide over the silica-NS surface.

Figure 10. Transmission electron microscopic (TEM) image of the product obtained by the hydrolysis of the cobalt pentandionato complex [$Co(acac)_2$], in hexadecaylamine (HDA) solvent with ~550 nm silica-NS in the reaction medium.

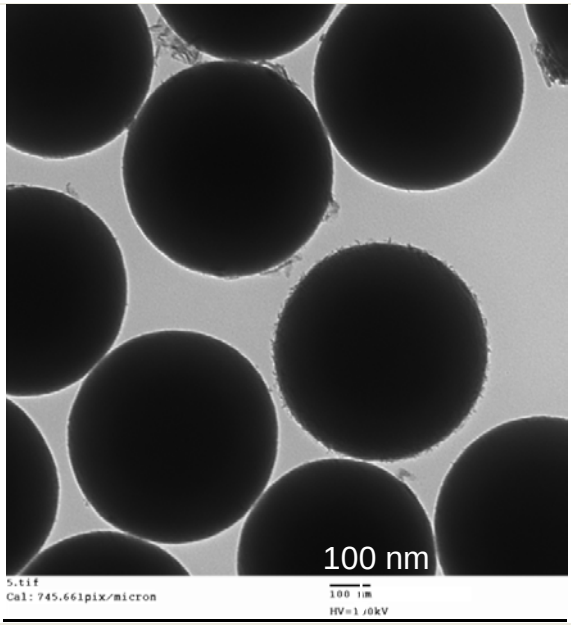

The same reaction was evaluated by lowering the starting concentration of the dissolved cobalt salt by nearly an order of magnitude that before. The TEM of the product shown in Fig. 10 provided no evidence for any appreciable coating of cobalt hydroxide over the silica-NS.

Cobalt hydroxide precipitated in the presence of cetyl triethyl ammonium bromide (CTAB).- the main attraction of this procedure was its simplicity and the relatively small amounts of chemicals, particularly the surfactant, used in the preparation. Surfactants, in general, make the post preparative cleaning of the product more challenging due to extensive frothing in aqueous solutions. As a result, less surfactant is preferred. Shown in Fig. 11 are the SEM images of the product.

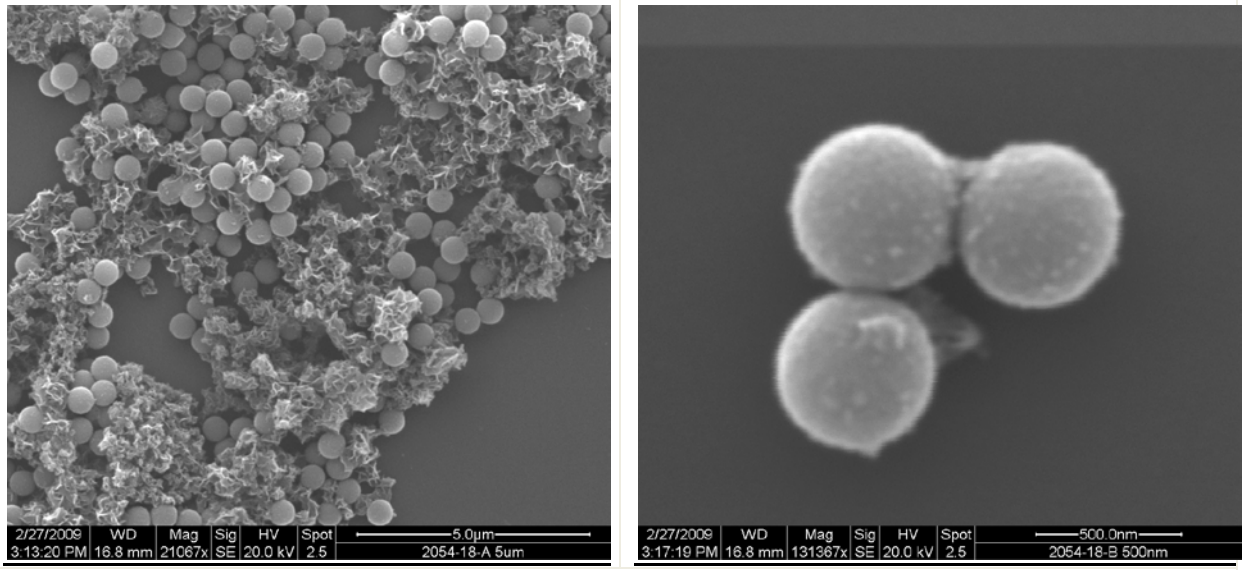

Figure 11. SEM images of monodispersed silica nanospheres of ~500 nm coated with cobalt hydroxide in the presence of the cetyl triethyl ammonium bromide (CTAB) surfactant. Low magnification image is on the left (scale bar = 5m) and the same high magnification image is on the left (scale bar = 500 nm).

Gross precipitation of the cobalt hydroxide is evident in the low magnification image of1. 10 (left). EDS analysis obtained for the broad area scan (Fig. 11-left) showed clear evidence for gross precipitation of cobalt hydroxide away from the silica-NS. The high magnification image on the right in Fig. 11, however, shows a slight hint of something coated on the surface. Although, it could be a thin coating of cobalt oxide it was not present in sufficient amounts to show up in the corresponding EDS spectrum. Therefore, the coating could contain relatively a small amount of cobalt oxide.

Cobalt hydroxide coated on silica nano-spheres under hydrothermal conditions.- The third procedure attempted to afford a coating of cobalt hydroxide over the silica-NS surface was the hydrolysis of a cobalt salt with urea under hydrothermal conditions. SEM views of the resulting product are shown Fig. 12. The high magnification SEM image on the right shows the heavily coated silica-NS have coalesced to form a continuous lumpy mass instead of individually coated nanospheres. We attempted strategies such as varying pH of the starting solution, cobalt salt concentration, and

incorporation of a non-ionic surfactant (P123) into the mixture etc. without success.

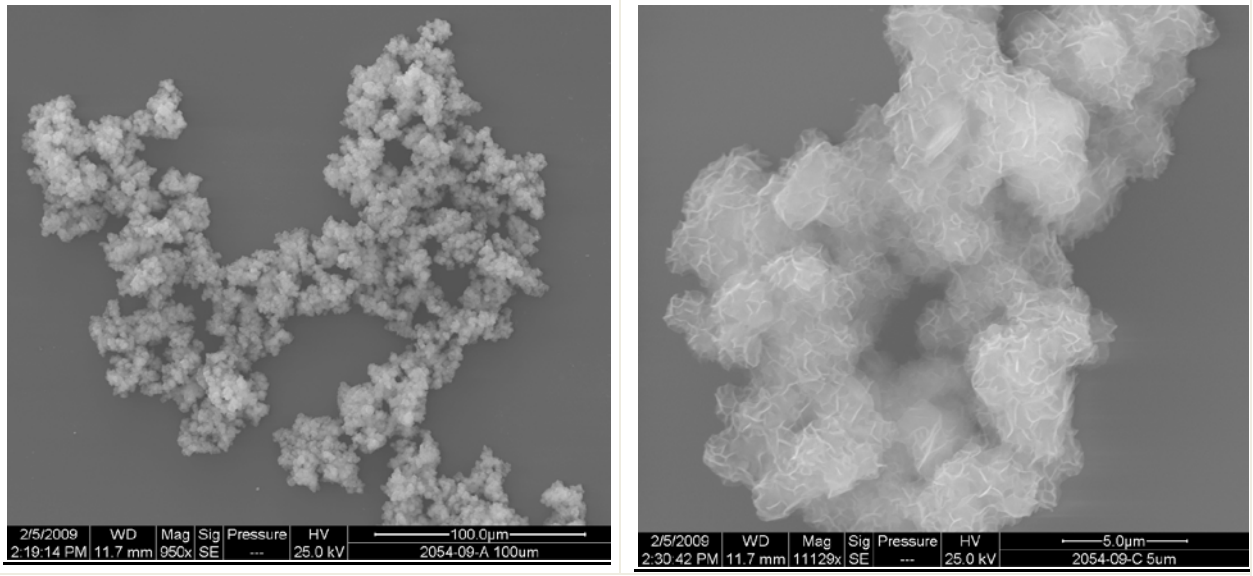

Figure 12. SEM image of the monodispersed silica nanospheres of ~500 nm coated with cobalt hydroxide under hydrothermal conditions. Low-resolution picture is on the left (scale bar = 100 □m) and the same high-resolution image is on the left (scale bar = 5 µm).

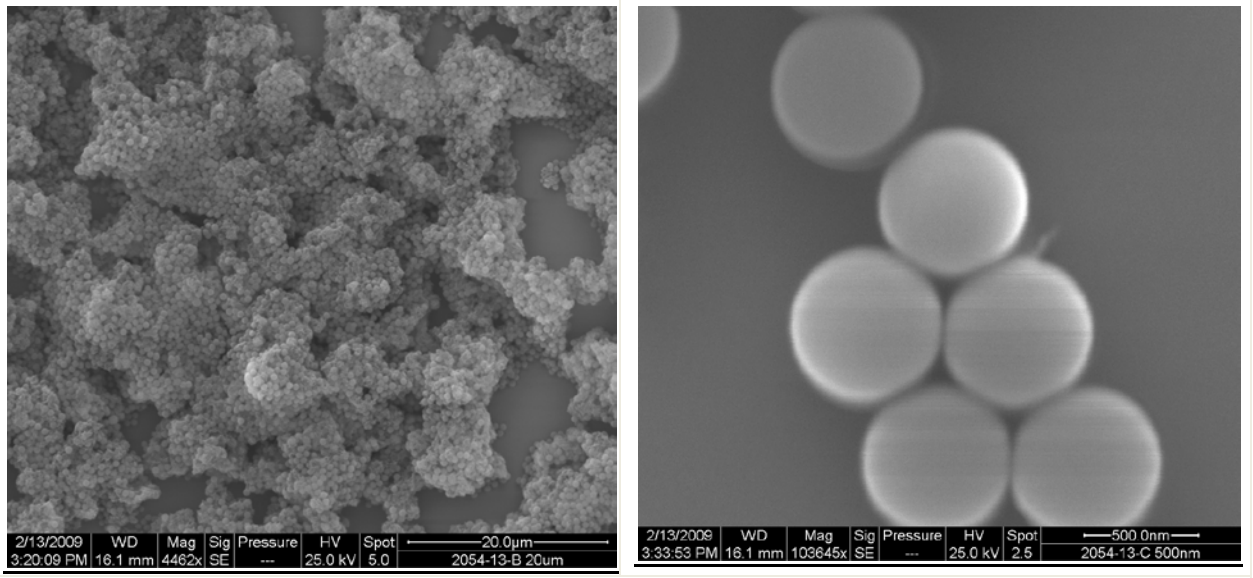

Figure 13. SEM image of the monodispersed silica nanospheres of ~500 nm coated with cobalt hydroxide using cobalt nitrate, sodium dodecyl sulphate (SDS), urea and deionized water taken in the molar ratios of 1 : 2 : 30 : 60. Low-resolution picture is on the left (scale bar = 20 µm) and the same high-resolution image is on the right (scale bar = 500 nm).

Cobalt hydroxide coated on silica nano-spheres in the presence of sodium dodecyl

sulphate (SDS) and urea.- We evaluated the procedure reported by Narayan et al. [4] on the preparation of Co_3O_4 nano-catalyst using cobalt nitrate, sodium dodecyl sulphate (SDS), urea and deionized water taken in the molar ratios of 1 : 2 : 30 : 60. We repeated the same reaction under two different conditions, a) reaction with as prepared silica nanospheres and b) reaction with silica nanospheres sensitized with $SnCl_2$.

Shown in Figs. 13 and 14 are the SEM images of the as prepared and Sn^{2+} sensitized silica nanospheres respectively after coating with cobalt hydroxide as mentioned above. We found no evidence for a cobalt hydroxide shell formed on as prepared silica nanospheres (Fig. 13) although, gross precipitation of cobalt hydroxide was clearly evident as confirmed by the corresponding broad area EDS scan.

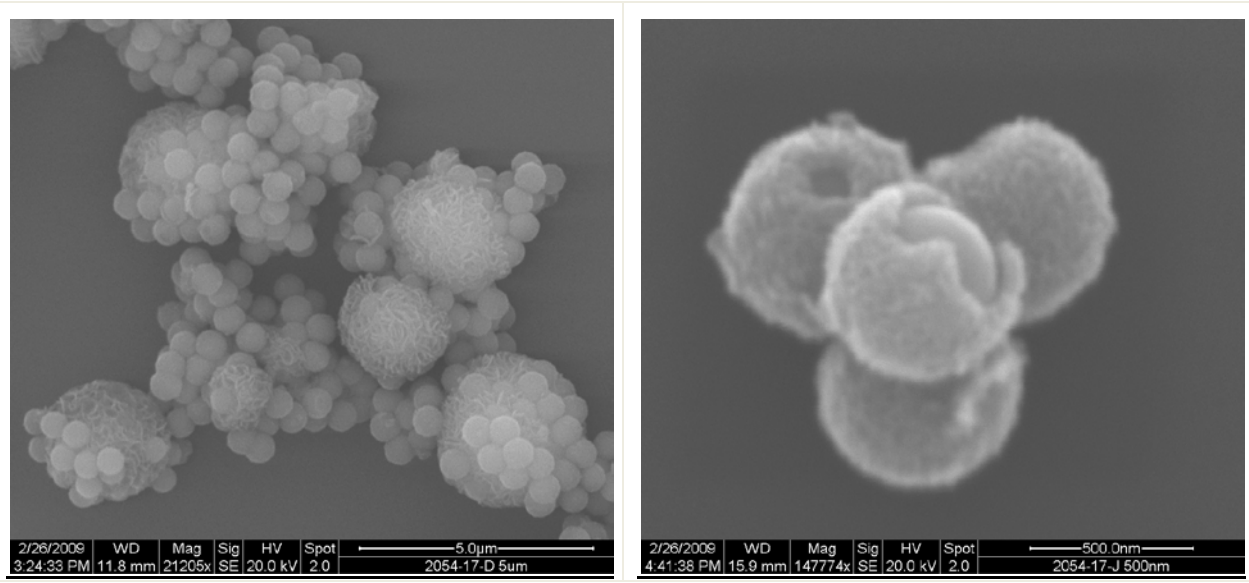

Figure 14. SEM image of the Sn^{2+} sensitized monodispersed silica nanospheres of ~500 nm coated with cobalt hydroxide as described under Fig. 12. Low-resolution picture is on the left (scale bar = 5 µm) and the same high-resolution image is on the left (scale bar = 500 nm).

On the other hand, we had ample evidence supporting the deposition of cobalt oxide on Sn^{2+} sensitized silica nanospheres under the same experimental conditions. The image shown in Fig. 14 in high magnification clearly shows the underlying silica nanosphere through the breached portion of the cobalt hydroxide shell. The latter appears to be loosely packed and has undergone damage during the post preparative washing of the product involving ultrasonic dispersion. The cobalt hydroxide coating appeared to be about 50 nm thick, although the amount of cobalt nitrate used in the preparation was only sufficient, in terms of Co_3O_4 density and total surface area of nanospheres, to form a 5 nm thick Co_3O_4 shell. The EDS spectra corresponding to the high magnification image of Fig. 14 confirms that the coating on the surface of silica nanospheres is indeed made of a cobalt-containing material.

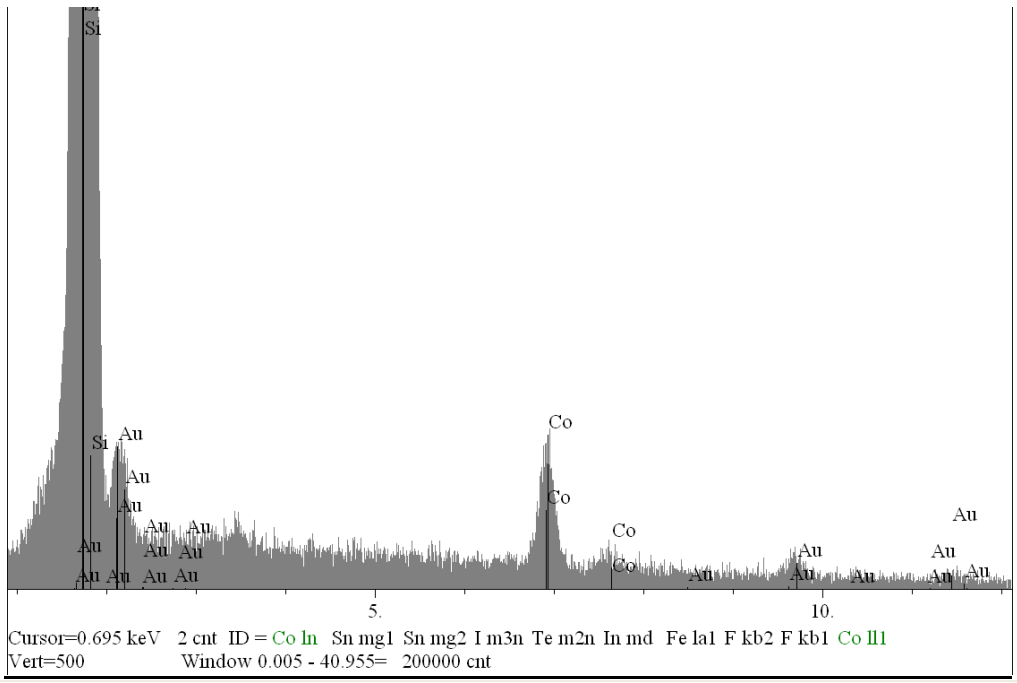

Figure 15. EDX analysis of the silica nanospheres corresponding to the high magnification image of silica nanospheres (Fig. 14-right) coated with the cobalt hydroxide shell.

One unsettling aspect of the result shown in4. 13 is the presence of large globules of cobalt hydroxide that has grown independent of the coating formed on the silica nanospheres. Despite the effectiveness of Sn^{2+} sensitization in forming a cobalt hydroxide shell on silica nanospheres, significant concentrations of Sn species could be observed in EDS scans for the coated products. Therefore, it was desirable to find another avenue to emulate the seeding-and-growth process of cobalt hydroxide on the surface of silica-NS without the use of Sn^{2+} sensitization.

Coatings of cobalt hydroxide on –NH_2-functionlaized silica nano-spheres.- Because of its ability to complex metal cations, –NH_2 groups anchored to the silica-NS surface were considered a possible alternative to Sn^{2+} sensitization. We successfully carried out the surface-functionalization of silica-NS with amine, -NH_2, groups by injecting 3-propylaminotrimethoxysilane (APTMS) into the same reactor once the seeded growth process to synthesize silica-NS was completed. Enough APTMS to grow approximately 5 molecular layers-thick shell of the condensed APTMS over fully grown silica-NS was used in this amine fictionalization-step. Seamless deposition of APTMS shell was evidenced in the SEM images of the product. Cobalt hydroxide deposition on these amine functionalized silica-NS was carried out using the procedure by Narayan et al. [4] as described previously. SEM images of the product are shown in Fig. 16.

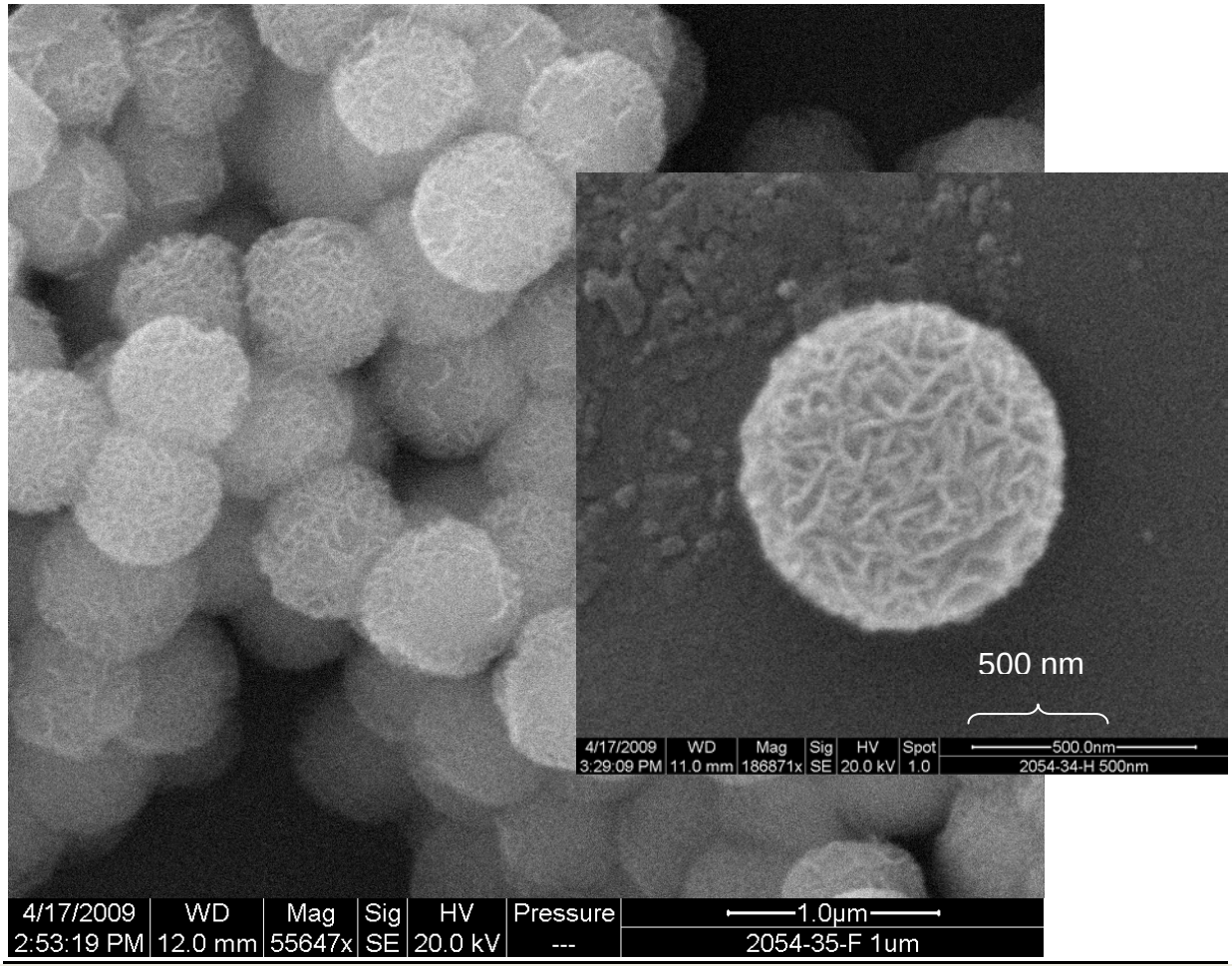

Figure 16. SEM images of amine-functionalized monodispersed silica-NS of ~500 nm coated with cobalt hydroxide by the reaction of cobalt nitrate, sodium dodecyl sulfate (SDS), urea and deionized water.

As shown in Fig. 16, the nanospheres appear to be uniformly coated with cobalt hydroxide which represents our first long-awaited success to prepare the fully coated material. Cobalt hydroxide appears to have deposited exclusively on the surface of the SiO_2 template as there was very little free cobalt hydroxide deposits evident while viewing the SEM. Amine-functionality present on the silica-NS appeared to have made this possible, as silica without the amine modification always resulted in significant amounts of cobalt hydroxide precipitated freely away from the template as described before. The cobalt hydroxide layer in Fig. 16 appears to possess a unique twine-like morphology with gullies between strands, possibly exposing the underlying silica core. This could have been to our advantage since, facile access to the silica core was essential later on when it was to be etched away after establishing the outer carbon shell. The coarse morphology of the deposit could also be advantageous considering its expected catalytic activity for oxygen reduction. Agitation of a dilute suspension of the product using a dip-type ultrasonic horn resulted in minimal damage to the cobalt oxide coating, suggesting that the coating was mechanically very robust.

Coating of the ~200 nm silica-NS with cobalt hydroxide.- Deposition of cobalt hydroxide shell over the ~200 nm silica-NS core was full of challenges. The same procedure outlined above for the 500 nm template was repeated after taking into account the difference in the surface areas of the two materials. Shown in Fig. 17 is a SEM view of the ~200 nm silica template coated with $Co(OH)_2$ equivalent to a nominal Co_2O_3 thickness of 3 nm (as done for the 500 nm silica-NS template).

Figure 17. SEM images of the ~200 nm silica template coated with $Co(OH)_2$ equivalent to a calculated thickness of 3 nm (same nominal thickness was used for 500 nm silica-NS).

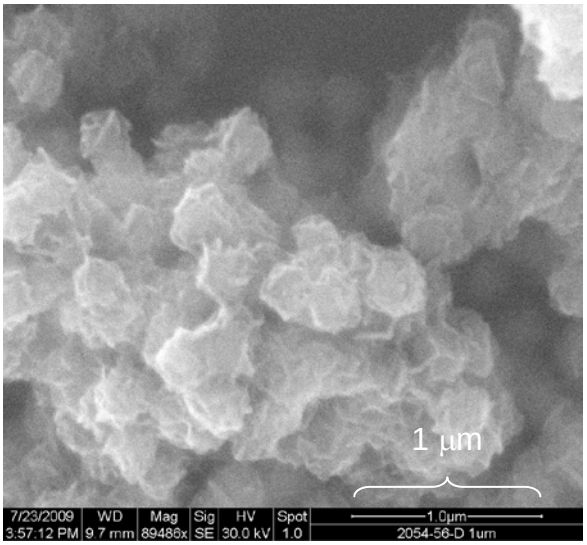

Obviously, $Co(OH)_2$ enough to provide a 3 nm-thick Co_2O_3 coating appeared to have led to a severely agglomerated product. Therefore, A more diluted reaction medium was evaluated as a potential solution to this problem. The SEM view of the $Co(OH)_2$-coated product resulting from the same amount of the cobalt precursor but at a concentration of half (diluted from 125 ml previously used , to 250 ml) is shown in Fig. 18.

Figure 18. SEM images of the ~200 nm silica template coated with the same amount $Co(OH)_2$ as the product shown in Fig. 17, but the reaction medium diluted by a factor of two.

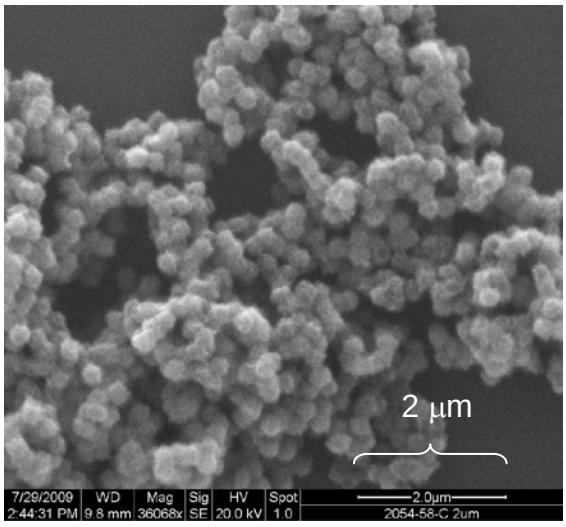

Although the resolution of Fig. 18 is only half as much as in Fig. 17, less severe agglomeration is evident in the latter. Further dilution of the reaction medium or reducing the concentration of the cobalt salt used in the reaction brought about only a

marginal improvement.

The recipes that were ultimately adopted for coating of ~200 and ~500 nm silica-NS with cobalt hydroxide are shown in Table 3. Two levels of cobalt loadings, from here on designated as 1X and 2X were developed for coating silica-NS of ~500 nm.

Table 3.Recipes developed for coating silica-NS with cobalt hydroxide.

	200-1X	500-1X	500-2X
Silica-NS, g	5.00	10.00	10.00
$Co(NO_3)_2.6H_2O$, g	0.34	0.69	1.37
SDS, g	0.68	1.36	2.72
Urea, g	2.13	4.25	8.50
Water (Total), ml	~500	~500	~500
Nominal CoO thickness, nm	0.2	0.5	1

3.1.3 Coating of cobalt oxide deposited silica nanospheres with glucose-derived carbon.-

Decomposition of glucose to carbon under hydrothermal conditions was examined. First, glucose was used alone to validate the hydrothermal decomposition process and to ensure the autoclave was functioning within its designed safety limits at the reaction temperature of 190^{o}C. Then, the same reaction was repeated in the presence of ~500 nm silica-NS coated with cobalt oxide to generate a carbon shell over the silica/cobalt oxide structure.

Figure 19. SEM images of carbon itself obtained in the hydrothermal decomposition of glucose at 190^{o}C.

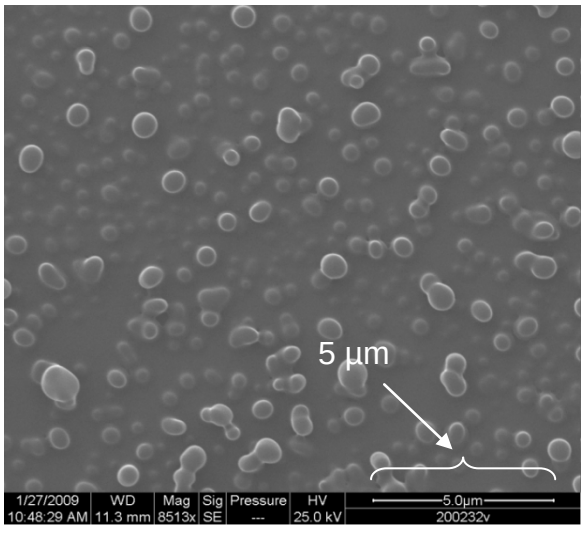

SEM image of the glucose-derived carbon is shown in Fig. 19. Carbon appeared as discrete particles agglomerated to much larger dimensions, on the order of 750 nm.

Figure 20. SEM images of carbon coated ~500 nm silica-NS/cobalt hydroxide core shell structure.

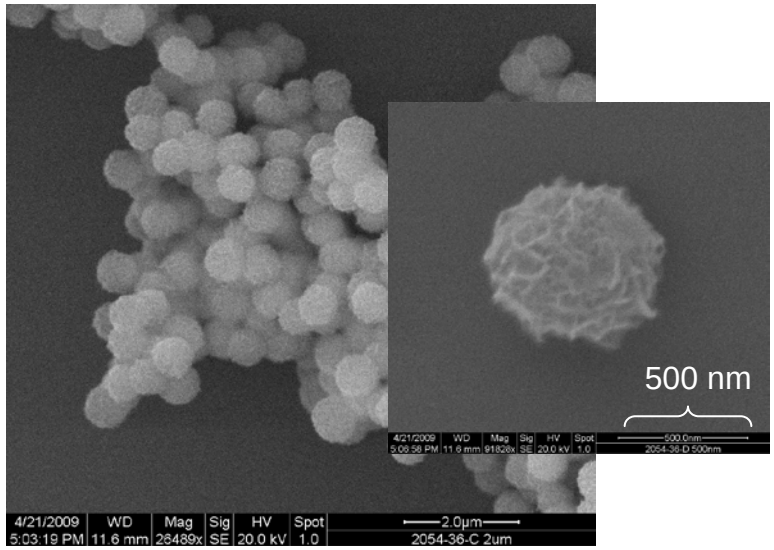

Surprisingly, when the same hydrothermal synthesis is carried out in the presence silica-NS coated with cobalt hydroxide in the reaction medium, the character of the carbon product has changed completely. Instead of forming isolated lumps carbon has deposited exclusively on the surface of silica-NS/cobalt hydroxide core-shell structure completely covering it, as depicted in Fig. 20. Broader area SEM views provided no evidence for independently formed carbon lumps. The glucose-derived carbon shell appeared to preserve the twine-like imprint of the underlying cobalt hydroxide seen in Fig. 16. The low contrast of the structure suggests that the carbon prepolymer layers have fully covered the surface, resulting in the pink-blue color of the initial $Co(OH)_2$-coated material turning to brown-gray. The latter changes to black when the product was heated at 700^{o}C in oxygen free argon carbonizing the prepolymer.

Coating of the ~200 nm silica-NS/cobalt hydroxide core shell structure with carbon.- The slight agglomeration present in the product shown in Fig. 18 grew worse upon carbon deposition.

Figure 21. SEM view of the cobalt hydroxide coated structure shown in Fig. 18 after coating with the carbon shell.

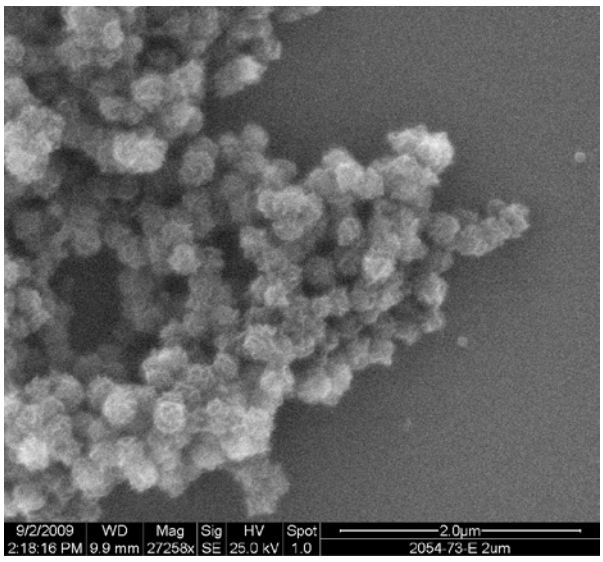

An SEM view of the resulting product is shown in Fig. 21. Our efforts to eliminate the agglomeration of the 200 nm silica-NS core/dual shell structure were not successful.

The recipes that were ultimately adopted for coating of ~200 and ~500 nm silica-NS/ cobalt hydroxide core/shell structures are shown in Table 4.

Table 4.Recipes developed for coating silica-NS/Co(OH) core/shell structures with carbon

	200-1X	500-1X, or 2X
Original Silica-NS used in Table 3 *	5.00	10.00
D-glucose, g	6.59	9.59
Water (Total), ml	~400	800
Nominal carbon thickness, nm**	22	40

* The entire product from the recipes given in Table 3 was used here, ** assuming 100% carbon yield from glucose

3.1.4 Removal of silica core from carbon coated silica-NS/$Co(OH)_2$ structures.

The last remaining step to secure the target cobalt-encapsulated carbon nanoshells was to etch away the silica template from the silica-NS/cobalt hydroxide/carbon, core/dual-shell structure. Our attempts to carry out this step with gram quantities of the core/dual-shell material afforded an intractable glass-like material which was not suitable for electrode fabrication. Etching was carried out in 2M NaOH at 60^{o}C overnight. This product was unlike the smooth, free-flowing material we had observed in previous runs at much smaller scale. A broad-area SEM view of this brittle, glass-like product is shown in Fig. 22.

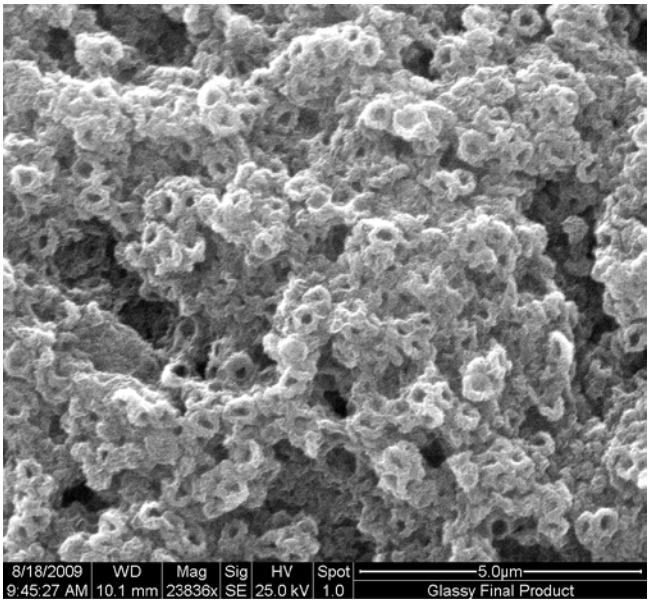

Figure 22. SEM images of the glassy, intractable product obtained in a scaled up preparation of the cobalt encapsulated carbon nanoshells.

Although the shell structure is identifiable, the shells are fragmented with pieces bonded together to form an agglomerated mass. The EDX spectrum shown in Fig. 23 indicates the presence of a substantial amount of silicon remaining in the sample.

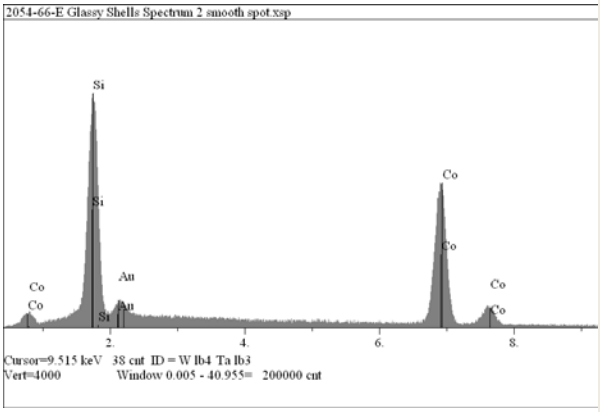

Elt.	Line	Intensity (c/s)	Error 2-sig	Atomic %	Conc		
Si	Ka	143.34	1.336	53.281	35.212	wt.%	
Co	Ka	115.99	1.202	46.719	64.788	wt.%	
				100.000	100.000	wt.%	Total

kV	20.0
Takeoff Angle	35.0°

Figure 23. SEM/EDX analysis of the product shown in Fig. 22

By comparing the EDX data for the material, before etching, about 14 atomic % of the original silicon was found to remain in the etched sample. Increasing the time of etching made no difference in the silicon content of the product. Since the alkali etchant 2M NaOH at 60^{o}C was known to be very effective on silica-NS, the most probable reason for the etched product to have a large percentage of silicon was the product of etching, sodium silicate, remaining in the sample. The brittle, glass-like product also could be an artifact of this remaining sodium silicate which, once dried, is known to turn into a glassy material. This broken shell structure shown in Fig. 22 was the first critical issue to solve.

The cobalt catalyst/carbon dual shell could have been strengthened simply, by increasing the thickness of one or both shells, provided the silica core remains accessible to the etchant across the two shell walls. This concern led us to examine the etching process with either shell individually.

Etching of the silica core in 500 nm silica-NS/carbon, core/shell structure.- During our initial work the ratio of glucose to silica-NS used for the carbon deposition was only a half as much as that in the recipe, “500-1X, or 2X “ given in Table 4. The same glucose stoichiometry was used here to form the carbon pre-polymer shell over 500 nm silica-NS. After etching away the silica core with 2M NaOH overnight, the product was freed of soluble silicates by extensive washing with DI-water as before. The resulting product indicated substantial fragmentation of shells. This difficulty could be circumvented by heat treating the pre-polymer coated product at 700^{o}C in oxygen free Ar, which resulted in carbonization of the pre-polymer phase. Etching and leaching of this product ensued as before which resulted in a very fluffy product with no glassy character whatsoever. The SEM view of the resulting empty carbon shells (Fig. 24) shows neither any whole or partial silicon core that remained un-etched or fragmented. The shells are perfectly spherical, as expected, and transparent as well. It appeared that the carbon shell itself was strong enough to withstand the etching and the subsequent work-up. Surprisingly, the dual shell structure (Fig. 22) with a similarly formed carbon shell had undergone total fragmentation.

We also evaluated empty carbon shells that formed by doubling the glucose stoichiometry equivalent to that in the recipe “500-1X, or 2X “ shown in Table 4. The corresponding SEM view is shown in Fig. 25.

Figure 24. SEM image of carbon shells constructing on the 500 nm silica templates after etching and leaching.

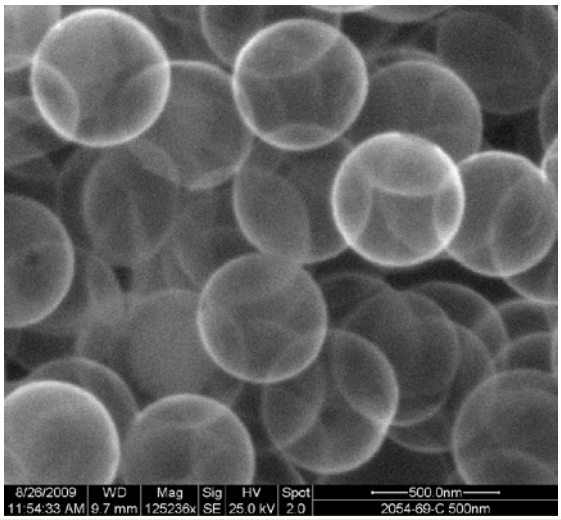

Figure 25. SEM image of carbon shells twice the thickness of those shown in Fig. 24, showing that the etching process can still be accomplished through the increased thickness.

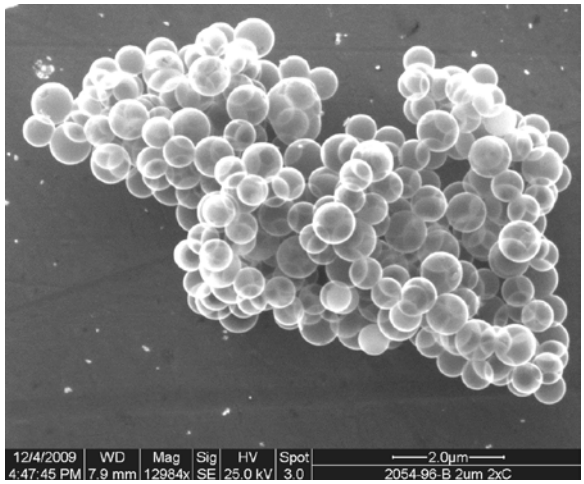

Figure 26. SEM/EDX spectrum of the product shown in5. 24 taken from a sample spread over a Cu substrate. There is no Si peak above the background noise level.

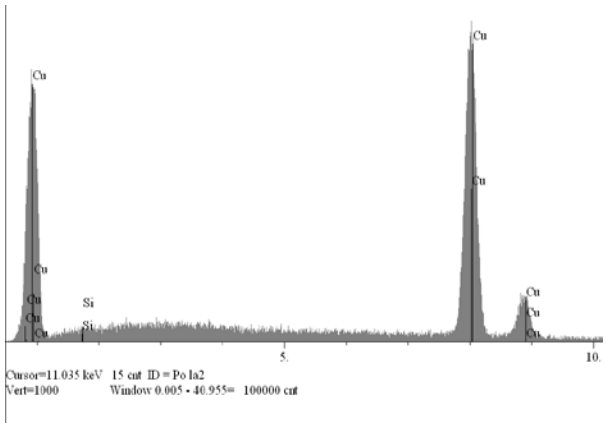

Again, shells shown in Fig 25 are fully transparent and show no fragmentation. The corresponding EDX spectrum shown in Fig. 26 indicates not more than a trace amount of silicon left in the etched/leached spheres despite the thicker carbon shell wall. These observations suggest that the carbon shell is strong and it offers no restrictions to etching of the silica core or to the elution process. It further suggests that the etching medium and the conditions used in the process are effective and do not require any adjustment. It also suggests that the thickness of the carbon shell can be doubled for strength's sake, if necessary, without affecting the etching step.

Etching of the silica core in 500 nm silica-NS/cobalt catalyst, core/shell structure.- Next. We focused on the mechanical robustness of the cobalt catalyst shell by itself. The $-NH_2$ derivatized ~500 nm silica-NS template was coated with a cobalt hydroxide shell as described earlier. The stoichiometry of the cobalt salt during our initial trials was eight times higher than that in the "500-1X" recipe given in Table 3. The cobalt hydroxide shell was heat treated as we had done for the dual shell structure prior to etching in 2M NaOH overnight. The objective was to determine whether the cobalt catalyst shell remained intact after etching and leaching. If the product was discrete shells and not agglomerated, glass-like material, we could simply coat carbon over that to form the target dual shell product.

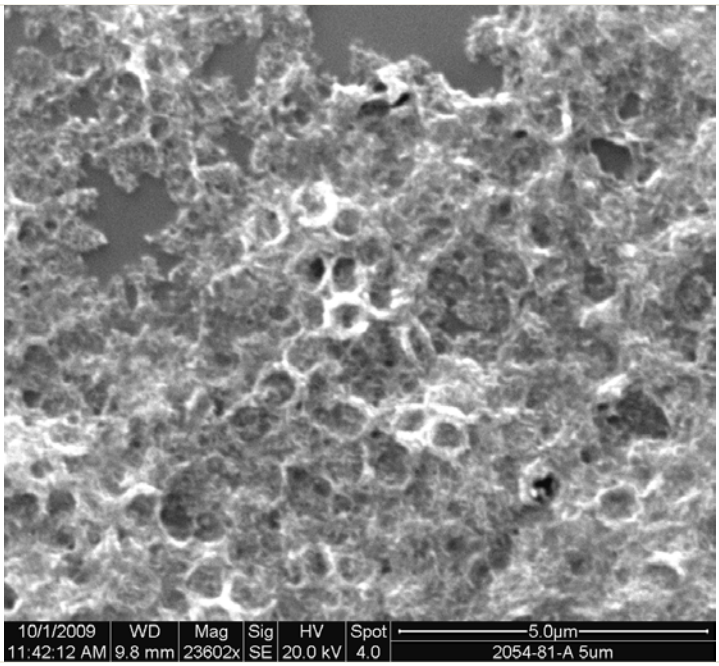

Figure 27. Broken Co shells resulting from the etching of the ~500 nm silica-NS/cobalt catalyst, core/shell (single shell) structure

Shown in Fig. 27 is the SEM view of the product that remained after etching away the silica core of the silica-NS/cobalt catalyst, core/shell structure. It appears that the cobalt-catalyst shells have either disintegrated into pieces or totally collapsed, forming chip-shaped structures upon removal of the silica core. More gentle post-etched procedures, for example filtering rather than centrifuging to separate products etc., failed to avoid the structural failure depicted in the figure. It highlights the need to have

the carbon shell in place, in order to support the underlying cobalt-catalyst shell before attempting to remove the inner silica core. Considering the mechanical robustness of the carbon shell itself (Figs. 24 and 25), key questions are why the cobalt catalyst/carbon dual shell is not mechanically robust and why the product obtained following etching/leaching is glassy, presumably, due to remaining sodium silicate (Fig. 22). We wondered about the possibility of the twine-like morphology of the cobalt catalyst layer with deep gullies (Fig. 16) somehow making the overlaid carbon shell mechanically weak. Therefore, in an effort to strengthen the dual nano-shell structure, attention was focused on the morphology of the cobalt-catalyst layer.

Manipulation of the morphology of the cobalt-catalyst layer.- As seen above, carbon shells alone are quite smooth and uniform, and their spherical shape provides them strength. One hypothesis for the mechanical failure of the dual-shell structure was that the twine-like strands of the cobalt-catalyst layer were too rough and had many sharp facets, which could be acting as stress centers and take away from the strength normally inherent to smooth spherical shells. This structure was then transferred to the carbon coating leaving a structure with many weak points leading to its failure. Our initial approach to mitigate this issue was to decrease the amount of cobalt until the faceted structures disappear or be sufficiently minimized to be dulled when carbon coated. If that was not enough, the thickness of the carbon shell could be increased enough to bury and smooth out any sharp facets instead of merely coating the existing structures with a thin, fragile layer of carbon.

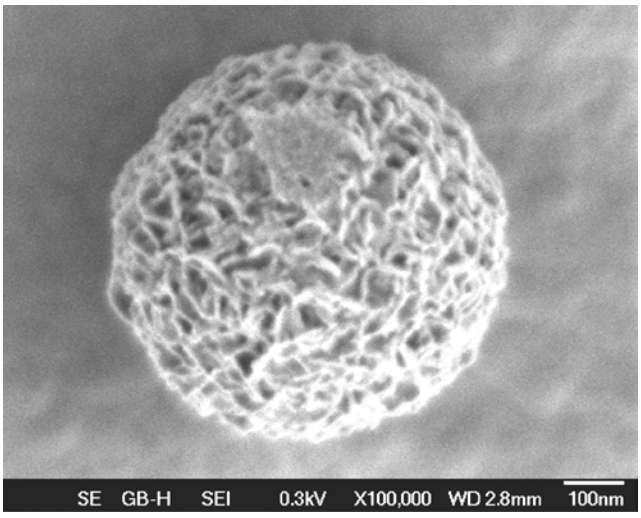

a)

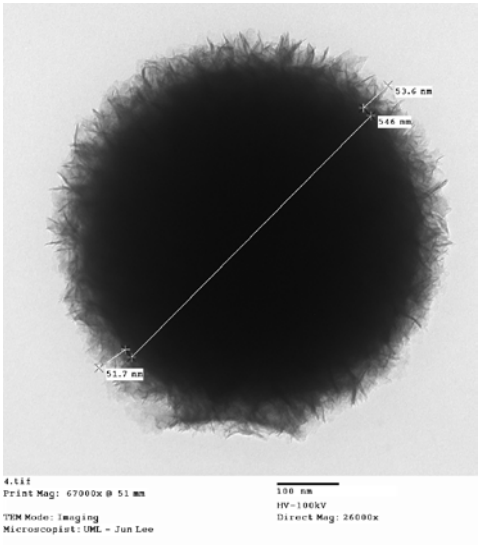

b)

Figure 28. a) SEM and b) TEM images of cobalt hydroxide coated silica nanospheres with ½ the amount of cobalt previously used (4 times the cobalt stoichiometry in the recipe " 500-1X" shown in Table 3).

Figs. 28 through 31 show the SEM views of the morphology of cobalt-catalyst layer resulting from a progressive reduction of the stoichiometry of the cobalt salt. The structure seen in. 28 shows a cobalt layer deposited with half the amount of cobalt as our usual process (4 times the stoichiometry under "500-1X" shown in Table 3). The

cobalt concentration was reduced by a factor of two each time to afford the structures depicted in Figs. 29 and 30 respectively.

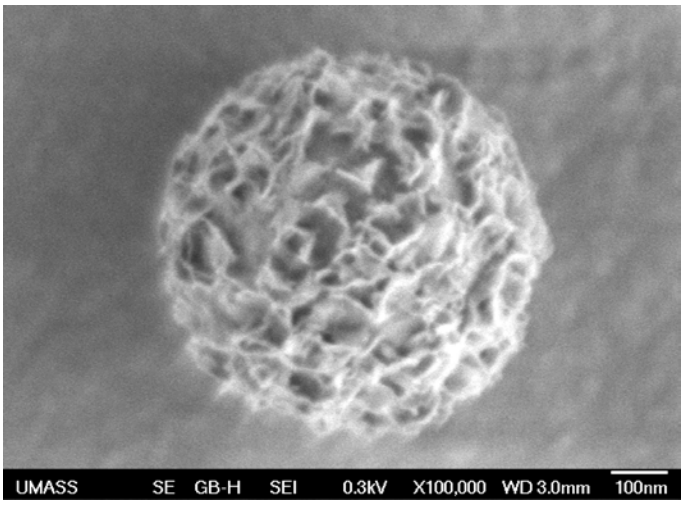

a)

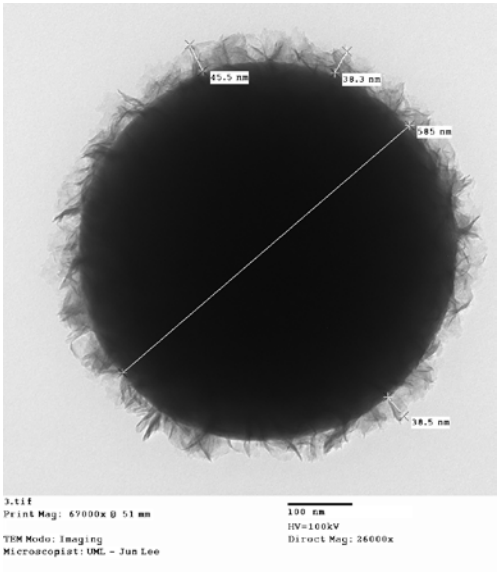

b)

Figure 29. a) SEM and b) TEM images of cobalt hydroxide coated silica nanospheres. Amount of the cobalt salt was 2 times the stoichiometry under "500-1X" shown in Table 3).

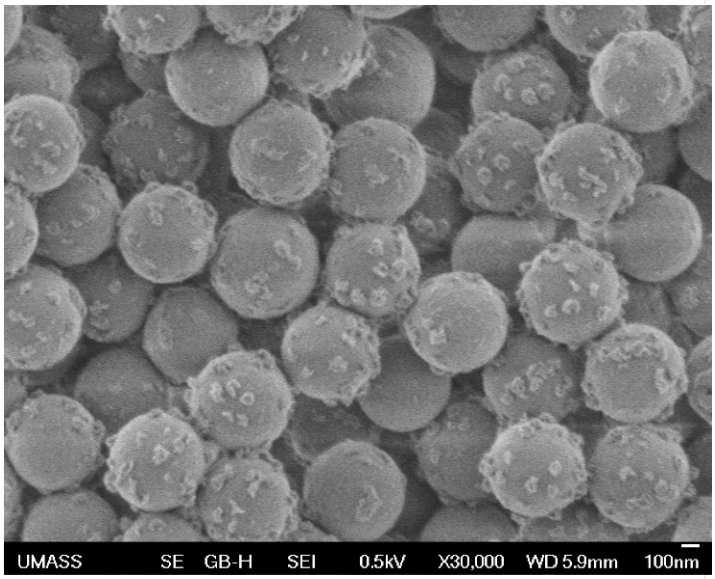

[a]

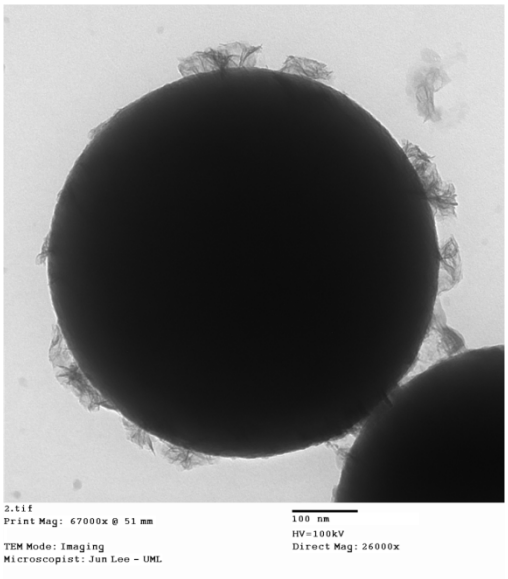

[b]

Figure 30. a) SEM and b) TEM images of Co-coated silica nanospheres showing studs of Co on the surface. Stoichiometry of the cobalt salt was equivalent to that under "500-1X" shown in Table 3).

This amount cobalt stoichiometry was halved again (equivalent to two times that in the recipe, "500-1X" shown in Table 3) for the structure seen in Fig. 29. The thickness of

the cobalt layers (as measured from the TEM images) decreased from ~52 nm to ~40 nm. It can also been seen in Fig. 29a) that there are some regions of the surface that seem smooth below the peaks of the cobalt ridges. It is hoped that further reducing the cobalt will lead to a layer that is entirely smooth like those regions. It is also interesting to note that the patch seen on the upper hemisphere of the nanosphere in Figure 28a) is not a flat region on the surface, but is a result of being attached to another sphere at some point during synthesis. We have seen these become less and less common (Fig. 29) as the stoichiometry of the cobalt salt was continually decreased.

Shown in Fig.30 are the SEM and TEM views of silica nano-spheres coated with 1/8th the amount corresponding to that for the structure in Fig. 28 (equivalent to that in the recipe, “500-1X” shown in Table 3). Instead of providing a complete coverage over the silica surface, as previously seen when a higher amount of the catalyst was used, the deposits have assumed a blunt, stud-like morphology. EDXS analysis confirmed the presence of cobalt in these islands, as expected. Its resolution was not sufficient, however, to ascertain the presence of any cobalt in the area between these islands, although a very thin layer of cobalt-hydroxide cannot be ruled out. It was hoped that this sparsely coated catalyst layer will allow the subsequent carbon coating to form a smoother (and stronger) layer as well as provide for easier etching of silica.

Effective synthesis of cobalt encapsulated carbon dual shells.- Based on our observations detailed above, synthesis of the core-dual shell structure, ~500 nm silica-NS/cobalt hydroxide/carbon was carried out by fixing the

- stoichiometry of the cobalt salt for cobalt hydroxide deposition at a level equivalent to that under “500-1X” shown in Table 3 (Fig. 30), and
- stoichiometry of glucose for carbon deposition at a level equivalent to that in the recipe, “500-1X, or 2X “ shown in Table 4. (Fig. 25).

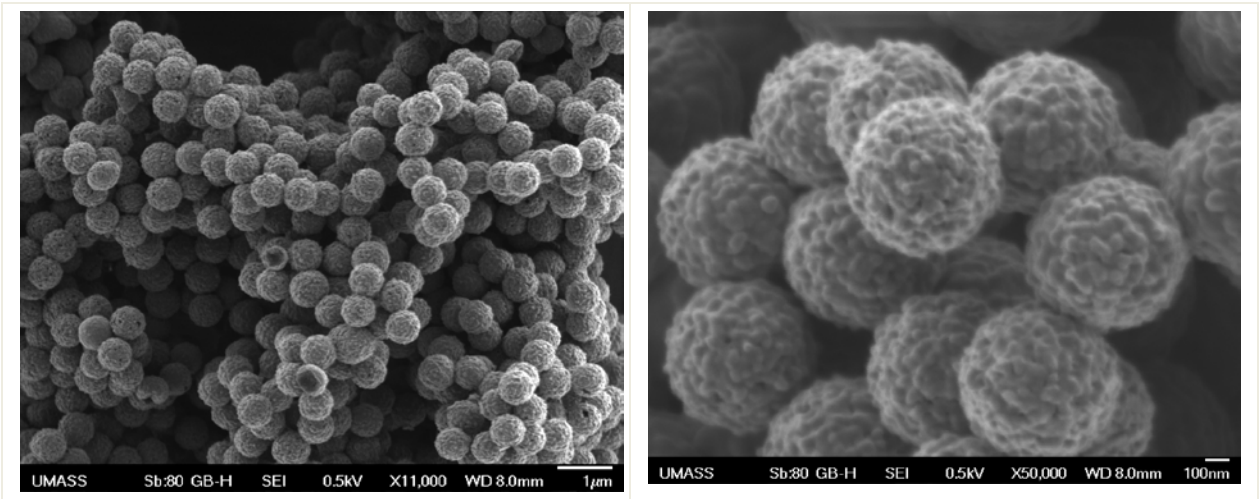

Figure 31. SEM images of the powdery (not glassy) end product, Co-catalyst/Carbon shells based on 500 nm silica template obtained in a successful synthesis. The expanded view is shown on the right.

The entire sequence of steps involved in the synthesis (Fig. 1) was successfully carried

out ending up with a very powdery (not at all glassy) material as originally anticipated based on background evaluations discussed above. SEM views of the product are shown in Fig. 31 while TEM views are shown in Fig. 32. The SEM images clearly show no agglomerated product and a textured surface. The surface with a rough, golf-ball like appearance is the result of the bumpy morphology of the underlying cobalt catalyst shell accentuated by the overlaying, thick carbon layer. The SEM view and the TEM images shown below demonstrate that the shells are not agglomerated in any way and are almost all intact. TEM images show the shells to be well etched out. The thickness of the carbon shell appears to be about 20 nm.

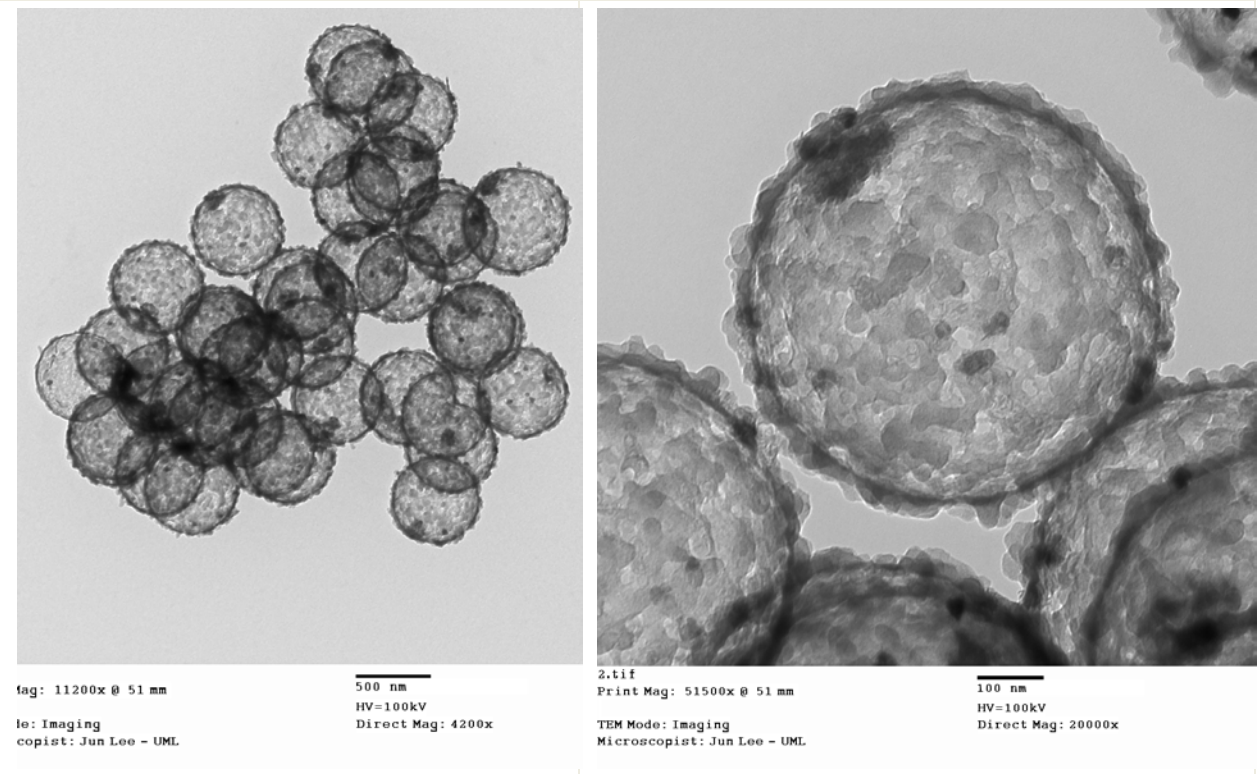

Figure 32. TEM images of the Co-catalyst/Carbon shells based on 500 nm silica template obtained showing the hollow dual shell structure. Expanded view on the right.

We could safely double the stoichiometry of the cobalt salt involved in the precipitation of cobalt hydroxide according to the recipe identified in Table 3 as “500-2X”. The product was a free-flowing powder without any agglomeration, as witnessed in SEM and TEM analysis (not shown).

Cobalt-catalyst encapsulated carbon nanoshells based on 200 nm silica templates-
The recipe that successfully led to the development of the dual nano-shell material discussed above was adopted to prepare the same with ~200 nm silica-NS after allowing for the difference in the surface area. High resolution SEM and TEM pictures of the product are presented below in Fig. 33. Despite the seemingly uneven growth of cobalt/carbon, the empty shell structure and non agglomerated nature of the product are clearly recognizable. In this case, careful adjustment of the amount of carbon used in the shell was necessary to prevent agglomeration.

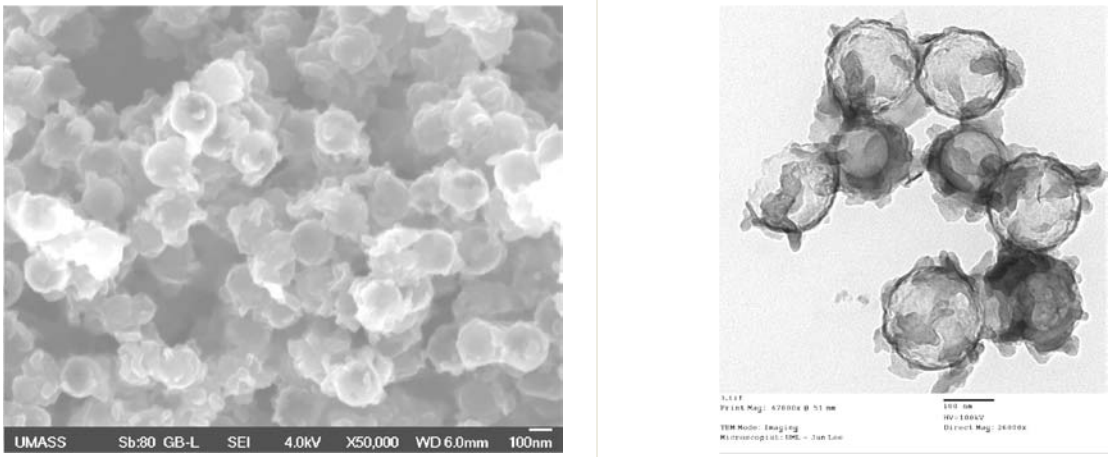

Figure 33. High resolution SEM and TEM of Co/C dual nanoshell structure on ~200 nm silica nanospheres.

Re-evaluation of the etching procedure.- Previously, etching in NaOH was done with a concentration of ~2 M and at 60°C for roughly 16-24 hours. We are particularly concerned about the status of the cobalt layer which was made nominally very thin to minimize its destabilizing effect of the overlaid carbon shell.. For this reason, we evaluated etching for only 4 hours. Figure 34a] shows a TEM image of these shells, and a subsequent EDXS spectrum (not shown) revealed a composition of 56 wt% C, 10 wt% O, 31 wt% Co and 3 wt% Si, which is similar to that obtained for the material etched longer.

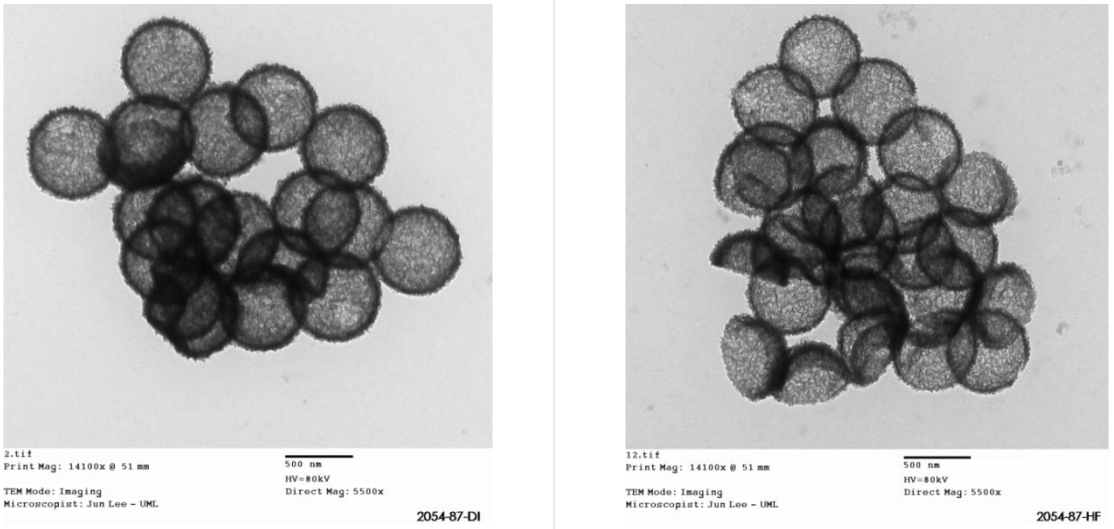

[a] [b]

Figure 34. TEM images of C/Co shells after having the silica cores etched with a) 2 M NaOH or b) 2% HF.

This level of silicon could very well be due to any lingering etching product, sodium silicate remaining in the structure. It appears that nearly all of the silica can be etched out of the cobalt/carbon shells in 2 M NaOH at ~60^{o}C in 4 hours.

We also evaluated another well known and widely used ethant for silica, 2 wt% aqueous HF as an alternative to NaOH. Following 2 hours etching, the product was thoroughly washed before evaluating by TEM as depicted in Fig. 34b. The EDXS evaluation (not shown) revealed a barely perceptible Si peak and a composition of 56 wt% C, 3 wt% O and 41 wt% Co. In comparison to the sample etched with NaOH, this sample seems to have lost some carbon (evident by the lower C:Co ratio) but has also removed more of the silica (evident by both the drop in Si peak and the drop in oxygen). There also appeared to be more broken shells in the HF etched sample as seen in other SEM and TEM images (not shown). In light of other related evaluations, we believed 2M NaOH etching for 4-6 hours would offer the best compromise.

3.2 Anchoring of the Cation and the Anion Conductive Ionic Brushes

Initially, we focused on introducing -COOH surface groups because these are easy to detect and quantify by titration, and the methods developed for COOH attachment are readily applicable to the attachment of the other groups of interest.

Figure 35. Hypophosphorous acid mediated reduction of diazonium salts and covalent attachment to carbon.

Covalent attachment of functional groups to the surface can be accomplished through the reaction of diazonium salts. Here, the reaction proceeds through a radical mechanism when the diazonium group is reduced using hypophosphorous acid (Fig. 35).

Synthesis of carboxypheny ldiazonium tetrafluoroborate.- Synthesis was carried out as described. The product was evaluated by IR as shown in Fig. 36.

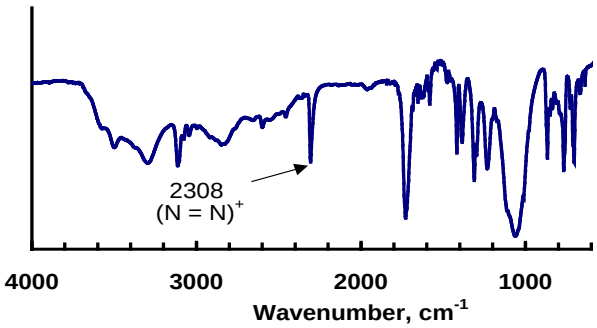

Figure 36. The synthesis of carboxyphenyldiazonium tetrafluoroborate and the IR spectrum of the product (right) showing characteristic diazonium stretch at 2308cm^{-1}.

-COOH functionalization of carbons.- Initially, control experiments were performed to

determine the background level of titratable groups on the XC-72/P2000 mixture (typically COOH groups). The general titration procedure used for all samples was to incubate the samples with NaOH solution and determine their acid content by back titrating the remaining hydroxide using HCl.

Titration of the untreated carbon mixture determined that the acid content was 0.055 mmol/g (6.3 x 10^{-9} mmol/cm^2) . Individually, XC-72 and P-2000 had 0.075 mmol/g (8.7 x 10^{-9} mmol/cm^2) and 0.034 mmol/g (3.9 x 10^{-9} mmol/cm^2), respectively. Next, a second control experiment in which the carbon mixture was stirred with hypophosphorous acid was performed. Following extensive washing with water, titration showed that the acid content had increased to 0.174 mmol/g (20.2 x 10^{-9} mmol/cm^2), indicating that some acid remained adsorbed on the carbon. As a third control experiment, the carbon was stirred with p-aminobenzoic and acid hypophosphorous acid. Here, the titratable acid content increased to 0.298 mmol/g (34.6 x 10^{-9} mmol/cm^2). This is not unexpected, since carbon is expected to strongly adsorb aromatic compounds

COOH functionalized carbon was prepared by reacting with carboxyphenyldiazonium tetrafluoroborate and hypophosphorous acid as described previously. Following reaction, washing and Soxhlet extraction, the acid content was measured as 1.01 mmol/g (117.1 x 10^{-9} mmol/cm^2). This was a significant increase in COOH groups compared to the background levels, and indicated that covalent attachment of COOH had occurred (without the CH_2Cl_2 soxlet extraction the acid content was 152.2 x 10^{-9} mmol/cm^2.) The reaction was repeated using only one equivalent of hypophosphorous acid. Here, the COOH content was 1.23 mmol/g, (143.1 x 10^{-9} mmol/cm^2). When two equivalents of sodium hypophosphite was used in place of the acid, the COOH content was measured to be 1.12 mmol/g (130.0 x 10^{-9} mmol/cm^2). In addition, the increase in weight of the carbon sample following the reaction correlated well with the moles of benzoic acid bound as calculated from the titration results. Similar reactions were done with glucose-derived carbon as well. The carbon was very hydrophobic and was found by titration to have a low acid content of 0.05 mmol/g, Following reaction with carboxyphenydiazonium tetrafluoroborate, the COOH content was found to have increased ~10 fold to 0.48 mmol/g. Similar levels were measured when the reaction was performed without H_2PO_3 reducing agent. Here, vigorous gas release was observed simply by mixing the carbon with the diazonium salt, showing the ready reaction between the two. Following reaction with carboxyphenydiazonium tetrafluoroborate, the carbon became significantly more hydrophilic and was readily wetted by aqueous solution (Fig. 37).

We applied the methods developed above to the functionalization of the hollow carbon spheres (500 nm) containing the Co catalyst. The carbon spheres were reacted with carboxyphenydiazonium tetrafluoroborate both in the presence and absence of one equivalent of H_2PO_3. The reaction was carried out in a limited scale of the reaction and as a result, assessment of surface –COOH groups was not done. However, as one would expect from covalently attached COOH surface groups, there had been a significant increase in hydrophilicity of the spheres, which form a stable suspension.

Figure 37. Unreacted bulk glucose-derived carbon (left) was very hydrophobic. Following addition of COOH groups to the surface (right), the sample became wettable.

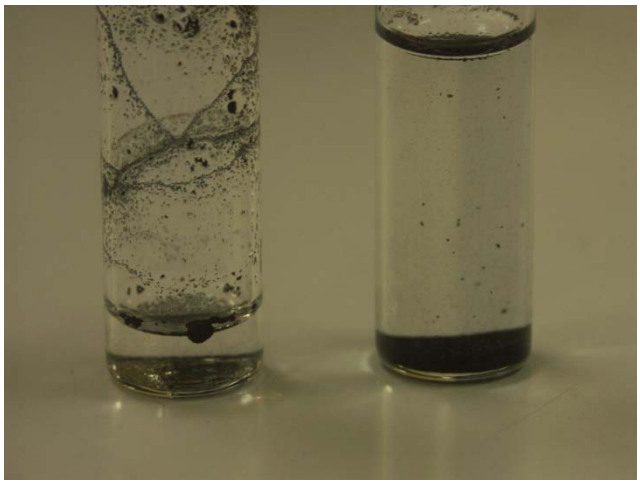

-SO_3H functionalization of carbons.- We also carried out reaction of carbons with the aryl sulfonicphenyldiazonium tetrafluoroborate in order to introduce $–SO_3H$ groups to the surface. The surface functionalization was successful, and under reductive reaction conditions using H_2PO_3, the SO_3H content was measured as 0.267 mmol/g. This was slightly lower than that achieved for COOH attachment, but still significantly higher than the baseline levels of hydrophilic groups. Higher levels of surface functionalization were achieved in the absence of H_2PO_3 (0.337 mmol/g SO_3H).

Functionalization of commercial carbons with quaternary amine groups.- Introduction of the quaternary ammonium functionality to the carbon surface was also of interest in the program. This was planned to accomplish via the $–NO_2$ groups which were introduced using the appropriate diazonium derivative synthesized in-house. Introduction of $–NO_2$ was a prelude to the modification of the carbon surface with quaternary ammonium groups as shown below.

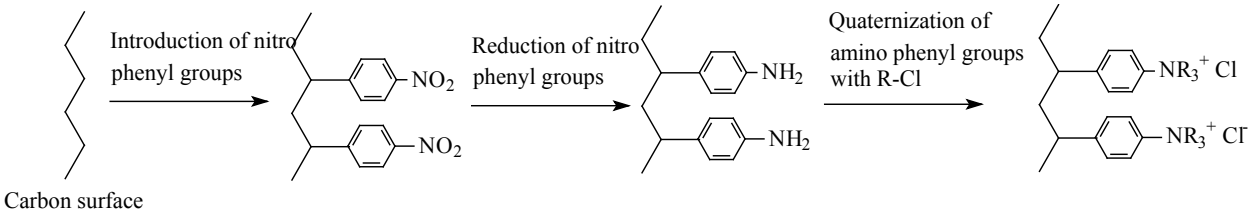

We used surface enhanced Raman scattering (SERS) on gold to detect the presence of –phenyl-NO_2 groups on the surface of carbon. Fig. 38 compares the SERS traces for carbon before and after modifying with the phenyl-NO_2 groups. In the published Raman spectra of neat nitrobenzene peaks located at ~854 (β,NO_2), 1005 (v_{12}, aromatic), 1110 (v_{13}, aromatic), and 1345 (v, NO_2) compare well to the peaks present in the spectrum for modified carbon.

We identified a few issues critical to derivatization of the carbon surface. They were,

- inability of FTIR to reliably detect the presence of various surface groups,

- elution of the encapsulated cobalt catalyst from the dual shell structure due to very acidic conditions used during the reaction of carbon with diazonium compounds as verified by EDXS analysis, and
- work-up to remove hypophosphorous acid after derivatization is extremely difficult because the carbon suspension becomes so fine which makes it very difficult to isolate by filtering or centrifuging. As a result, preparation of materials in quantities sufficient to fabricate electrodes was impractical.

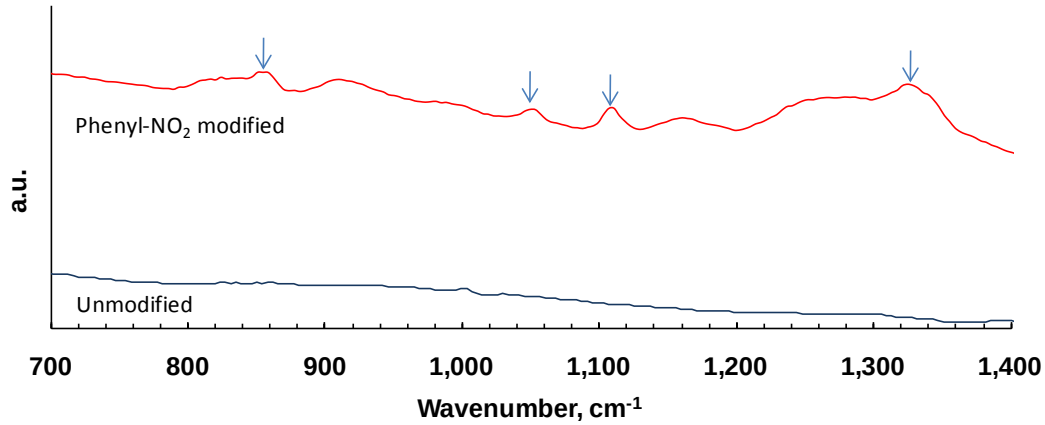

Figure 38. SERS spectra of carbon before and after modifying with phenyl-NO_2 groups.

3.3 Li/O_2 Cell Fabrication

Electrolyte design and component procurement were described in the experimental section. The electrolyte co-solvent methyl n-propylcarbonate, MPC was synthesized in-house and purified as described.

3.3.1 Preparation of electrode structures based on glucose derived carbon shells

Because of the low tap-density and regular shape of carbon shells, fabrication of composite electrodes in a manner similar to those using commercial carbons was not effective. The resulting coating was not mechanically robust, and after drying the coating disintegrated with the slightest disturbance. It appeared that the carbon shells failed to stick to each other or to the nickel mesh substrate. This could be related to the relatively small binder to surface area ratio caused by the extreme low density of the bulk material when a polymer binder is used in quantities (wt %) similar to that typically used in electrodes based on regular carbons.

This adherence issue could be sufficiently mitigated by increasing the bonder content to 30 weight %. The resulting electrodes, although still showing some peeling, could be processed into electrodes usable in fabricating cells. A SEM cross sectional view of the coated structure is shown in Fig. 39. The image clearly shows that there is no tight adhesion between the composite layer and the Ni mesh on a microscopic level.

Figure 39. SEM view of a cross section of the composite coating made of carbon shells indicating that the composite layer has separated from the Ni mesh substrate.

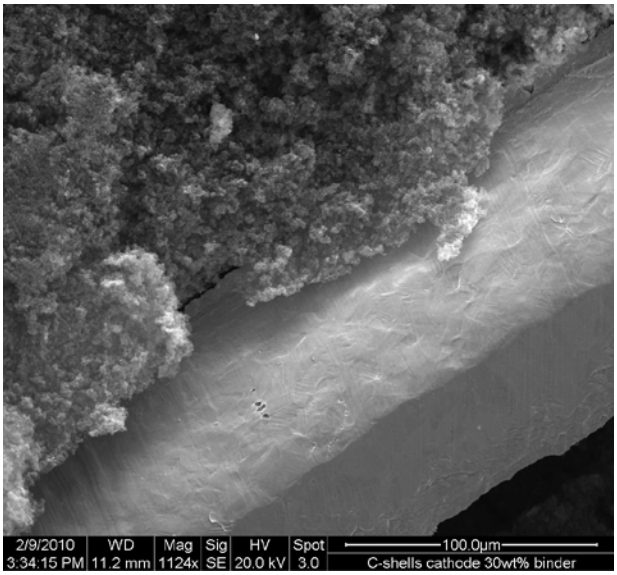

An SEM image of the same composite coated structure is depicted in Fig. 40. The carbon shells making up the electrode are clearly visible there and they have survived well through the electrode fabrication process that involved compaction. Microscopic cracks and the inhomogeneously distributed PTFE binder are also evident. The backscattered image of the same location showed brighter regions (not shown) corresponding to an accumulation of more fluorine and hence a higher PTFE content. This indicates an in-homogeneously distributed (and possibly excessive) binder.

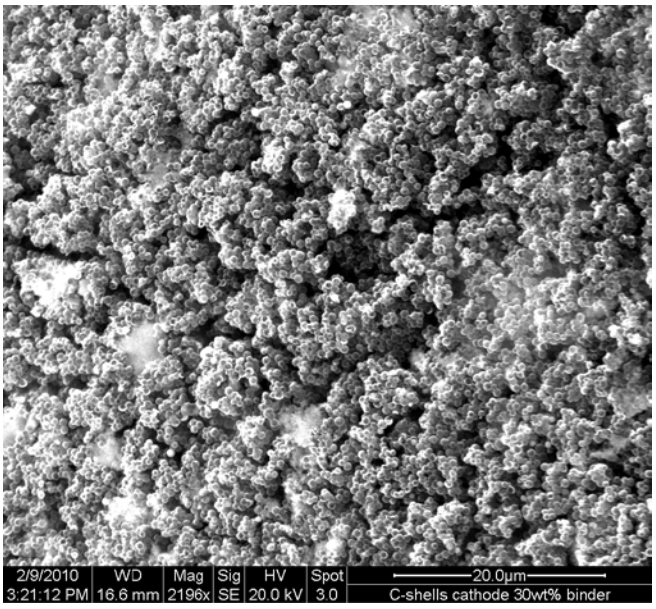

Figure 40. SEM view of the composite surface shown in Fig 39.

Adhesion of these electrodes could be substantially improved when applied to a carbon coated Ni mesh. In this case the Ni mesh was given a thin coating of carbon by

exposing it to hexane vapor in a stream of oxygen-free nitrogen at 700^{o}C. After coating the mesh with the composite, it was dried and pressed at the ambient temperature at 18,000 lbs. for 20 sec. We routinely used such electrodes in our cell studies.

3.4 Performance of Li/O_2 Cells

Screening of potential electrolyte solvents, lithium salts, and polymeric cathode binders suitable for Li/O_2 cells was carried out using cathodes based on a 50:50 by weight blend of commercially available carbons (Black Pearls 2000 and Vulcan XC-72). The former carbon is a synthetic high porosity carbon of approximately 2000 m^2/g while the latter is widely used as a conductive additive in various electrode formulations. The key objective of this broad screening process was to identify the most desirable candidates for the three battery components mentioned above which we hoped to be used, later on in Li/O_2 cells based on the target Co@C materials.

3.4.1 Evaluation of Li/O_2 cells with cathodes made of BP2000/XC-72 blends

Screening of electrolyte solvents.- We evaluated a series of binary and ternary electrolytes containing a common mixture of lithium salts viz. Li-imide and LiBOB. at the 97.5/2.5 mol ratio. The common electrolyte compositions are,

- Binary: First solvent 46.3 mol% / second solvent 46.3 mol% / Li-imide 7.2 mol% / LiBOB 0.2 mol%)
- Ternary: First solvent 30.8 mol% / second solvent 30.8 / Third solvent 30.8 mol% / Li-imide 7.2 mol% / LiBOB 0.2 mol%)

In general, electrolytes consisting of high dielectric solvents such as carbonates and acetamides favor high conductivity, and ether solvents such as glymes favor good oxygen solubility and both these attributes are necessary for the Li/O_2 cell to function properly. Even within a particular category each solvent possess a unique combination of properties such as boiling point, melting point, viscosity, and the donor number etc., Therefore, a suitable blend of solvents is often necessary to achieve the optimum electrolyte properties desirable for a particular application. We evaluated a series of electrolytes in the binary solvents, EC/PC (electrolyte designation, C1D1), PC/DME (C2D1), PC/DEGME (C3D1), PC/DMA (C4D1), PC/DMFA (C5D1), PC/MPC (C6D1), and in the ternary solvents MPC/DEGME/DMFA (C7D1), PC/DEGME/DMFA (C8D1) in Li/O_2 cells using cathodes made of blended commercial carbons, BP2000 and XC-72. These solvent combinations and the corresponding electrolyte designations were identified in Table 2.

The voltage vs. capacity profiles for Li/O_2 cells containing each electrolytes are depicted in Fig. 41. Both binary and ternary blends containing DMFA appear to stand out from the rest, and of these the cell containing the ternary solvent, C8D1, shows the highest capacity. We used this solvent blend as the basis for screening lithium salts and polymeric cathode binders as described next.

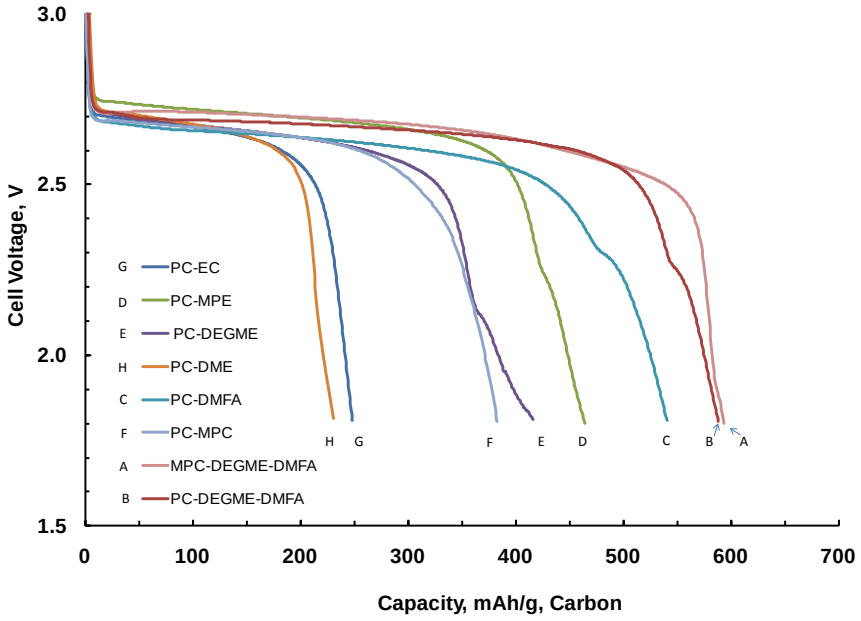

Figure 41. Discharge behavior for Li/O_2 cells containing electrolytes based on binary and ternary solvents identified in the figure containing a blend of Li-imide and LiBOB. Discharges were made at 0.3 mA/cm^2 to 1.8 V at room temperature in pure oxygen. Electrode area was 10 cm^2. The cathodes were made of a 50:50 mixture of Black Pearls 2000 and Vulcan XC-72 containing the PTFE binder (6.3 wt%).

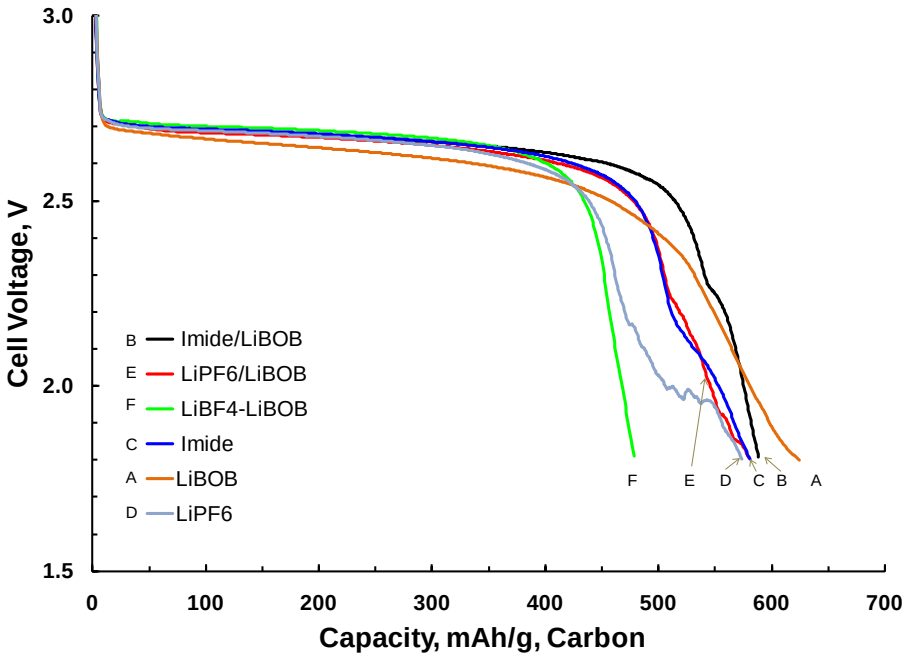

Figure 42. Discharge behavior for Li/O_2 cells with electrolytes made of single and mixed lithium salts in the PC/DEGME/DMFA baseline solvent. Electrolyte salts are identified in the figure. Discharged at a current density of 0.3 mA/cm^2 in pure oxygen. Details of the cathodes are given in Fig. 41.

Screening of lithium salts and their blends - We screened electrolytes made of single Li salts and mixtures dissolved in the PC/DEGME/DMFA mixed solvent in Li/O_2 cells. Key features of this series of cells were,

- cathodes made of, a 50:50 mixture of Black Pearls 2000 and Vulcan XC-72 containing the PTFE binder (6.3 wt%),
- common electrolyte composition, PC 30.8 mol% / DEGME 30.8 mol% /DMFA 30.8 / total lithium salt 7.5 mol%,
- Salt/(electrolyte) designations identified in Table 2 as: Li-imide/LiBOB(C8D1), $LiPF_6$/LiBOB(C8D2), $LiBF_4$/LiBOB(C8D3, Li-imide(C8D4), LiBOB(C8D5), $LiBF_4$(C8D6).

Fig. 42 compares the voltage vs. specific capacity characteristics of Li/O_2 cells corresponding to each of these electrolytes. The highest specific capacity was obtained using 100% LiBOB. However, because of its drooping potential profile that remains below the others, the second best salt(electrolyte) was chosen for our continuing work. The Li-Imide/LiBOB mixed salt (electrolyte, C8D1) afforded a specific capacity that is only ~5% lower than LiBOB alone with an average discharge voltage, at least 50 mV higher.

Screening of the cathode binders - Three water-based cathode binders were of interest. They were, emulsified PTFE (60wt%), 2:1 (by weight) SBR/CMC blend, and lithium acrylate.

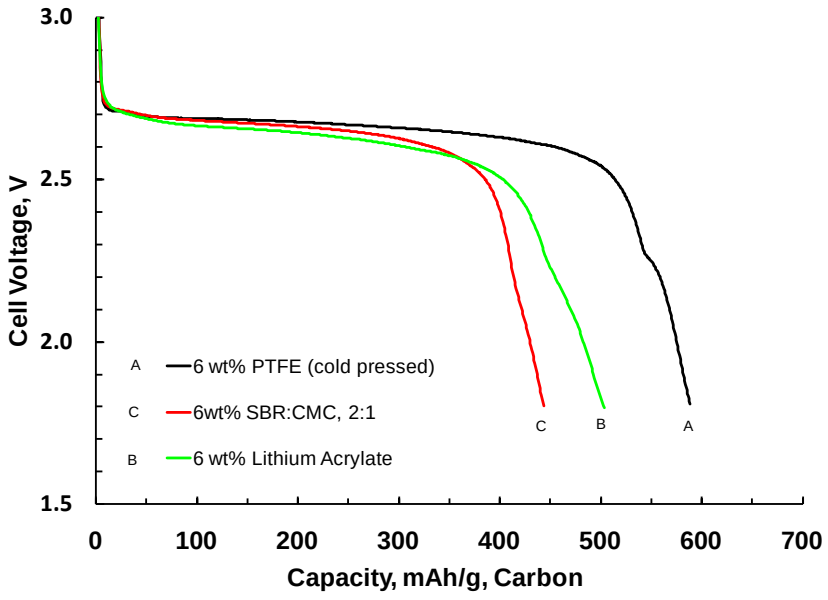

Figure 43 Comarative perfomence of cahodes containing 6 wt% waer-based binders in Li/O_2 cells. The electrolyte was C8D1, PC 30.8 mol% / DEGME 30.8 mol% /DMFA 30.8 / Li-Imide 7.3 mol% / LiBOB 0.2 mol%. Cathodes contained Discharges were at 0.3 mA/cm^2 to 1.8 V cutoff at room temperature in pure oxygen. Electrode area 10 cm^2.

Of the three binders identified in Fig. 43 , the cathodes containing the PTFE binder (cold pressed) provided the highest specific capacity and therefore were chosen for our continuing work. Typically, electrodes containing PTFE are baked at temperatures higher than 320^{o}C before use in order to vitrify the bonder. But we found that treatment undesirable compared to cold pressing due problems such as delamination at edges and consistently low capacities in Li/O_2 cells.

Discharge behavior of cathode made of commercial carbon blends.- Typical discharge behavior of cathodes based on the blend, Black Pearls 2000 and Vulcan XC-72 carbon in Li/O_2 cells is illustrated for two cells in Fig. 44. The most favorable combination of the electrolyte solvent, lithium salt and the cathode binder identified above was used in these cells. A Celgard 2400 propylene microporous film (facing the lithium side) in contact with a nonwoven glass fiber paper and soaked with the electrolyte was used as the ionic separator. Discharges were made at the current density of 0.1 mA/cm^2 over the 10 cm^2 electrode.

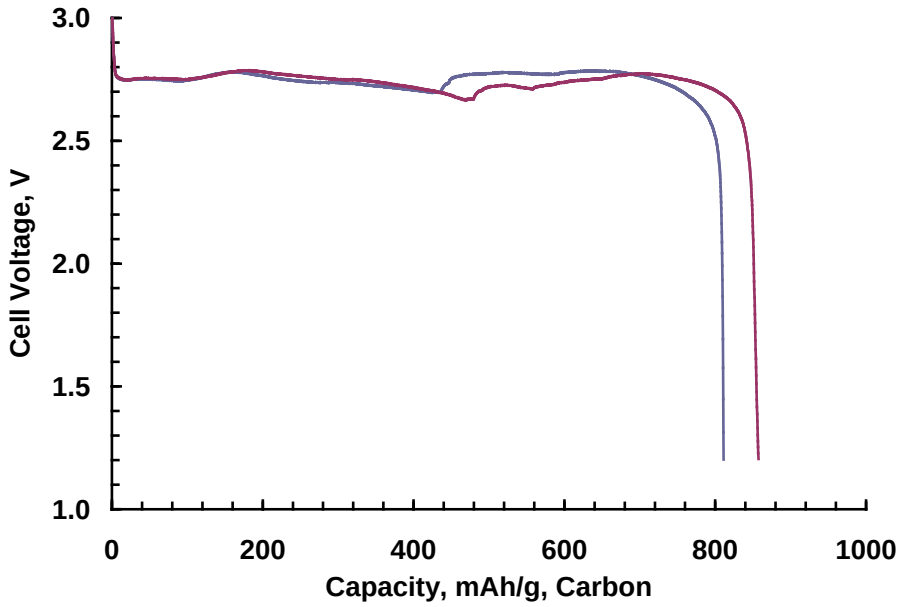

Figure 44. Discharge behavior of two Li-air cells with cathode composites based on a Vulcan XC72/Pearl-2000 blend. Discharged at 0.1 mA/cm^2 to 1.2 V at room temperature in dry O_2. Electrode area, 10 cm^2. The cathode had 6.3 w% PTFE binder. The electrolyte, PC 59.1 w%/EC 21.9 w%/ Li-imide 18.7 w%/LiBOB 0.3 w%.

Since the cathode is facing the lithium anode only on one side and oxygen on the other, it is of interest to determine whether the end-of-discharge condition is the result of the electrode choking on the side facing oxygen. Shown in Fig. 45 are the EDXS elemental maps of a cross section of a spent cathode. The electrode was recovered after discharge and was cleaned thoroughly in a soxlet extractor to remove any remaining electrolyte before the analysis. One difficulty with the EDXS analysis is its inability to detect lithium. Therefore, distribution of oxygen in the electrode was considered indicative of the areas where the deposits of lithium oxide exist. The oxygen map in Fig. 45 indicates a more or less uniform distribution of the lithium salt throughout the bulk of

the electrode, indicating that the electrode is active in all areas of the cathode alike during the low current discharge. There was no preferential accumulation of oxides even near the current collector which suggests that the composite is a good electronic conductor, and the entire electrode bulk is accessible to the electrolyte.

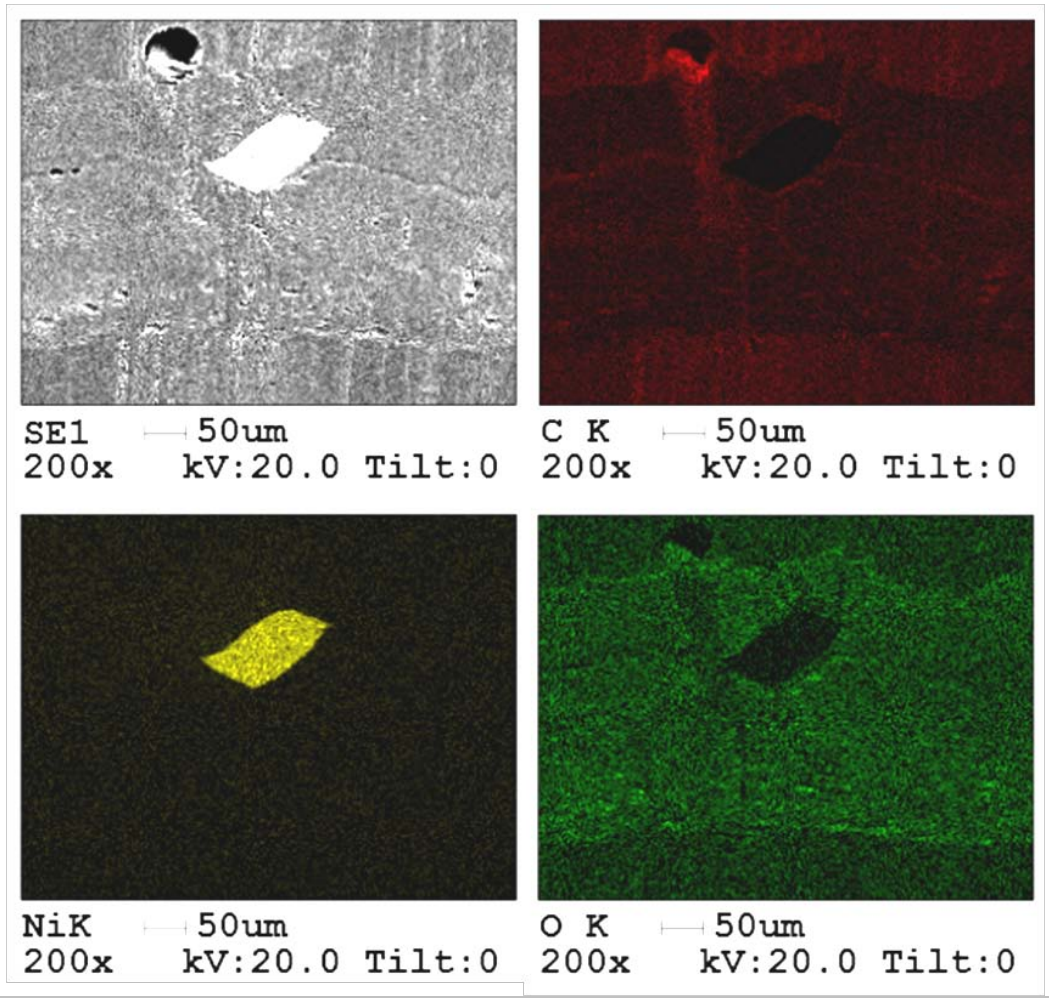

Figure 45. EDXS elemental mapping maps showing, clockwise from the top left, SEM cross section of the electrode, carbon, oxygen and nickel. The side facing lithium is towards bottom.

Good bonding of the composite to the Ni current collector is also evident in Fig. 45. The electrode contained the PTFE binder, and it was compacted at the ambient temperature, at 18000 lbs for 20 seconds.

Discharge behavior of catalyzed commercial carbon cathodes in Li/O_2 cells.- We also evaluated cathodes made of the commercial carbon blend coated with catalysts such as polyaniline, B_2O_3, and Co-Mn, and some of these, after undergoing various treatments. Catalysis of the oxygen reduction reaction in fuel cell cathodes by nitrogen doped carbon (obtained via pyrolysis of N-containing polymers) has been well documented.

[12,13]. Pyrolysis of a polyaniline coating is a convenient way to produce a surface layers of nitrogen coated carbon. Further enhancement in the electrochemical reduction of oxygen can be achieved by complexing PANI with metals, e.g. Co. We also noted the effectiveness of nano-structured Co-Mn-oxide as a bi-functional catalyst in oxygen reduction (ORR) and oxygen evolution reactions (OER) as reported recently [14]. B_2O_3 was yet another material of interest. Although not a catalyst, a recent literature report has shown that B_2O_3 modification caused the oxygen groups on the surface of hard carbon to increase, making its interaction with the electrolyte more favorable. A substantial improvement in the Li intercalation had occurred, as a result [15]. Realizing the potential of these materials to improve the performance of our Li/O_2 cells, we evaluated a series of cathodes based on the modified blend on commercial carbons. Discharge characteristics of all these cells were similar to those depicted in Fig. 44. The observed specific discharge capacities relative to the carbon weight are expressed in Table 5 for 1.8V and 1.2V discharge cutoffs at a discharge current of 0.3 mA/cm^2.

Table 5. Performance of catalyzed carbon cathodes in Li/O_2 cells*.

Carbon modification	Sp. Capacity at 1.8V cutoff, mAh/g	Sp. Capacity at 1.2V cutoff, mAh/g
Unmodified BP Pearls 2000 and Vulcan XC-72 blend	603.4	630.2
"A": PANI coated, not heat treated at 700^{o}C	447.0	515.0
"A": duplicated	448.2	534.6
"B": "A" heat treated at 700^{o}C	512.8	527.8
"C": "A" cobalt complexed, not heat treated at 700^{o}C	409.3	432.9
"C": duplicated	451.0	480.8
"D": "C" heat treated at 700^{o}C	486.0	500.0
"D": duplicated	508.0	554.0
"E": PANI deposition, $CoCl_2$ complexation, heat treatment at 700^{o}C, and H_2SO_4 etching.	542.4	568.0
"E": duplicated	647.3	718.9
"E": duplicated	715.2	740.7

12) C. Jin, T.C. Nagaiah, W. Xia, B. Spliethoff, S. Wang, M. Bron, W. Schuhmann and M. Muhler, "Metal-free and electrocatalytically active nitrogen-doped carbon nanotubes synthesized by coating with polyaniline" *Nanoscale*, **2**, 981 (2010).
13) R. Kobayashi and J-i Ozaki, "Novel N-Doped Carbon Cathode Catalyst for Polymer Electrolyte Membrane Fuel Cells Formed on Carbon Black" *Chemistry Letters*, **38**, 396 (2009).
14) Y.Gorlin and T. F. JaramilloX. *J. Am. Chem. Soc., Electrochem. Soc.,* **132,** 13612 (2010).
15) X. Wu, Z. Wang, L. Chen, and X. Huang, *J. Electrochem. Soc.,* **151**, A2189 (2004).

"F": carbon surface modified with B_2O_3	497.0	528.2
"F": duplicated	482.0	520.0
"G": Carbon surface modified with 50:50 mol% Co-Mn catalyst	497.0	528.2
"G": duplicated	541.3	659.7
"G": duplicated	620.1	713.2

* 50:50 weight% mixture of commercially available carbons, Black Pearls 2000 and Vulcan XC-72.

None of these modifications brought about a significant improvement in the capacity over the unmodified carbon blend. Probably, the surface of carbon is already catalytic enough or catalysis of the oxygen reduction has no relevance to the processes or factors that limit how far the oxygen reduction proceeds at the low current density employed. There was some marginal improvement with the annealed PANI complexed with cobalt followed by H_2SO_4 etching. But the results are rather sporadic and inconclusive.

Residual capacities of spent carbon cathode following the first discharge.- Another intriguing aspect we have noticed with the Li/O_2 cells using carbon based cathodes is the residual capacity of the cathode following the discharge. In this case, once the discharge ended the cell was left in open-circuit for few hours, and then the cell could be re-discharged accumulating more capacity. After repeating this process for 25 times, the cathode still had some residual capacity, although it progressively got smaller. Capacities observed in such repeated discharges for cathodes based on the baseline blend of commercial carbons and the glucose-derived carbon are shown in Table 6.

Table 6. Discharge capacities observed in the first and the subsequent discharges.

Type of carbon cathode	Capacity, mAh/g (carbon) observed after a particular discharge					
	First	Second	5 th	10 th	25 th	Total
Glucose-derived	126.4	488.0	3.6	3.6	1.9	560.0
Baseline commercial carbon blend	906.1	19.8	4.5	2.5	1.0	1013.6

For the cathode made of the commercial carbon blend, the capacity observed in the second discharge is just 2% of that for the discharge. In all, 12% additional capacity was accumulated in 25 discharges. In contrast, for the glucose-derived carbon the first discharge capacity was low, about 14% of that for the commercial carbon blend. But the capacity resulting in the second discharge was almost four times (386%) higher than the first discharge. From that point onwards, both carbons show similar capacities that got smaller progressively. Although the exact reason for these observations remains unclear, there could be a few possible causes. Li-salt precipitating in the first discharge

could have improved the wetability of the glucose derived carbon, so that additional surface area may have become available for the second discharge. It could also be due to a reorganization of the lithium oxide coating, re-exposing some of the carbon surface that got covered during the first discharge. It is also possible that the liquid electrolyte gradually wets the inner regions of the oxide deposit, so that the ionic flow towards the carbon surface is reestablished during the time the cell is maintained at rest, enabling renewed electrochemical activity. This behavior of the glucose-derived carbon is somewhat unsettling because the target dual shell material has its carbon shell made of the glucose-derived carbon.

Behavior of –SO_3H functionalized carbon cathodes in Li/O_2 cells.- Voltage vs. specific capacity profile for the –SO_3H derivatized commercial carbon blend is shown in Fig. 46. The discharge profile for the unmodified carbon is also provided for comparison. What is immediately noticeable is that the surface functionalization has not caused a significant change in the capacity of a cathode. The improvement shown is well within the cell-to-cell variation we observed with hand-made prototype cells. The capacity for the discharge at high current (3 mA) is also in the same range as that shown in Fig 41.

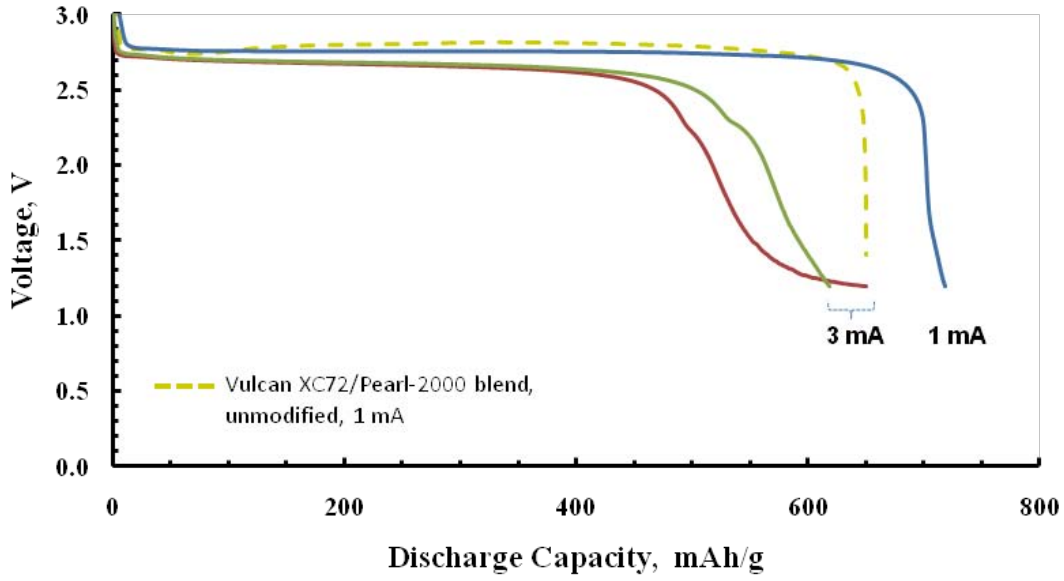

Figure 46 Discharge behavior of Li/O_2 cells with the cathode made of BP-200/XC-72 blend derivatized with the aryl-SO_3H functionality. Discharged to 1.2 V at room temperature in dry O_2. Electrode area, 10 cm^2. The cathode had 6.3 w% PTFE binder. The electrolyte: electrolyte was C8D1, PC 30.8 mol% / DEGME 30.8 mol% /DMFA 30.8 / Li-Imide 7.3 mol% / LiBOB 0.2 mol%.

Glucose-derived carbon derivatized with the aryl-SO_3H functionality was also evaluated in Li/O_2 cells. The capacity has increased nearly four times as a result compared to the un-derivatized material (also include in the figure). This magnitude of increase is reminiscent of a similar increase in the capacity of the same carbon (un-derivatized) when the spent cathode was allowed to rest and then re-discharged as shown in Table 6. Improved wetability of the derivatized surface may be the most plausible cause for

the increased capacity. The overall capacities, however, at 1 and 3 mA currents are still low compared to the commercial carbon blend described above. A possible catalytic effect of the aryl-SO_3H group can be ruled out as a result.

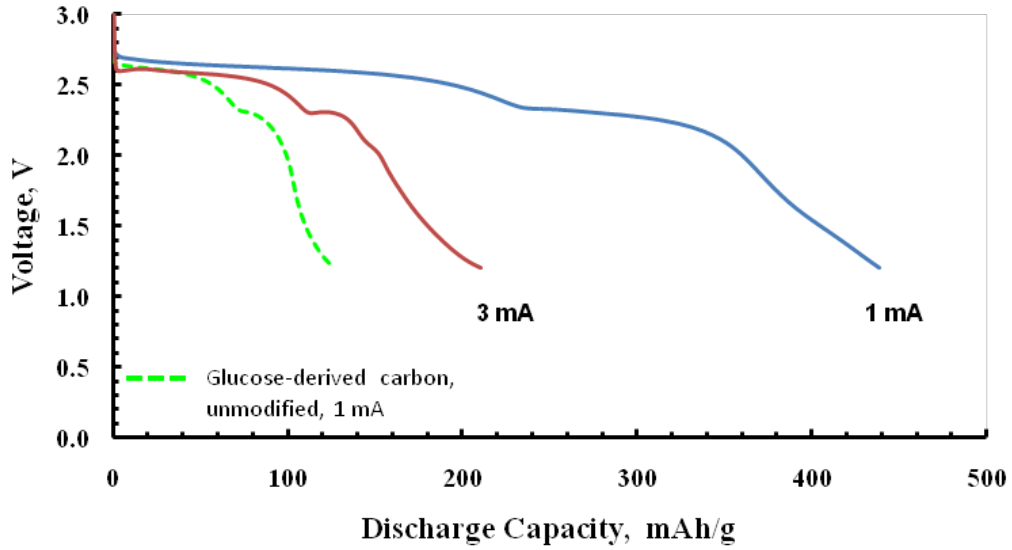

Figure 47 Discharge behavior of Li/O_2 cells with the cathode made of glucose-derived carbon derivatized with the aryl-SO_3H functionality. Discharged to 1.2 V at room temperature in dry O_2. Electrode area, 10 cm^2. The cathode had 6.3 w% PTFE binder. The electrolyte: electrolyte was C8D1, PC 30.8 mol% / DEGME 30.8 mol% /DMFA 30.8 / Li-Imide 7.3 mol% / LiBOB 0.2 mol%.

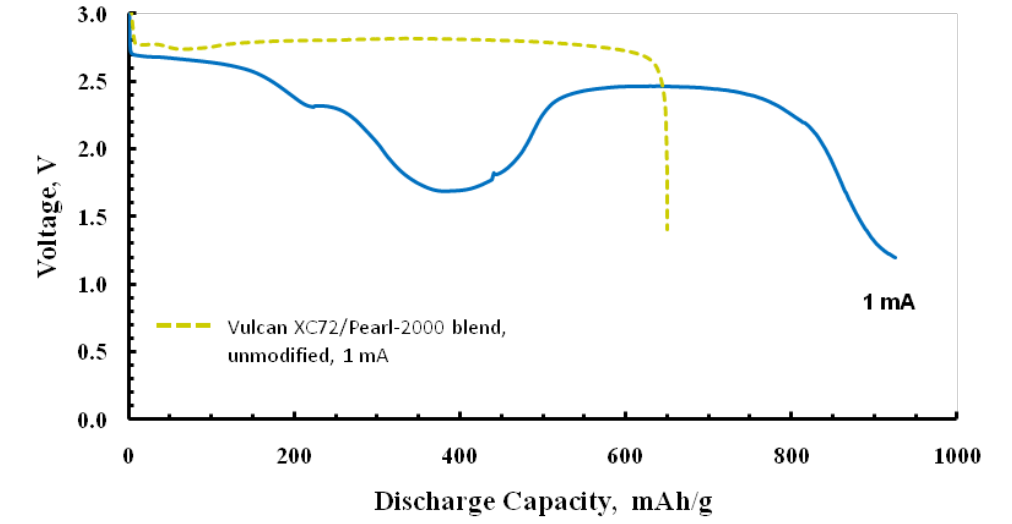

Figure 47 Discharge behavior of Li/O_2 cells with the cathode made of BP-200/XC-72 blend derivatized with the aryl-quaternary ammonium functionality. Discharged to 1.2 V at room temperature in dry O_2. Electrode area, 10 cm^2. The cathode had 6.3 w% PTFE binder. The electrolyte: electrolyte was C8D1, PC 30.8 mol% / DEGME 30.8 mol% /DMFA 30.8 / Li-Imide 7.3 mol% / LiBOB 0.2 mol%.

Behavior of aryl–quaternary ammonium functionalized carbon cathodes in Li/O_2 cells.- Shown in Fig. 48 is the voltage vs. specific capacity profile for the blend of commercial carbons derivatized with the aryl-quaternary ammonium functionality. The discharge profile for the unmodified carbon is also provided for comparison. The discharge curve for the modified carbon is highly deformed although it ended up with much higher capacity compared to the unmodified material. We have seen this behavior in more than one occasion, although in some electrodes the dip in the center portion reached the cutoff potential before recovery. As a result, we consider these experiments very preliminary. Behavior of the electrode made of the glucose derived carbon is more or less the same as the one with the sulfonate modification in Fig. 47. Again, there is a substantially improved capacity resulting from the modification. An electrode surface which is now more wettable a possible reason for the improved capacity.

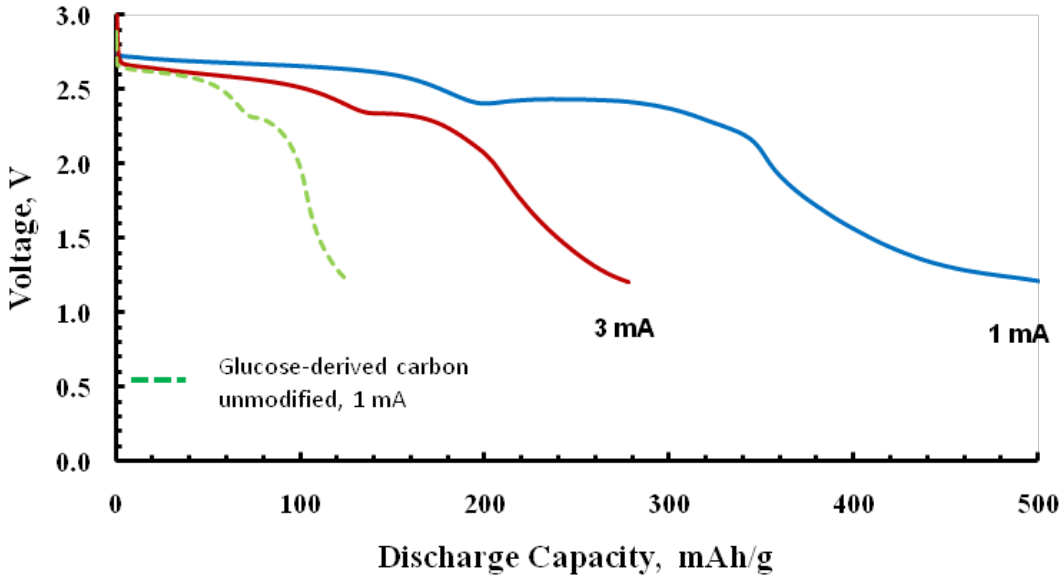

Figure 49 Discharge behavior of Li/O_2 cells with the cathode made of glucose-derived carbon derivatized with the aryl-quaternary ammonium functionality. Discharged to 1.2 V at room temperature in dry O_2. Electrode area, 10 cm^2. The cathode had 6.3 w% PTFE binder. The electrolyte: electrolyte was C8D1, PC 30.8 mol% / DEGME 30.8 mol% /DMFA 30.8 / Li-Imide 7.3 mol% / LiBOB 0.2 mol%.

3.4.2 Evaluation of Li/O_2 cells with cathodes made of Co@C

Evaluation of Li/O_2 cells based on the blend of commercial carbon described above allowed identification of the most desirable electrolyte solvent blend, lithium salt and the binder for the cathode. We applied these findings in the fabrication of Li/O_2 cells with cathodes made of Co@C.

Cell voltage versus capacity (mAh per g carbon) profiles for the cathodes made from 500 nm-Co@C material in Li/O_2 cells are shown in Fig. 50 at different discharge currents. As noted earlier the Co@C appears to have a very low tap density and the fabrication of usable electrodes from it proved to be extremely challenging.

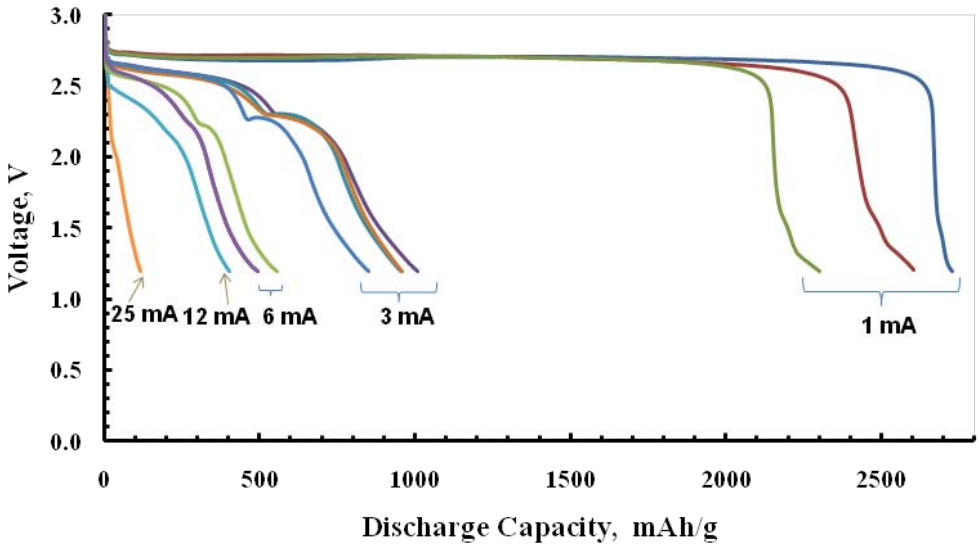

Figure 50. Cell voltage versus discharge capacities as a function currents for the 500nm-Co@C/O_2 cathode based on "1X" (Table 4) material in the electrolyte, C8D1, PC 30.8 mol% / DEGME 30.8 mol% /DMFA 30.8 / Li-Imide 7.3 mol% / LiBOB 0.2 mol%. Discharges were made in pure oxygen until the voltage reached 1.2V. Cathode area = 10 cm^2.

Improved techniques finally enabled fabrication of good quality electrodes with 20 w% of the PVDF binder. The discharge behavior of these electrodes made of 500nm-Co@C material at different current densities is shown in Fig. 50. Multiple discharges at a single current are depicted to illustrate the realm of reproducibility of the results. Two things are immediately noticeable. First, the specific capacities at the 1 mA discharge rate is nearly four times higher than that for the blend of commercial carbons. Second is the large gap in the discharge capacities between the cells discharged at 1mA and 3 mA. We speculate that the points of contacts among spherical structures maintain the electronic conductivity throughout the structure, and these points of contacts are protected from getting buried under a layer of lithium oxide by PTFE surrounding those contacts. In any case, any mechanism that limits the discharge capacity of regular carbons at high currents appears to be still operative in cathodes made of Co@C. The specific capacity at 3 mA current is still very high compared to that for electrodes made of regular commercial carbon. Therefore, the Co@C is sill unique as an electrode material for Li/O_2 batteries.

Another peculiar feature in the curves shown in Fig. 50 is that the shape of the discharge profile at lower discharge is different from that for higher discharges. The curve appears to have three segments. Two plateaus are clearly visible at high currents and a third ill-defined plateau is barely recognizable at the very end of discharge. The two high voltage plateaus may be related to the formation of two lithium oxides, Li_2O and Li_2O_2, while the third plateau could be the reduction of carbon itself. There appears to be a rate limitation of some form associated with the second plateau, because at low currents it appears to extend further, making the discharge profile appear more rectangular and providing more specific capacity.

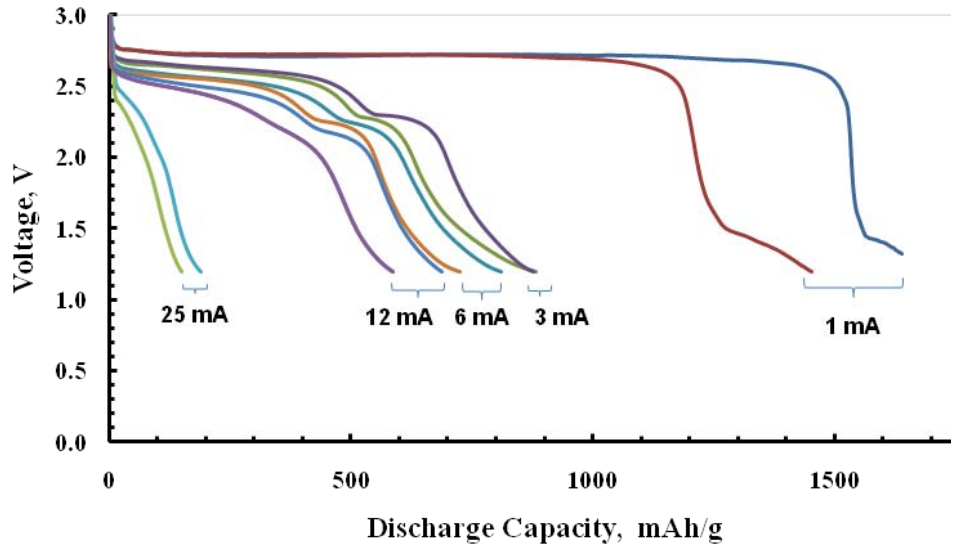

Figure 51. Cell voltage versus discharge capacities as a function currents for the 500nm-Co@C/O_2 cathode based on "2X" (Table 4) material in the electrolyte, C8D1, PC 30.8 mol% / DEGME 30.8 mol% /DMFA 30.8 / Li-Imide 7.3 mol% / LiBOB 0.2 mol%. Discharges were made in pure oxygen until the voltage reached 1.2V. Cathode area = 10 cm^2.

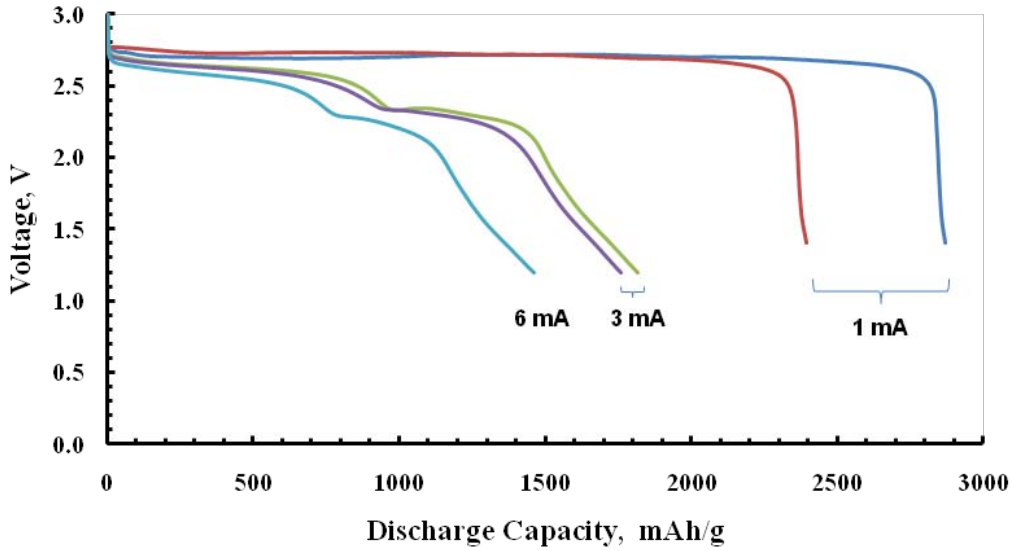

Figure 52. Cell voltage versus discharge capacities as a function of currents for the ~200nm-Co@C/O_2 cathode based on "1X" (Table 4) material in the electrolyte, C8D1, PC 30.8 mol% / DEGME 30.8 mol% /DMFA 30.8 / Li-Imide 7.3 mol% / LiBOB 0.2 mol%. Discharges were made in pure oxygen until the voltage reached 1.2V. Cathode area = 10 cm^2..

The same discussion is valid for the 500-Co@C material with twice as much cobalt as before ("2X" recipe in Table 4). Corresponding discharge profiles at different currents

are shown in Fig. 51. Overall discharge capacities appear to be smaller than the “1X” Co@C material seen above. Probably, a part of the carbon surface area is unavailable for the oxygen reduction because of the islands of the catalyst occupying it. Following a steep reduction of the discharge capacity, in responding to a modest increase in the discharge current, the capacity does not vary much over a narrow range of increasing currents. Further increase in the current seems to reduce the discharge capacity sharply once again. This could be in response to a rate limitation associated with the first plateau of the discharge profile.

Much improved specific capacities could be realized by fabricating electrodes with the 200 nm-Co@C material as depicted in Fig 52. For example, specific capacities have approached 3000 mAh/g and 2000 mAh/g at the discharge currents of 1 and 3 mA respectively. The effect of more surface area accessible with the 200 nm Co@C material may be responsible for this enhanced activity. Regardless of the exact cause, extremely high specific capacities make 200 nm-Co@C the material of choice for Li/O_2 cells.

Distribution of the lithium oxide product in spent Co@C/O_2 cathodes.- Cathodes made of Co@C materials have two types of locations, inside the empty shells and outside among shells, for the insoluble lithium oxide product to accumulate. We were interested to find out whether lithium oxide is preferentially formed inside the shells where the catalyst is located. In order to verify this we carried out the EDX analysis of a cathode made of 500 nm-Co@C material before and after the cathode was discharged in a Li/O_2 cell. Again, oxygen was considered indicative of the presence of the lithium oxide product.

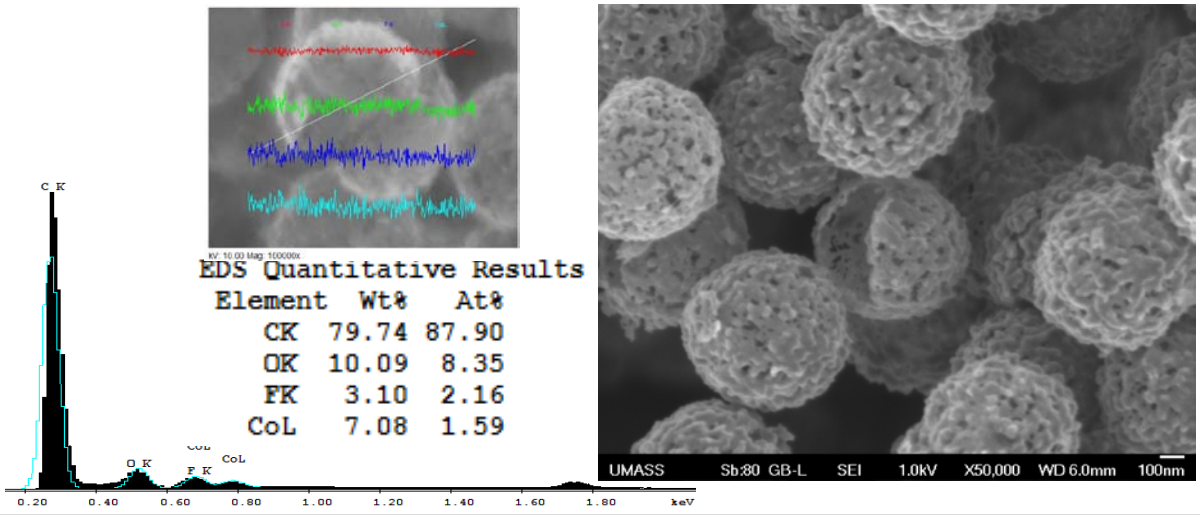

Figure 53. SEM view, EDX spectrum and analysis, and elemental distribution map obtained for a cathode made of 500 nm-Co@C with Teflon as the binder ***before discharge*** in a Li/O_2 cell. The colored curves in the element distribution map are in the same order as are shown in the analysis, carbon in red and cobalt in torques color.

Shown in Fig. 53 are the SEM view, EDX spectrum and analysis, the elemental distribution scan across few shells before discharging in the Li/O_2 cell. What is

remarkable is that the shells have survived through the electrode fabrication process without suffering much damage. It is also surprising that there is so much space among the shells even after the 10 cm^2 (1.6 in^2) electrode was compacted at 18,000 lbs. EDS analysis show some residual oxygen, probably arising from oxygen-carrying groups on carbon.

We examined cross section of a Co@C electrode before and after it was discharged in a Li/O_2 cell, as shown in Fig. 54. There is absolutely no sign of the oxide product formed preferentially inside shells. Unfortunately, the EDX-elemental scans over a shell, cut-across during the sample preparation do not show any local variation of any element including cobalt which is supposed to on the inside wall of the shells. Our attempts to more or less localize this analysis across the thickness of a shell wall were not successful as it was apparently beyond the capability of the present instrument. What is apparently shown is an average result for a depth of at least several layers of shells.

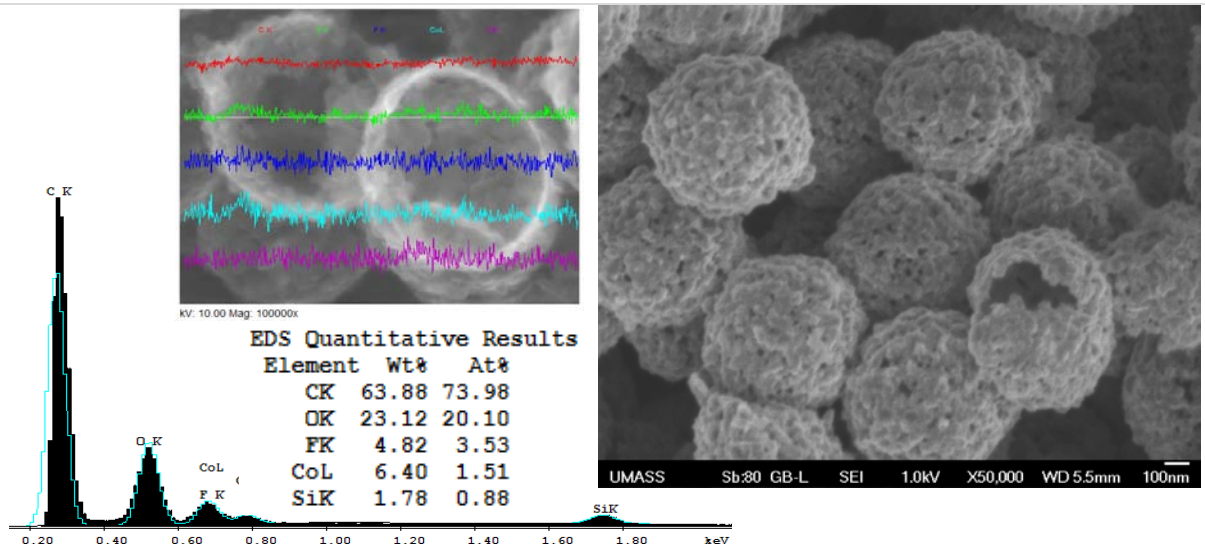

Figure 54. SEM, EDX spectrum and analysis, and elemental distribution across a sliced shell in the structure ***after discharge*** in a Li/O_2 cell. The colored curves in the element distribution map are in the same order as are shown in the analysis, carbon in red and silicon in pink.

A substantial increase in the oxygen content, however, is evident in the EDX analysis included in Fig. 54 as expected from a cathode fully discharged in a Li/O_2 cell. Surprisingly, the void structure of the electrode has not altered significantly in comparison that in Fig. 53, although the specific discharge capacity for this particular electrode was over 1500 mAh/g of carbon. The oxide deposit appears to have coated smoothly over the nano-shells with apparently a modest increase in its thickness.

Effectiveness of the encapsulated cobalt as an oxygen catalyst.- The presence of a potent oxygen catalyst inside the nanoshells was supposed to facilitate the distribution of lithium oxide preferentially inside the empty shells. However, this assertion was not supported by the data shown in Fig. 54. It is, therefore, desirable to find out more about the effectiveness of the encapsulated cobalt species as an oxygen catalyst. To this end, we evaluated carbon nanoshells sans the catalyst in Li/O_2 cells using similar test

conditions as used for the cobalt encapsulated catalyst.

Shown in Fig. 55 is the voltage versus capacity behavior of carbon nanoshells in composites containing 30wt% PTFE binder. Carbon nanoshells were synthesized similar to 500 nm-Co@C, except no cobalt catalyst was involved. The cell was discharged to a 1.2V cutoff and, after an extended stay open-circuit, discharging was done for a second time.

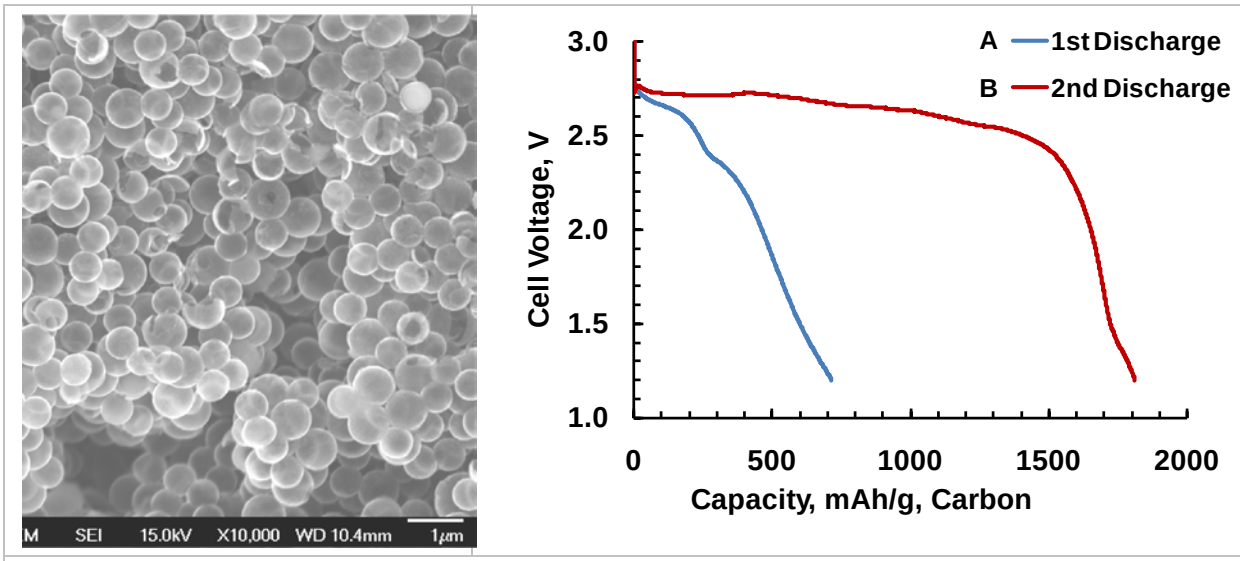

Figure 55. Cell voltage versus capacity profile of a composite laminate of carbon nanoshells with 30wt% PTFE binder evaluated in a Li/O_2 cell containing the C8D1, PC 30.8 mol% / DEGME 30.8 mol% /DMFA 30.8 / Li-Imide 7.3 mol% / LiBOB 0.2 mol%. Discharges were done at 0.1 mA/cm^2 to 1.2 V at room temperature in pure oxygen. Electrode area 10 cm^2. Shown on the left, SEM view of the electrode after the first discharge.

As we had seen before in Table 6 for glucose derived carbon (not shells), the second discharge in Fig. 55 afforded much higher capacity than the first approaching 1884 mAh/g. Capacities obtained in subsequent discharges were very small, suggesting that the capacity of the cathode has been exhausted by the end of the second discharge. The total discharge capacity involved in both discharges approaches that for 500nm-Co@C depicted in Fig. 50. This revelation cast some doubt about the exact role the encapsulated cobalt plays in 500 nm Co@C-based Li/O_2 shells. The exceptionally smooth morphology of the carbon shells in Fig. 55 contrasting the rugged, Swiss cheese-like morphology of 500 nm Co@C pictured in Fig. 53 adds more complications. It raises an important question whether the high capacity observed in the discharge of the 500 nm Co@C/O_2 cathode (Fig. 50) is due to a catalytic effect of the encapsulated cobalt or due to the differences in the morphology. Unfortunately, no definite answer can be found based on the data currently available.

Rechargeability of the Co@C/O_2 cathode in Li/O_2 cells.- Demonstration of rechargeability evaluation of the Co@Co/O_2 cathode in Li/O_2 cells was a key objective of this effort. Shown in Fig. 56 is the cyclability evaluation of Li/O_2 cell with a cathode made of 500nm-Co@C material. Lower cobalt:carbon ratio was used ("1X" material in Table 4)

during synthesis. The initial discharge at 1 mA afforded an excellent specific capacity. The first charge to terminal voltage of 4.3V resulted in a capacity of 550mAh/g, which is a fair value. The second discharge capacity was higher that that involved in the first charge which probably involved some residual discharge capacity discussed above. Unfortunately, cycling did not proceed any further even at this low current. We were not successful in many attempts made at improving the cyclability any further.

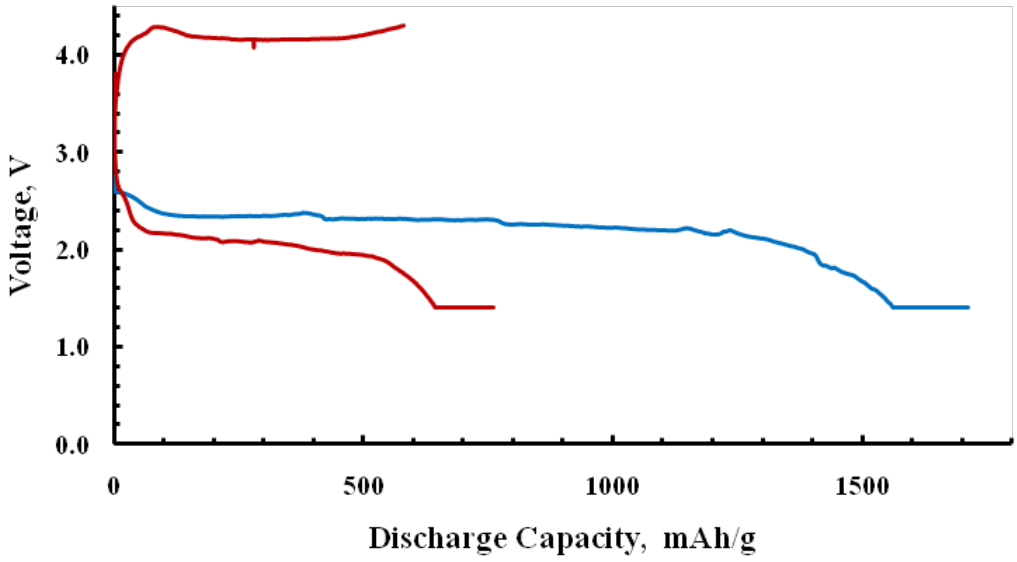

Figure 56. Cell voltage versus specific capacity profiles for the 500nm-Co@C/O_2 cathode in the electrolyte C8D1, PC 30.8 mol% / DEGME 30.8 mol% /DMFA 30.8 / $LiPF_6$ 7.3 mol% / LiBOB 0.2 mol% at +- 1mA. in pure oxygen from 1.2 to 4.3V. 10 cm^2.

Alternative substrates for Co@C/O_2 cathodes.- Despite the high binder content used, the low tap density of Co@C materials makes the bonding between the open pore Ni mesh was still questionable. We prepared a unique substrate by coating the Ni mesh with a Cu_2O layer and then reducing it at 550^oC with hydrogen. This created a substrate with a continuous coating of porous copper. We used this Ni/porous copper substrate to cast electrodes with 500nm-Co@C material. The discharge behavior of cells based on this substrate is shown in Fig. 57. The discharge behavior of an electrode coated on the regularly used carbon-coated Ni mesh is also included for comparison.

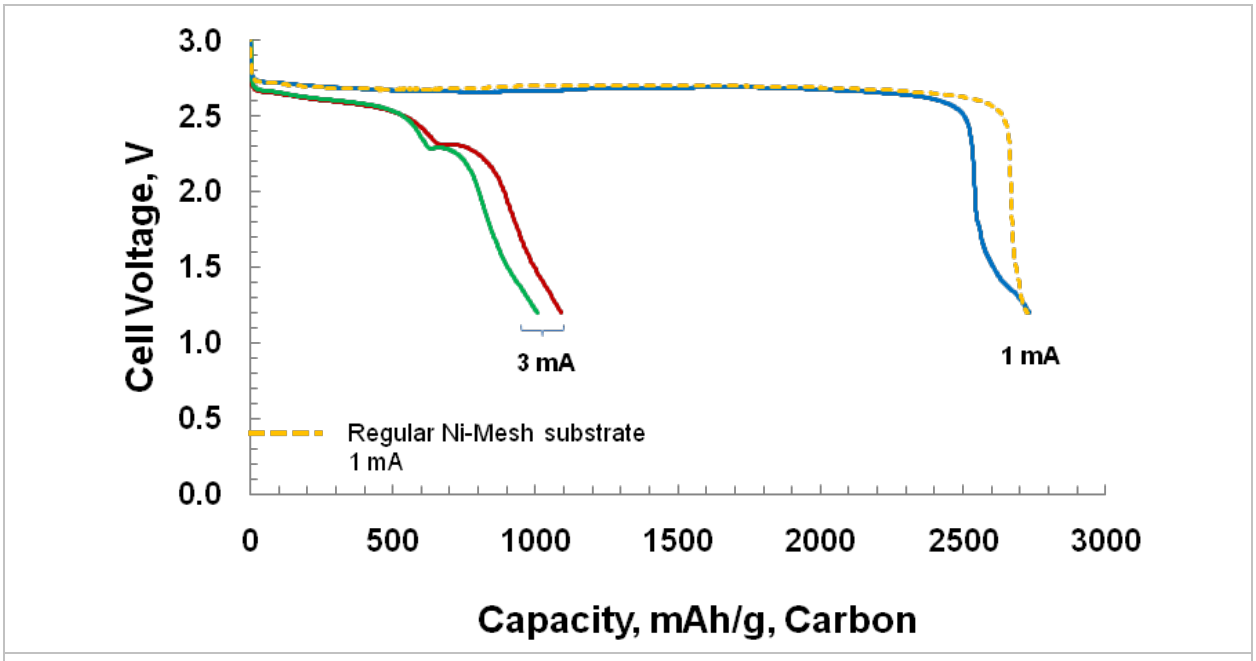

Fig 57. Cell voltage versus discharge capacities for the 500 nm-Co@Ci/O_2 cathode of "1X" composition (Table 4) applied on a copper-coated Ni mesh at different currents in tee electrolyte, C8D1, PC 30.8 mol% / DEGME 30.8 mol% /DMFA 30.8 / Li-Imide 7.3 mol% / LiBOB 0.2 mol%. Discharges were made in pure oxygen until the voltage reached 1.2V. Cathode area = 10 cm^2.

The continuous coating of the substrate with porous copper should establish a better contact with the composite containing the Co@C material and therefore, to provide superior capacity. However, the data in Fig. 57 are comparable to those obtained with the regular Ni substrate. The bonding of the Ni mesh appeared to be as good regardless its open pores. We found no advantage of using the porous Cu substrate.

4 CONCLUSION

We have attempted all Tasks included in this effort fully and obtained promising results. Synthesis of the cobalt encapsulated carbon nanoshells was full of challenges that were successfully overcome. Silica-NS templates of 500 and ~200 nm sizes were prepared using a spreadsheet-based work plan. The process was scaled up to produce about 50g at a time in a one liter reactor. Deposition of the cobalt catalyst and the carbon shell were perfected leading to the synthesis of Co@C materials with two cobalt/carbon ratios. We evaluated a broad matrix of variables pertaining to Li/O_2 cells using a liquid electrolyte. Electrolyte solvent blends, lithium slat blends, and cathode binders were of interest. This matrix was evaluated using a blend of two commercial carbons. Based on the evaluations of a large number of Li/O_2 cells, the electrolyte, PC 30.8 mol% / DEGME 30.8 mol% /DMFA 30.8 / Li-Imide 7.3 mol% / LiBOB 0.2 mol% emerged as the best composition. Cold pressed carbon composites with the PTFE binder turned was found to provide the highest capacities involved in O_2 reduction. Ionic groups anchored to the surface of the commercial carbon blend were not effective in improving the performance of Li/O_2 cells based on them.

Guided by the results of the preliminary evaluations involving commercial carbons, we evaluated Co@C/O_2 cathodes based on the silica templates of 500 nm and 200 nm. The dual shell architecture of these materials was well-preserved in the electrodes regardless of the high pressure used in electrode fabrication. The Co@C electrodes exhibited capacities in the 2500 to 3000 mAh/g range in Li/O_2 cells at low current density (0.1mA/cm^2) whereas cathodes based on the commercial blend provided capacities in the 800 mAh/g range. Higher discharge currents resulted in a sharp decrease in the capacity, but without losing the capacity advantage of the Co@C material. Despite the very high capacities observed for Co@C materials, there was no evidence to support that lithium oxide was preferentially deposited inside nanoshells. Uniform coverage of lithium oxide over the entire exposed carbon surfaces was observed instead. Despite the very high discharge capacities observed with the Co@C/O_2 cathode, it was poorly rechargeable. Only one charging cycle with nearly equal specific capacities was possible